INFORMATION TO USERS

This manuscript has been reproduced from the microfilm master. UMI films the text directly from the original or copy submitted. Thus, some thesis and dissertation copies are in typewriter face, while others may be from any type of computer printer.

The quality of this reproduction is dependent upon the quality of the copy submitted. Broken or indistinct print, colored or poor quality illustrations and photographs, print bleedthrough, substandard margins, and improper alignment can adversely affect reproduction.

In the unlikely event that the author did not send UMI a complete manuscript and there are missing pages, these will be noted. Also, if unauthorized copyright material had to be removed, a note will indicate the deletion.

Oversize materials (e.g., maps, drawings, charts) are reproduced by sectioning the original, beginning at the upper left-hand corner and continuing from left to right in equal sections with small overlaps.

Photographs included in the original manuscript have been reproduced xerographically in this copy. Higher quality 6" x 9" black and white photographic prints are available for any photographs or illustrations appearing in this copy for an additional charge. Contact UMI directly to order.

University of Alberta

LIQUID MALDISTRIBUTION AND MASS TRANSFER EFFICIENCY IN RANDOMLY PACKED DISTILLATION COLUMNS

by

FUHE YIN ©

A thesis submitted to the Faculty of Graduate Studies and Research in partial fulfillment
of the requirements for the degree of **Doctor of Philosophy**

in

Chemical Engineering

Department of Chemical and Materials Engineering

Edmonton, Alberta
Fall, 1999

The author has granted a non-exclusive licence allowing the National Library of Canada to reproduce, loan, distribute or sell copies of this thesis in microform, paper or electronic formats.

The author retains ownership of the copyright in this thesis. Neither the thesis nor substantial extracts from it may be printed or otherwise reproduced without the author's permission.

L'auteur a accordé une licence non exclusive permettant à la Bibliothèque nationale du Canada de reproduire, prêter, distribuer ou vendre des copies de cette thèse sous la forme de microfiche/film, de reproduction sur papier ou sur format électronique.

L'auteur conserve la propriété du droit d'auteur qui protège cette thèse. Ni la thèse ni des extraits substantiels de celle-ci ne doivent être imprimés ou autrement reproduits sans son autorisation.

0-612-46953-0

Canada

University of Alberta

Library Release Form

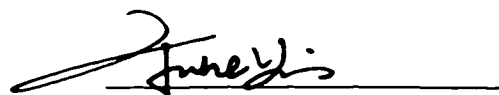Name of Author: **Fuhe Yin**

Title of Thesis: **Liquid Maldistribution and Mass Transfer Efficiency in Randomly Packed Distillation Columns**

Degree: **Doctor of Philosophy**

Year this Degree Granted: **1999**

Permission is hereby granted to the University of Alberta Library to reproduce single copies of this thesis and to lend or sell such copies for private, scholarly, or scientific research purposes only.

The author reserves all other publication and other rights in association with the copyright in the thesis, and except as hereinbefore provided, neither the thesis nor any substantial portion thereof may be printed or otherwise reproduced in any material form whatever without the author's prior written permission.
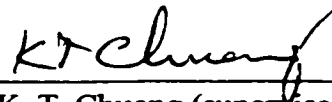
Fuhe Yin

10668-93 Street

Edmonton, Alberta

Canada T5H 1X9

Date: _Sept. 29, 1999_

University of Alberta
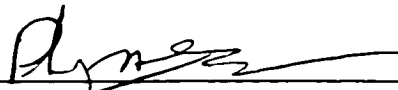
Faculty of Graduate Studies and Research

The undersigned certify that they have read, and recommend to the Faculty of Graduate Studies and Research for acceptance, a thesis entitled **Liquid Maldistribution And Mass Transfer Efficiency in Randomly Packed Distillation Columns** submitted by **Fuhe Yin** in partial fulfillment of the requirements for the degree of **Doctor of Philosophy** in **Chemical Engineering**.

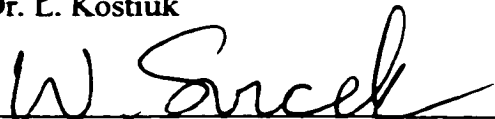Dr. K. T. Chuang (supervisor)

Dr. K. Nandakumar (supervisor)

Dr. P. A. J. Mees

Dr. S. Liu

Dr. L. Kostiuk

Dr. W. Y. Svrcek (external examiner)

Date: September 17, 1999

ABSTRACT

The design and scale-up of packed columns have been traditionally based on one-dimensional models due to the lack of understanding of flow distributions in the packing. This often leads to unreliable design and limits the application of packed columns, particularly on large scales.

The objective of this thesis is to develop theoretical models to predict flow distribution and separation efficiency of randomly packed columns, thus providing more rigorous design tools for such columns.

To study the liquid distribution in a randomly packed column, a 0.6 m diameter air-water column has been constructed with a special liquid collector equipped at the bottom of the column. This liquid collector was installed to serve three purposes, namely, (1) to measure the liquid radial distribution, (2) to support the packing, and (3) to distribute the inlet gas flow.

The effects of liquid distributor design, operating condition, packed bed height, and liquid physical properties on liquid distribution have been experimentally determined. Two different designs of liquid distributor were used: one was a standard commercial ladder-type distributor, another was a modification of the first one which only allowed the liquid to enter the central region of the column (covered 43% of the column cross sectional area). The liquid distributions were measured over a relatively wide range of operating conditions: the gas flow rate was varied from 0 to 3.0 kg/m^{2}s with three different liquid flow rates: 2.91, 4.78 and 6.66 kg/m^{2}s. The packed bed height was varied from 0.9 m to 3.5 m to examine the flow distribution development along the

bed height. Three different systems (water/air, aqueous detergent solution/air, and Isopar/air) were employed to study the effect of liquid properties such as surface tension and viscosity on liquid distribution. These systems were chosen since they had relatively large differences in surface tension and viscosity. The measured liquid distribution data were used to validate the models developed in this study.

The predictive models for hydrodynamics and mass transfer in randomly packed columns have been established. These models were based on theoretical volume-averaged Navier-Stokes equations and mass transfer equations. The complicated two-phase flow behavior and mass transfer characteristics in randomly packed columns have been modeled in the following aspects: (a) flow resistance offered by the solid packing, (b) pressure drop of two-phase flow across the packed column, (c) liquid and gas spreading (dispersion for volume fraction), (d) inter-phase mass transfer and effective mass transfer area, (e) mass dispersion in both radial and axial directions, (f) turbulent flow, and (g) void fraction variation in radial direction.

The models were solved with the aid of the modern Computational Fluid Dynamics (CFD) package CFX4.2 developed by AEA technology plc. The predicted liquid flow distribution, pressure drop, concentration profile and separation efficiency (HETP) were compared with experimental data obtained in this study and FRI (Fractionation Research, Inc.) data at various conditions. In general the predictions agree well with the experimental data, indicating the suitability of the proposed models for the simulation of hydrodynamics and mass transfer in randomly packed columns.

ACKNOWLEDGEMENTS

I wish to express my deep gratitude to my supervisors, Dr. K.T. Chuang and Dr. K. Nandakumar for their guidance and encouragement throughout this program.

I would also like to thank the University of Alberta for the awarding of the Ph.D. scholarship.

My thanks are also due to Dr. S. Liu for his helpful discussions, Mr. A. Afacan for his suggestion and assistance in the experimental work, and the Department Machine Shop and Instrument Shop for building the test column.

Table of Contents

List of Tables

List of Figures

Chapter 1

INTRODUCTION

1.1 Introduction

Packed columns have been widely used in separation processes such as distillation, absorption and liquid-liquid extraction due to their low pressure drops, high capacities and efficiencies. The main function of packing is to create interfacial area for mass transfer between vapor and liquid phases. Packing types can be divided into two categories: random and structured. Structured packing is generally proprietary and is much more expensive than random packing of similar geometric area (the surface area per unit volume). Their application also tends to be limited by the incomplete performance documentation (Bravo and Fair, 1982). Hence this study will be mainly focused on random packing.

The separation efficiency of a packed column is normally expressed by Height Equivalent to a Theoretical Plate (HETP) (Treybal, 1987). It is therefore of great interest to the industrial designer to be able to predict the HETP accurately. However, there is a large scatter in the HETP values published in the literature. For example, for 25 mm packing a 2-3 fold variation in the HETP has been reported from different researchers (Bolles and Fair, 1982; Hoek et al., 1986; Kunesh et al., 1987; Kister, 1992; Shariat and Kunesh, 1995).

The main reason for the large variations in HETP is generally believed to be the non-uniformity of liquid distribution in packed columns. As much as a 50~75% decrease

in packing performance caused by a poor liquid distribution has been reported by Nutter et al. (1992). The non-uniform liquid distribution is usually referred to as liquid maldistribution. Ideally, both the liquid and vapor phases should be uniformly distributed in the packing for the maximum efficiency. Although the vapor distribution in the packing can generally be regarded as more or less uniform (Kouri and Sohlo, 1987, 1996; Stichlmair and Stemmer, 1987; Olujic and de Graauw 1989), the liquid distribution is usually far from uniform due to the radial variation of void fraction of packing and the poor initial distribution of liquid. In particular, the liquid maldistribution effect does not scale up properly and hence the data generated on a small diameter column are of questionable value in scaling up to large diameter columns.

1.2 Objective of Thesis

The objectives of this research are:

(1) to obtain a better understanding of the two-phase flow hydrodynamics and mass transfer in randomly packed columns, and

(2) to develop CFD based models to predict liquid flow distribution and mass transfer efficiency in randomly packed columns.

To achieve these goals, both experimental and theoretical studies were carried out in this research. In the experimental part, the liquid distribution in a relatively large scale column (0.6 m in diameter) was studied. Many factors were thought to affect the flow distributions in a randomly packed column. These factors can be classified into two categories: (1) structural factors: including the size and type of packing, the design of the liquid distributor, and the packed bed height; (2) operational factors: including the flow

2

rates of liquid and gas, and the physical properties of the liquid (viscosity, surface tension, and density). The experimental results not only can offer a better insight into the liquid distributions in randomly packed columns, but also can serve the purpose to validate our models. In the simulation part, the volume-averaged Navier-Stokes equations and mass transfer equations were solved with the aid of the modern Computational Fluid Dynamics (CFD) package CFX4.2 (AEA Technology plc, 1997).

1.3 Structure of Thesis

The ultimate goal of this research is to establish the CFD based models to predict mass transfer efficiency in randomly packed distillation columns. Mass transfer efficiency is found to strongly depend on the liquid flow distribution in the packing. Therefore, every aspect affecting the liquid flow distribution must be first fully studied and understood before we can move to modeling of the mass transfer process. The arrangement of this thesis follows this guideline.

This thesis consists of seven chapters. In Chapter 2, the previously published work relevant to this study is reviewed and discussed. First we look at the previous experimental and model studies on the flow distributions in randomly packed beds, then related mass transfer studies involving the effect of liquid maldistribution is discussed. The void fraction variation in randomly packed bed is a key factor that affects the flow patterns. Thus we also give a discussion of the measuring methods of the void fraction variation in Chapter 2. Along with the discussion of the previous work, the further work that needs to be done in these areas is pointed out. In Chapter 3, the experimental set-up and the procedures for measuring the liquid distribution in our laboratory are presented.

3

The effects of packed bed height, liquid distributor design, liquid and gas flow rate, and liquid physical property on liquid distribution have been investigated. The typical experimental results are also given in this chapter. Chapter 4 demonstrates how to model flow distributions in packed columns using the volume-averaged Navier-Stokes equations. The necessary models to model the flow resistance offered by the solid packing, the interface drag force between gas phase and liquid phase, the liquid and gas spreading (volume fraction dispersion coefficients), and void fraction variation are established. The comparison of the simulation results based on our models and the experimental data is shown in Chapter 5. With the detailed knowledge of flow fields, the volume-averaged mass transfer equations to determine the concentration fields for mass transfer processes are solved in Chapter 6. To validate the models, data obtained by Fractionation Research, Inc. (FRI) on 15.9 mm, 25.4 mm, and 50.8 mm metal Pall rings in a packed distillation column of 1.22 m diameter are used. The models were also tested against the data under two different operating pressures of 33.3 kPa and 165.5 kPa and a wide range of F-factors. The last chapter, Chapter 7, concludes the main points of this study and lists some recommendations for further work.

4

1.4 References

AEA Technology plc, (1997) *CFX-4.2: Solver.* Oxfordshire OX11 ORA, United Kingdom.

Bolles, W. L. and Fair, J. R., (1982) Improved Mass-Transfer Model Enhances Packed-Column Design. *Chem. Eng.* **July**, 109-116.

Bravo, J. L. and Fair, J. R., (1982) Generalized Correlation for Mass Transfer in Packed Distillation Columns. *Ind. Eng. Chem. Process Des. Dev.* **21**, 162-170.

Hoek, P. J., Wesselingh, J. A. and Zuiderweg, F. J., (1986) Small Scale and Large Scale Liquid Maldistribution in Packed Columns. *Chem. Eng. Res. Des.* **64**, 431-449.

Kister, H. Z., (1992) *Distillation Design*, McGraw-Hill, New York.

Kouri, R. J. and Sohlo, J., (1987) Liquid and Gas Flow Patterns in Random and Structured Packings. *I. Chem. E. Symp. Ser.* No. 104, B193-B211.

Kouri, R. J. and Sohlo, J., (1996) Liquid and Gas Flow Patterns in Random Packings. *Chem. Eng. J.* **61**, 95-105.

Kunesh, J. G., Lahm, L. and Yanagi, T., (1987) Commercial Scale Experiments That Provide Insight on Packed Tower Distributors. *Ind. Eng. Chem. Res.* **26**, 1845-1850.

Nutter, D. E., Silvey, F. C. and Stober B. K., (1992) Random Packing Performance in Light Ends Distillation. *I. Chem. E. Symp. Ser.* No. 128, A99-A107.

Olujic, Z. and de Graauw J., (1989) Appearance of Maldistribution in Distillation Columns Equipped with High Performance Packings. *Chem. Biochem. Eng.* **4**, 181-196.

Shariat, A. and Kunesh, J. G., (1995) Packing Efficiency Testing on a Commercial Scale with Good (and Not So Good) Reflux Distribution. *Ind. Eng. Chem. Res.* **34**, 1273-1279.

Stichlmair, J. and Stemmer, A., (1987) Influence of Maldistribution on Mass Transfer in Packed Columns. *I. Chem. E. Symp. Ser.* No. 104, B213-B224.

Treybal, R. E., (1987) *Mass-Transfer Operations*, McGraw-Hill.

Chapter 2

LITERATURE REVIEW

2.1 Introduction

The adverse effect of liquid maldistribution (non-uniform liquid distribution) on the separation efficiency of packed columns has long been recognized and several experimental and theoretical studies have been carried out on the subject. One of the sources of liquid maldistribution is the high liquid wall flow. The formation of liquid wall flow is mainly due to the higher void fraction in the wall region. The orientation of packing near the column wall is also important for the determination of wall flow especially for the old, non-flow-through packings. This chapter presents a survey of the previous studies on the liquid maldistribution and its effect on the mass transfer efficiency. Owing to the importance of the void fraction variation in determining the flow distribution in randomly packed columns, the related studies on this subject will also be discussed in this chapter.

2.2 Liquid Maldistribution in Randomly Packed Columns

2.2.1 Experimental Studies

Baker et al. (1935) were the first to undertake a comprehensive experimental study on the liquid flow distribution in randomly packed columns. They measured the liquid distribution by collecting the liquid at the bottom of the column using a specially designed support plate which divided the column cross section into four equal cross-

7

sectional area concentric rings, with each collecting section amounting to 25% of the column cross sectional area. They examined the liquid distribution in packed columns of different diameters using broken stones, spheres, saddles, etc. as packings. They found that the ratio of column diameter to the packing diameter (D_c/d_p) had a significant effect on the liquid distribution in packed columns. The general trend was that the proportion of liquid accumulated on the column wall increased with the decrease of D_c/d_p ratio. Serious liquid maldistribution resulted when this ratio was less than 8. Therefore, a well known rule of thumb for the design of packed columns has evolved, viz., the ratio of column diameter to the packing diameter should be greater than 8 to avoid the adverse effect of wall flow on the packing separation efficiency (Wankat, 1988). They also found that the initial liquid distribution was very important for the liquid distribution in the packings. In a 0.3 m diameter packed column, a packing height of at least 3 m was required for the liquid to reach the fully developed flow pattern when the single-stream liquid was introduced into the center of the column.

Scott (1935) studied the liquid distribution in a column filled with 12.7 mm Lessing rings, 6.35 mm and 12.7 mm graded cokes, respectively. All experiments were carried out with water introduced at the top of the column as a point source, and there was no gas or air stream passing up the column. By measuring the liquid flow rates at different locations over a horizontal plane at the bottom of the column, he demonstrated that the liquid showed a tendency to spread towards the column wall. He also found that the liquid wall flow increased with the increase of the packed bed height. He stated that the reason for the liquid to accumulate at the column wall was due to the orientations of the packings in the near wall region. The packings near the wall were found to lie on the

8

wall surface mainly in two directions, either with their axes being at right-angle to or in parallel with the wall surface, very few of the rings were in a position oblique to the wall surface.

Porter et al. (1968) investigated the liquid spreading as it trickled down a randomly packed column. A Plexiglass™ square box containing the random packing was used in the experiments. Water was introduced into the column as a line source. There was no gas stream circulating through the column. Most of their experiments were carried out with 12.7 mm ceramic Raschig rings but some measurements were also made with 12.7 mm Intalox saddles, 15.9 mm metal Pall rings, and 25.4 mm Raschig rings. The liquid distribution in the packing was obtained by measuring the rate of liquid flow from small sampling areas at the bottom of the column. They found that the liquid distribution in the packing was far from uniform. It was observed that the liquid rivulets were formed as the liquid flowed down the column. These rivulets sometimes could run into one another and coalesce to form larger rivulets, and sometimes could break up into smaller rivulets.

Bemer and Zuiderweg (1978) measured the liquid spreading and flow patterns in a 0.2 m column as a function of the wettability of the packing, packing size, bed height, flow rate and liquid surface tension. Water or water-butanol mixtures were fed into the packed column as a point source in the absence of a gas stream. Their support plate was divided into 177 sampling sections to measure the liquid flow distribution at the bottom of the column. The radial spreading was found to be dependent only on the packing size. Little or no effect could be found of liquid surface tension on the spreading. However,

9

this finding is contrary to the conclusions of Onda et al. (1973) who found that liquid spreading increased with the increase of liquid surface tension.

A more detailed study on the liquid distribution in the random packing was published by Hoek et al. (1986). A Plexiglass™ column of 0.5 m diameter with various bed heights up to 2 m was employed in their experiments. The random packings used were glass Raschig rings, stainless steel Pall rings, as well as ceramic and polypropylene Intalox saddles. The superficial liquid velocities used were 5, 10 and 15 mm/s. There was no gas stream used. To study the flow distribution on the scale of packing elements, they divided their bottom support plate into 657 square (16×16 mm) liquid catching cells and 24 cells touching the column wall. The liquid flow rate from each cell was measured separately and thus the flow distribution across the column cross section could be obtained. However, this fine degree of resolution was not suitable for the study of the overall migration of liquid toward the column wall. In order to study the rate of the migration, they performed the radial integration of the flows from the catching cells. They proposed that a distinction should be made between small scale maldistribution and large scale maldistribution. Small scale maldistribution refers to the liquid distribution on the scale of the packing elements and is mainly determined by the size and shape of the packings and the random structure of the packed bed. They showed that small scale maldistribution was not influenced by the packed bed height and the initial liquid distribution and thus could be regarded as the inherent property of the packing (Hoek et al., 1986). This aspect of the flow distribution has also been found by Albright (1984) in his simulation of liquid flow in a packed column. He referred this feature as natural flow distribution of packings. Albright (1984) concluded that every packing has a natural

10

liquid flow distribution. An initial distribution that is better than the natural one will degrade to it quickly. Conversely, a poor initial liquid distribution, caused by the ill-design and/or malperformance of the liquid distributor, will ultimately improve to the natural flow pattern after a certain packed bed height, though sometimes at a very slow rate. The height required to attain the natural flow pattern depends on the type and size of packings, the random structure of the packed beds, the design of the liquid distributor, and the flow rates of process fluids. The adverse effects of this small scale maldistribution on the separation efficiency, although unavoidable, are generally not very serious and sometimes may be compensated by the radial mixings of fluids (Hoek et al., 1986). On the other hand, large scale liquid maldistribution required special attention when designing large diameter packed columns. Large scale maldistribution is usually caused by the heavy wall flow and the non-uniform initial liquid distribution at the top of the packed bed. The formation of the wall flow is due to the increased local void fraction in the near wall region. The poor initial liquid distribution is caused by the ill-designed or poorly installed liquid distributors.

The liquid maldistribution in the presence of gas flow has not been well studied. Kouri and Sohlo (1987, 1996) studied the liquid and gas flow distributions as a function of packed bed heights, liquid and gas flow rates, and the initial inlet profiles of the liquid and gas in a 0.5 m diameter column. The random packings examined were ceramic Intalox saddles and plastic Pall rings. The main emphasis of their work was on the interaction between the countercurrent gas and liquid phases. They observed that the liquid distribution over the bulk region of the packed bed became more uniform as the gas flow rate was increased provided that the initial gas distribution was uniform. They

also found that the developing length for the liquid to reach the fully developed flow pattern depended on the gas flow rate. When there was no gas circulating through the packed column, the packed length of 2.0 m was required for the liquid to approach the fully developed state for the 25 mm Pall rings at the liquid flow rate of 2.5 kg/m²s, but this length was reduced to about 1.0~1.5 m as the gas flow rate increased to 2.7 kg/m²s. This kind of effect of gas flow on the liquid distribution in packed columns was also observed by Dutkai and Ruckenstein (1970). In a study of liquid spreading in a packed column of 0.15 m diameter, they demonstrated that the liquid spreading coefficient increased with the gas loading up to 70% of flooding.

As for the gas distribution in a packed column, it is generally believed that the gas phase is always more or less uniform provided that the initial distributions of gas and liquid are even (Kouri and Sohlo, 1987, 1996; Stichlmair and Stemmer, 1987; Olujic and de Graauw 1989). According to these studies, the radial spreading of gas is a much faster process as compared with that of the liquid. Even a severely maldistributed inlet gas may become uniform within a very short bed height. For example, to study the gas distribution in a packed column of a diameter 0.5 m, Kouri and Sohlo (1996) introduced the gas only in the central part of the column, which occupied about 64% of the column cross sectional area, they found that a bed height less than 0.5 m was sufficient to smooth out the non-uniform initial distribution of gas, and concluded that the uniform gas distribution may be assumed throughout the column.

As can be seen, the problem of liquid maldistribution in packed columns has long been recognized and has been a subject of extensive studies. However, most of the previous liquid distribution studies have been carried out in small packed columns with

12

diameters usually less than 0.3 m without the presence of gas flow. The packings examined were usually Raschig rings, Berl saddles, etc. The use of these packings is very limited in industry. Nowadays more and more large diameter columns packed with modern, high efficiency packings such as Pall rings and Mini rings are built to improve the capacity and efficiency. The flow behavior in such columns needs to be further investigated because in practice two-phase flow (liquid and gas) rather than single liquid phase flow (no gas flow) is encountered. There is also a great need to investigate the effect of the gas loading on the liquid distribution and thereby to provide some guidelines for the industrial design of such columns.

2.2.2 Model Studies

Several models have been proposed to predict the liquid distribution in a packed column. These include the random walk model (Scott, 1935; Tour and Lerman, 1939), the diffusion model (Cihla and Schmidt, 1957; Porter and Jones, 1963; Jameson, 1966; Dutkai and Ruckenstein, 1968, 1970; Onda et al., 1973; Bemner and Zuiderweg, 1978; Hoek et al., 1986), and Zone/stage model (Zuiderweg et al., 1993). The Zone/stage model calculating mass transfer based on the predicted liquid flow distribution by using diffusion model, and will be discussed later in Section 2.3.

2.2.2.1 Random Walk Model

Scott (1935) and Tour and Lerman (1939) proposed that the liquid spreading through unconfined tower packing (no wall effect was evident) was of a random nature and that it followed the Gaussian probability distribution. These researches used the

13

following equation to describe the liquid distribution in a radially unconfined bed irrigated by a point source

$$f(z) = \frac{1}{\sqrt{2\pi}\, s} \exp\left(- z^2 / 2s^2 \right)$$ (2-1)

where $f(z)$ is the fraction of liquid flow per unit area at a distance z from the distributor, and s is the standard deviation which depends on the packing particle size and the packed bed height.

According to this model, when the liquid flows onto a piece of packing element in the column, it will divide and displace in horizontal directions. The chance of it flowing in each horizontal direction, i.e. inward toward the center of the column or outward toward outside is the same. This model was confirmed experimentally by Tour and Lerman (1939). They showed that it could be used satisfactorily to predict the flow distribution when the feed stream was initially introduced to the unconfined column through a point source at the column axis or line source at low or moderate liquid flow rates. However, it could not be used to calculate the local flow rates in a packed column with other arbitrary forms of initial distribution of the feed stream, such as a uniform inlet, which is of commercial importance. It also could not be used to predict the flow behavior in the wall regions due to its equal chance assumption (Jameson, 1966). Hoftyzer (1964) argued that the results from the random walk model were of little practical importance due to the assumption of no wall influence.

14

2.2.2.2 Diffusion Model

Cihla and Schmidt (1957) introduced the radial diffusion model, Equation (2-2), to calculate the movement of the liquid flow in a packed column

$$\frac{\partial f}{\partial z} = D\left(\frac{\partial^2 f}{\partial r^2} + \frac{1}{r}\frac{\partial f}{\partial r} + \frac{1}{r^2}\frac{\partial^2 f}{\partial \theta^2} \right) \qquad (2\text{-}2)$$

Where f is the local liquid flow rate per unit area, that is, the local superficial liquid velocity as a function of the cylindrical coordinates r, z, and θ. D is the liquid spreading coefficient, which must be determined from liquid distribution experiments. It should be noted that, the liquid spreading coefficient D has units of m instead of the traditional units m^2/s. This is due to the replacement of the customary time variable, t (s) by the height, z (m) in the left hand side of Equation (2-2).

When the liquid is introduced into a column with radial symmetry, the above equation can be reduced to

$$\frac{\partial f}{\partial z} = D\left(\frac{\partial^2 f}{\partial r^2} + \frac{1}{r}\frac{\partial f}{\partial r} \right) \qquad (2\text{-}3)$$

Now the local liquid velocity is only a function of spatial position r and z. In order to solve Equation (2-3), three boundary conditions are required, that is, (1) at $z=0$ (at the top of the packed bed), the inlet profile of liquid, $f(r,0)$; (2) at $r=0$ (at the axis of the packed bed), $\frac{\partial f}{\partial r} = 0$. These two boundary conditions are easy to be established from the physical grounds, the third one, the wall boundary condition (at $r=R$), however, is very difficult to define. Different researchers have tried different ways to establish this wall boundary condition.

15

Cihla and Schmidt (1957) treated the column wall as a perfect liquid reflector, that is

$$\frac{\partial f}{\partial r} = 0 \quad \text{at } r=R \tag{2-4}$$

This boundary condition, coupled with the other two boundary conditions, allows the diffusion equation to be solved, but it is physically incorrect. Equation (2-4) simply means that any liquid which flows on to the column wall will be immediately returned to the nearby packings in the column, and thus there will be no liquid accumulated on the wall. However, as mentioned before, numerous experiments have demonstrated that the liquid does build up at the column wall.

Porter and Jones (1963) used the following wall boundary condition to take account of the liquid wall flow

$$f(R,z)=aw(z) \tag{2-5}$$

where $f(R,z)$ is the density of wetting immediately near the column wall at the axial position z. $w(z)$ is the total liquid flow rate on the wall at a axial position z, and a is an empirical constant. This wall boundary condition is more realistic than that of Cihla and Schmidt (Equation (2-4)) and allows a certain amount of liquid to build up on the wall. However, the wall flow predicted by this condition is usually much larger than the experimental data (Dutkai and Ruckenstein, 1968; Stanek, 1994). Templeman and Porter (1965,1968) pointed out that this boundary condition was an over simplification.

Dutkai and Ruckenstein (1968, 1970) considered that the penetration of liquid into the wall region followed the adsorption-desorption mechanism with the adsorption rate being proportional to $f(R,z)$ and desorption rate to $w(z)$

16

$$-2\pi RD\left(\frac{\partial f}{\partial r}\right)_{r=R} = kf(R,z) - k'w(z) = \frac{dw(z)}{dz}$$ (2-6)

where k and k' are the empirical constants.

Kolar and Stanek (1965) proposed a wall boundary condition very similar to Equation (2-6) based on the idea similar to the wall treatment in convective heat transfer. Onda et al. (1973) argued that the driving force for the liquid to accumulate on the wall should be the difference between the equilibrium wall flow rate $w^*(z)$ and the practical wall flow $w(z)$

$$-2\pi RD\left(\frac{\partial f}{\partial r}\right)_{r=R} = c[w^*(z) - w(z)] = \frac{dw(z)}{dz}$$ (2-7)

where c is an empirical constant. This boundary condition gives results very close to those obtained based on the boundary condition of Equations (2-5) or (2-6) (Onda et al., 1973; Stanek, 1994).

In reality the factors affecting the liquid wall flow are very complex. These include the type and size of packings, the ratio of column diameter to particle diameter (D_c/d_p), the packed bed height, the gas and liquid flow rate, and the physical properties of the system. All the above wall boundary conditions fail to take all the factors into account. The difficulties in the formulation of a proper wall boundary condition make the application of the diffusion model unreliable. Bemer and Zuiderweg (1978) showed that the experimental local flow rate deviated greatly from the flow rate predicted by the diffusion model.

With the advance of modern computers and computational fluid dynamics, it is now possible to use more rigorous models to capture the flow hydrodynamics in

17

randomly packed columns. We propose to use volume-averaged Navier-Stokes equations to model the flow behavior in randomly packed columns.

2.3 Effect of Liquid Maldistribution on Mass Transfer Efficiency

Mass transfer in packed columns has been studied extensively due to its importance in many industrial processes such as distillation, absorption, and stripping. The mass transfer coefficients (individual and overall) have been correlated in terms of the gas and liquid loadings, and physical properties of the system being separated. The effect of the packing itself on the mass transfer has been included in terms of its specific surface area and nominal diameter. However, these studies are usually based on the assumption that the flow distributions of both vapor and liquid phases are uniform along the column cross section.

Liquid maldistribution in a packed column tends to reduce the mass transfer efficiency. Manning and Cannon (1957) examined the effect of liquid maldistribution on the packing separation efficiency. For the calculation of the quantitative effect of a small amount of liquid channeling in the packed column, they assumed that a small portion of the liquid which may flow though the column without taking part in any mass transfer between the phases. They demonstrated that as little as 1% of liquid channeling may cause a 44% efficiency lose. They also pointed out that liquid maldistribution effect on separation efficiency depended on the number of theoretical plates and the relative volatility of the system being separated.

Mullin (1957) also found that the liquid maldistribution has a detrimental effect on the packed column separation efficiency. To investigate this, he modeled the packed

column as two parallel columns and set different liquid flow rates in each of the columns but keeping the gas flow rate the same. These two columns were conceptually divided by an imaginary impermeable membrane, so no exchange of mass occurred between the two columns. Through a McCabe-Thiele plot, he demonstrated that the slope of the operating line decreased due to the liquid maldistribution and therefore the operating line moved towards the equilibrium line. More stages were thus required for a given separation when compared to the uniform flow distribution case.

Huber and Hiltbrunner (1966) further developed the concepts of Manning and Cannon (1957) and Mullin (1957) by allowing cross mixing of liquid and vapor. The radial cross mixing is the result of the side-movement of liquid and vapor due to the deflection of packing elements. Liquid maldistribution in the packing will cause concentration gradients along the column cross section, and the cross mixing will cancel out the difference in concentrations. Based on their studies, they concluded that in columns with a ratio of D_c/d_p less than 10, the cross mixing is large enough to compensate for the maldistribution effect and only very serious liquid flow maldistribution would cause a significant separation efficiency loss. On the other hand, when this ratio is greater than 30, the lateral mixing may not be effective enough to offset the influence of the liquid maldistribution. Therefore in a large diameter packed column, the liquid maldistribution problem is more serious than that in a small diameter column.

More recently, Zuiderweg et al. (1993) proposed a Zone/stage model to calculate the effect of the maldistribution on the efficiency of a packed column. In this model, the packed column is divided radially into a number of concentric zones, with each zone being of the same width and height. The height of a zone is chosen to be equal to the

19

basic HETP, which is a function of the system properties and the packing and can be determined in a laboratory scale column. The width of each zone is arbitrarily set to be 2~3 times the packing diameter. The calculation is divided into two steps. The first step is to calculate the liquid flow distributions based on the diffusion model and a uniform flow pattern is assumed for the vapor phase. The second step is the mass transfer calculation based on the equilibrium stage concept. The mass transfer calculation is iterative with end conditions based on the overall material balance being satisfied. With this model, they studied the effect of different kinds of initial liquid distributions on the separation efficiency. The general conclusion derived from their work is that the overall efficiency is very sensitive to the initial liquid distribution, especially in large diameter packed columns.

Stichlmair and Stemmer (1987) took a different approach to model the mass transfer process in a packed column in the presence of liquid maldistribution. In their experiments, they used hot water and air as the working system. The temperature profiles of the water at different packed bed height were measured. The behavior of temperature profiles should be similar to that of the concentration profiles in a real mass transfer system based on the analogy between heat and mass transfer. The shape of the temperature profile indicates the degree of liquid maldistribution. For example, if the temperature profiles are horizontal lines, this implies that there is no maldistribution present in the liquid and gas phases. Based on the temperature profiles, they calculated the number of transfer units by considering the packed column as a large number of hypothetic parallel channels with different gas and liquid loads. In each channel, the plug flow patterns were assumed in both the liquid and gas phases. They concluded that liquid

20

maldistribution has a severe effect on separation efficiency. Up to 50% of the mass transfer efficiency may be lost due to liquid maldistribution even with good initial liquid distribution.

More thorough experimental studies on mass transfer in a randomly packed column in the presence of liquid maldistribution were carried out in the FRI (Silvey and Keller 1966; Kunesh, et al. 1987; Shariat and Kunesh, 1995). The test column was 1.22 m in diameter and 3.66 m in height. Four sizes of carbon steel Pall rings were employed: 15.9, 25.4, 50.8, and 88.9 mm. The test systems were cyclohexane/n-heptane (C_6/C_7) at 33.3 and 165.5 kPa and isobutane/n-butane at 1138 kPa. Two designs for liquid distributors were tested, a notched trough distributor which is a standard commercial distributor manufactured by US Stoneware and a tubed drip pan (TDP) fabricated by FRI with approximately 104 drip tubes per meter square. They found that the TDP distributor gave a much better separation efficiency than the notched trough distributor, indicating the strong influence of the liquid distributor design on the column performance. When installing the liquid distributor, one major concern is how much the effect will be if the liquid distributor is not level. FRI studies showed that small amounts of non-levelness of the TDP-type liquid distributor only had a minimal effect. There was no obvious decrease in column efficiency if a liquid distributor uniformly tilted such that the ratio of highest to lowest flow rate was 25%. Similar results were obtained for the case of a distributor sagging (center to wall or vice versa) under load. This means that a certain amount of uniform liquid maldistribution resulting from the distributor will not cause a serious problem. However, if a discontinuity occurs (such as non-irrigation in the near wall region or the obstruction of some drip points), the consequence could be severe. By

21

blanking a chordal segment of the liquid distributor containing 11% of the pour points, FRI found that the packing HETP increased at least 50%, or the separation efficiency reduced by about 33%.

The mass transfer process strongly depends on the liquid flow distribution in packed columns. The correct prediction of concentration profiles depends on a detailed knowledge of the liquid and vapor velocity profiles. Owing to the extremely complex nature of the two-phase flow in packed columns, a simple empirical equation cannot provide a reliable prediction. Kister (1992) wrote: "Adequate prediction of the effect of maldistribution on efficiency requires a procedure that knits a maldistribution model together with a stage calculation model. ..., For rigorous computations, a rigorous model for maldistribution must be interknitted with a rigorous stage model. A proper model would be extremely complex and appears to be many years down the road." It is one of the objectives of this study to find such rigorous models to predict mass transfer efficiencies involving liquid maldistribution.

2.4 Void Fraction Variation in Randomly Packed Columns

Void fraction ε_p is defined as the ratio of the void volume to the volume of the packed bed. In the literature, it is also referred to as voidage or sometimes porosity. The void fraction ε_p will show kind of distribution in the radial direction due to the effect of column wall. Void fraction variation is one of the most important characteristics of randomly packed columns, and many attempts have been made to measure and model the radial void fraction variations in packed beds. Most of these measurements are based on

22

one of the following techniques: (1) water replacement, (2) a method based on fixing the bed with wax or resin, and (3) photometric method.

Water replacement is probably the simplest way to measure the void fraction in packed beds. From the amount of water needed to fill the voids in the packed bed, the void fraction can be determined. This method has been used by Dixon et al. (1984), Dixon (1988), and Foumeny and Roshani (1991). The main difficulties associated with the water replacement method include the elimination of air pockets and the determination of the meniscus level. Failure in overcoming these problems will result in errors in the determination of void fraction.

The procedure to use a hot wax or resin to measure the void fraction is somewhat more involved. After the bed is filled with packing, the hot wax or resin is introduced into the bed from the bottom. The function of wax or resin is to keep the packing elements in position. The flow rate of wax or resin must be kept low enough so that it does not disturb the packing and trap any air within it as it fills the voids in the bed. After the wax or resin solidifies, the bed is cut into annular rings and the volume of each small ring is determined. The small rings are then heated and the wax is allowed to melt. After separating the packing from the wax, the void volume is determined from the weight of wax and its density. The average void fraction for that small ring can then be readily determined from the void volume and the total volume. Roblee et al. (1958) used this technique to measure the radial void fraction variation in a cardboard cylinder. The packings utilized were spheres, cylinders, Raschig rings, and Berl saddles. The same method was also used by Benenati and Brosilow (1962) to study the effect of D_c/d_p (bed

23

diameter to packing particle diameter) on the radial void fraction variation of lead shot in a cylindrical column.

The advantage of this method is that it allows an accurate determination of the radial void fraction profiles. However, the obvious shortcoming of this method is that the bed must be destroyed.

The photometric method is based on the different absorptivity of the packing material and the matrix material to X-rays or Gamma-rays. This method has been used by Thadani and Peebles (1966), Schneider and Rippin (1988), and Toye, et al. (1998). The advantage of this method is that it is nondestructive and permits measurement at various points of the bed cross section. It is also suitable for systems with complex geometry (such as beds with internal cooling tubes, Schneider and Rippin (1988)). Furthermore it can be used to measure the void fraction of commercially important packings such as metal Pall rings.

The typical void fraction profiles for a bed of uniform spheres from the above studies can be described as follows. The void fraction reaches its upper limiting value of 1.0 at the wall, falls to its minimum value at approximately 1 parking radius from the wall, and then continues cycling through several maxima and minima before settling out at a constant value in the bulk of the bed. The wall effect extends into the bed about 5 packing diameters for a bed of uniform spheres. For other types of packings, such as Raschig rings and Berl saddles, the wall effect becomes negligible after one packing diameter from the wall.

For spheres, many theoretical studies have been carried out to model the void fraction variation in the radial position (Beavers et al., 1973; Vortmeyer and Schuster,

24

1983; Govindaro and Froment, 1986; Dixon, 1988; Kufner and Hofmann, 1990; Foumeny and Roshani, 1991; Zou and Yu, 1996). Vortmeyer and Schuster (1983) used an exponentially decaying function to model the radial average void fraction variation

$$\varepsilon_p = \varepsilon_{p_b}\left[1 + K_1 \exp\left(1 - K_2 \frac{R-r}{d_p}\right)\right] \qquad (2\text{-}8)$$

where ε_{pb} is the void fraction in the bulk region of the bed. K_1 and K_2 are model constants. Normally K_2 has a value of 2. At the column wall, $r=R$, the void fraction must have the value of 1.0, so K_1 can be determined as

$$K_1 = \frac{1 - \varepsilon_{p_b}}{\varepsilon_{p_b} \exp(1.0)} \qquad (2\text{-}9)$$

For the commercially important packings, such as Pall rings and Mini rings, there is currently no correlation available in the literature.

2.5 Summary

The published studies on liquid maldistribution, mass transfer efficiency involving the effect of liquid maldistribution, and void fraction measurements and predictions were reviewed and discussed.

Liquid distribution was usually studied in small diameter columns packed with old packings such as Raschig rings and Berl saddles without gas flow. Liquid distribution was found to be non-uniform in randomly packed columns. The effect of gas flow and liquid physical properties on liquid distribution was less studied.

The effect of liquid maldistribution on mass transfer efficiency was found to be important. FRI found that the packing HETP increased at least 50% if a chordal segment of the liquid distributor containing 11% of the pour points was blanked.

The void fraction in a packed column was shown to be higher in the wall region that that in the bulk region. The models for predicting void fraction radial variation were developed for packed beds of spheres. For commercially important packings, such as Pall rings and Mini rings, there is currently no correlation available.

2.6 Nomenclature

a   Empirical Constant in Equation (2-5), m^{-2}

c   Empirical Constant in Equation (2-7), m^{-1}

D   Liquid Spreading Coefficient, m

D_c Packed Bed Diameter, m

d_p Size of Packing, m

f   Liquid Superficial Velocity, $m\ s^{-1}$

k   Empirical Constant in Equation (2-6), m

k' Empirical Constant in Equation (2-6), m^{-1}

K_1 Empirical Constant in Equations (2-8), (2-9)

K_2 Empirical Constant in Equation (2-8)

Q   Total Liquid Flow Rate of the Point Source, $m^3\ s^{-1}$

r Radial Coordinate, m

R   Radius of the Packed Bed, m

z   Axial Coordinate, m

w   Wall Flow Rate, $m^3\ s^{-1}$

w^* Equilibrium Wall Flow Rate, $m^3\ s^{-1}$

Greek Symbols

ε_p Void Fraction

θ Angular Coordinate

Subscript
b   Bulk Bed

27

2.7 References

Albright, M. A., (1984) Packed Tower Distributors Tested. *Hydrocarbon Processing* Sept., 173-177.

Baker, T., Chilton, T. H. and Vernon, H. C., (1935) The Course of Liquor Flow in Packed Towers. *Trans. AIChE.* **31**, 296-313.

Beavers, G. S., Sparrow, E. M. and Rodenz, D. E., (1973) Influence of Bed Size on the Flow Characteristics and Porosity of Randomly Packed Beds of Sphere. *Trans. ASME, J. App. Mech.* **40**, 655-660.

Bemer, G. G. and Zuiderweg, F. J., (1978) Radial Liquid Spread and Maldistribution in Packed Columns Under Different Wetting Conditions. *Chem. Eng. Sci.* **33**, 1637-1643.

Benenati, R. F. and Brosilow, C. B., (1962) Void Fraction Distribution in Beds of Spheres. *AICHE J.* **8**, 359-361.

Cihla, Z. and Schmidt, O., (1957) A Study of the Flow of Liquid When Freely Tricking over the Packing in a Cylindrical Tower. *Coll. Czech. Chem. Commun.* **22**, 896-907.

Dixon, A. G., DiCostanzo, M. A. and Soucy, B. A., (1984) Fluid-Phase Radial Transport in Packed Beds of Low Tube-to-Particle Diameter Ratio. Int. *J. Heat Mass Transfer.* **27**, 1701-1713.

Dixon, A. G., (1988) Correlations for Wall and Particle Shape Effects on Fixed Bed Bulk Voidage. *Can. J. Chem. Eng.* **66**, 705-708.

Dutkai, E. and Ruckenstein, E., (1968) Liquid Distribution in Packed Columns. *Chem. Eng. Sci.* **23**, 1365-1373.

Dutkai, E. and Ruckenstein, E., (1970) New Experiments Concerning the Distribution of a Liquid in a Packed Column. *Chem. Eng. Sci.* **25**, 483-488.

Foumeny, E. A. and Roshani, S., (1991) Mean Voidage of Packed Beds of Cylindrical Particles. *Chem. Eng. Sci.* **46**, 2363-2363.

Govindaro, V. M. H. and Froment, G. F., (1986) Voidage Profiles in Packed Bed of Sphere. *Chem. Eng. Sci.* **41**, 533-539.

Hoek, P. J., Wesselingh, J. A. and Zuiderweg, F. J., (1986) Small Scale and Large Scale Liquid Maldistribution in Packed Columns. *Chem. Eng. Res. Des.* **64**, 431-449.

Hoftyzer P. J., (1964) Liquid Distribution in a Column with Dumped Packing *Trans. IChemE.* **42**, T109-117.

Huber, M. and Hiltbrunner, R., (1966) Fullkorperrektifizierkolonnen mit Maldistribution. *Chem. Eng. Sci.* **21**, 819-832.

Jameson, G. J., (1966) A Model for Liquid Distribution in Packed Columns and Trickle-Bed Reactors. *Trans. Inst. Chem. Engrs.* **44**, 198-206.

Kister, H. Z., (1992) Distillation Design, McGraw-Hill, New York.

Kolar, V. and Stanek, V., (1965) Distribution of Liquid over Random Packing. *Coll. Czech. Commun.* 30, 1054-1059.

Kouri, R. J. and Sohlo, J., (1987) Liquid and Gas Flow Patterns in Random and Structured Packings. *I. Chem. E. Symp. Ser.* No. 104, B193-B211.

Kouri, R. J. and Sohlo, J., (1996) Liquid and Gas Flow Patterns in Random Packings. *Chem. Eng. J.* **61**, 95-105.

Kufner, K. and Hofmann, H., (1990) Implementation of Radial Porosity and Velocity Distribution in a Reactor Model for Heterogeneous Catalytic Gas Phase Reactions (TORUS-MODEL). *Chem. Eng. Sci.* **45**, 2141-2146.

Kunesh, J. G., Lahm, L. and Yanagi, T., (1987) Commercial Scale Experiments That Provide Insight on Packed Tower Distributors. *Ind. Eng. Chem. Res.* **26**, 1845-1850.

Manning, R. E. and Cannon, M. R., (1957) Distillation Improvement by Control of Phase Channeling in Packed Columns. *Ind. Eng. Chem.* **49**, 347-349.

Mullin, J. W., (1957) The Effect of Maldistribution on the Performance of Packed Columns. *Indust. Chem.* **33**, 408-417.

Olujic, Z. and de Granuw, J., (1989) Appearance of Maldistribution in Distillation Columns Equipped with High Performance Packings. *Chem. Biochem. Eng.* **4**, 181-196.

Onda, K., Takeuchi, H., Maeda, Y. and Takeuchi, N., (1973) Liquid Distribution in a Packed Column. *Chem. Eng. Sci.* **28**, 1677-1683.

Porter, K. E. and Jones, M. C., (1963) A Theoretical Prediction of Liquid Distribution in a Packed Column with Wall Effect. *Trans.Inst. Chem.Engrs.* **41**, 240-247.

Porter, K. E., Barnett, V. D. and Templeman, J. J., (1968) Liquid Flow in Packed Columns. Part II: The Spread of Liquid over Random Packings, *Trans. Inst. Chem. Engrs.* **46**, T74-T85.

Porter, K. E. and Templeman, J. J., (1968) Liquid Flow in Packed Columns. Part III: Wall Flow. *Trans. Inst. Chem. Engrs.* **46**, T86-T94.

Roblee, L. H. S., Baird, R. M. and Tierney, J. M., (1958) Radial Porosity Variations in Packed Beds. *AIChE J.* **4**, 460-464.

Schneider, F. A. and Rippin, D. W. T., (1988) Determination of the Local Voidage Distribution in Random Packed Beds of Complex Geometry. *Ind. Eng. Chem. Res.* **27**, 1936-1941.

Shariat, A. and Kunesh, J. G., (1995) Packing Efficiency Testing on a Commercial Scale with Good (and Not So Good) Reflux Distribution. *Ind. Eng. Chem. Res.*, **34**,1273-1279.

Silvey, F. C. and Keller, G. J., (1966) Testing on a Commercial Scale. *Chem. Eng. Prog.* **62**, 68-74.

Scott, A. H., (1935) Liquid Distribution in Packed Towers. *Trans. Inst. Chem. Engrs.* **13**, 211-217.

Stanek, V., (1994) Fixed Bed Operations: Flow Distribution and Efficiency. Ellis Horwood Ltd.

Stichlmair, J. and Stemmer, A., (1987) Influence of Maldistribution on Mass Transfer in Packed Columns. *I. Chem. E. Symp. Ser.* No. 104, B213-B224.

Templeman, J. J. and Porter, K. E., (1965) Experimental Determination of Wall Flow in Packed Columns *Chem. Eng. Sci.* **20**, 1139-1140.

Thadani, M. C. and Peebles, F. N., (1966) Variation of Local Void Fraction in Randomly Packed Bed of Equal Spheres. *I. E. C. Proc. Des. Dev.* **5**, 265-268.

Toye, D., Marchot, P., Crine, M., Pelsser, A. –M. and L'Homme, G., (1998) Local Measurement of Void Fraction and Liquid Holdup in Packed Columns Using X-ray Computed Tomography. *Chem. Eng. and Process.* **37**, 511-520.

Tour, R. S. and Lerman, F., (1939) Unconfined Distribution of Liquid in Tower Packing, *Trans. AICHE.* **35**, 709-718.

31

Vortmeyer, D. and Schuster, J., (1983) Evaluation of Steady Flow Profiles in Rectangular and Circular Packed Beds by a Variational Method. *Chem. Emg .Sci.* **38**, 1691-1699.

Wankat, P. C. (1988) Equilibrium Staged Separations. Prentice-Hall Inc., Englewood Cliffs, New Jersey.

Zou, R. P. and Yu, A. B., (1996) Wall Effect on the Packing of Cylindrical Particles. *Chem. Eng. Sci.* **51**, 1177-1180.

Zuiderweg, F. J., Kunesh, J. G. and King, D. W., (1993) A Model for the Calculation of the Effect of Maldistribution on the Efficiency of a Packed Column. *Trans. IchemE.* **71**, Part A, 38-44.

Chapter 3

LIQUID DISTRIBUTION MEASUREMENTS

3.1 Introduction

As discussed in Chapter 2, most of the previous studies on liquid distribution were carried out in small diameter columns packed with Raschig rings and Berl saddles without gas flow. There is a dearth of experimental data on liquid distribution in large scale columns filled with commercially important packings, such as Pall rings, Mini rings, etc., especially when the column operates with two-phase flow (both liquid and gas flow are present). Furthermore, more data is required that shows the effect of liquid physical properties on the liquid distribution.

This chapter describes the experimental set-up used in our laboratory to measure the liquid distribution with or without the presence of gas flow. The experimental results obtained will also be shown, discussed, and the important conclusions will be presented.

3.2 Experimental Set-Up

The experimental apparatus consisted of a cylindrical column, an air blower with variable speed DC motor, a liquid feed pump, a commercially designed liquid distributor, a specially designed liquid collector (also served as support plate and gas distributing device) and the necessary flow rate indicating and controlling meters. A schematic diagram of the experimental set-up is shown in Figure 3.1. Water was pumped to the

33

liquid distributor at the top of the column. It then flowed downward through the packing and exited at the bottom of the column through the liquid distribution measuring device. The liquid flow rate was measured and controlled by a calibrated rotameter. The gas (air) flow to the column was supplied by an air blower through the gas inlet pipe which was normal to the column axis. Air was distributed across the bottom of the packed column via a number of gas rising tubes (chimneys) fixed to the inside of the liquid collector. The down-flow liquid and up-flow gas resulted in the countercurrent operation of the column. Each gas rising tube had a small cap fixed on the top that prevented liquid from entering it. The flow rate of air was measured by a hot-wire anemometer which was located on the gas inlet pipe adjacent to the column.

The column itself consisted of a number of transparent Plexiglass™ cylindrical sections. Each Plexiglass™ section had a inside diameter of 0.6 m and a height of 1.5 m. The use of transparent Plexiglass™ sections allowed for visual observation of the flow behavior in the packed column. The base of the column was made of stainless steel. A small window (0.2 m in diameter) was cut in the wall of this stainless steel section to facilitate removal of the column packing.

The column was dry-packed by hand to a desired depth with the 25.4 mm stainless steel Pall rings. Prior to use the new Pall rings were repeatedly washed with a detergent solution until all traces of machine oil were removed. The packing was then thoroughly rinsed with water.

The liquid distributor was installed on the top of the packing and carefully leveled after installation.

34

The stainless steel Pall rings are the most common random packings in use, hence were chosen for use in this study. The Pall ring was first developed by BASF (Badische Anilin und Soda-Fabrik in Ludwigshafen-am-Rhein, Germany) (Eckert et al., 1958) by cutting windows in the wall of the Raschig ring and bending the small arms inward while maintaining the height and diameter of the rings equal. Unlike the Raschig rings, the openings in the wall of the Pall rings allow the gas phase to pass through, thus reducing the flow resistance (pressure drop) and increasing the operating capacity. Furthermore, the extra small arms or tongues within the rings can guide liquid to flow inside of the rings, thus enhancing liquid distribution (Kister, 1992). Pall rings also have higher efficiency than Raschig rings (Kister, 1992). The Pall rings used in this study were provided by Koch-Glitsch, Inc., USA, and its main characteristics are listed in Table 3.1. The corresponding characteristics of Raschig rings are also included for comparison purpose.

3.3 Design of the Liquid Collector

The liquid distribution was measured at the bottom of the column. As the liquid flowed out of the packing, it was separated into several radially defined regions by a specially designed liquid collector. This liquid collector served three purposes: to collect liquid, to support the packing, and to distribute the inlet gas flow. It consisted of a number of concentric cylinders as shown in Figures 3.2 and 3.3. The width of each collecting region (except the central, near wall and wall regions) was 50 mm, or about 2 diameters of the 25.4 mm Pall ring. The diameter of the central cylinder was 200 mm. In

35

this study, the whole column cross section was divided into six annular sampling regions, labeled as region I, II, III, IV, V, and Wall starting from the center region. The collecting area of each sampling region is shown in Table 3.2.

Table 3.2 shows that each collecting region represented a different column cross sectional area. The wall region, or the outmost annular ring, accounted for 3.12% of the total column cross sectional area. This means that the width of this region was only 4.7 mm. It is obvious that a different choice of wall region width will give a different amount of liquid wall flow. There are a number of ways for selecting the wall region width. For example, Baker et al. (1935) divided the bottom of their column into four equal area concentric rings, that is, the wall region accounted for 25% of the total column cross section. In Kouri and Sohlo 's experiments (1987, 1996), the wall region was designed to occupy 11.64% of the column cross section. In both of these two cases, the wall region collected not only the wall liquid but also some liquid away from the wall.

Porter and Templeman (1965, 1968) utilized a liquid collector in which the width of the wall region was only about 3 mm. This corresponded to about 4% of the column cross section for a 0.3 m diameter column. The same wall region width was also used by Dutkai and Ruckenstein (1970). With such a small width, the wall region received only a negligible amount of liquid from the bulk of the bed, thus giving a better representation of the liquid running down the column wall. There is yet another way to specify the width of the wall region, that is, the width of one packing particle diameter has been used to define the wall region by Jameson (1966) and Gunn (1978). It is possible that, for large packing particles, this width of wall region also collected a relatively large amount of liquid from

36

the bulk of the bed. To differentiate the wall liquid from the bulk liquid, a small wall region (4.7 mm in width) was used in this study.

The liquid flowing into the liquid collector was removed through liquid drain tubes. For the collecting regions I-V, the liquid drain tubes were placed immediately under the liquid collector. For the wall region, the liquid was removed through the column wall via two flexible rubber tubes. The diameter of each liquid drain tube and the number of liquid drain tubes in each collecting region are listed in Table 3.3.

The uniform initial gas distribution over the bottom column cross section was ensured by the appropriate arrangement of the gas rising tubes. For the ease of construction, each gas rising tube was designed with the same diameter (25.4 mm). Since the liquid collecting area was different from region to region, the number of gas rising tubes within each collecting region was adjusted to ensure a uniform gas distribution.

Assuming that the cross sectional area of the ith collecting region is A_i and the number of the gas rising tubes in this region is n_i, then from the simple mass balance, we can get

$$n_i q = A_i v \qquad (3-1)$$

where q is the gas flow rate passing through each of the gas rising tubes and v is the average gas velocity over the ith liquid collecting region.

To ensure the uniform gas distribution over the total column cross section, the above relationship should be satisfied for each region. It should be noted that area A_5 includes the area of the wall region since there is no gas rising tubes in this region due to its very small width. The number of the gas rising tubes can then be readily determined according to Equation (3-1). The results are given in Table 3.3.

3.4 Procedure and Range of Studies

Each experiment commenced with the packing being loaded into the dry column to a desired height. The liquid distributor was then installed on the top of the packing and carefully leveled. At the fixed packed bed height, water was first introduced into the column through the liquid distributor and its flow rate was set to a predetermined value. The air blower was then started to provide air to the column for the case of two-phase flow study. The air flow rate was adjusted to the desired value by adjusting the speed of the air blower. A check was regularly made on the gas and liquid flow rates to ensure that the conditions did not vary during the operation. About 20 minutes were needed for the liquid to reach a steady state in the column after flow rates were set. It was found that the liquid flow rate through each liquid drain tube was almost independent of time after 20 minutes.

To measure the flow distribution, the liquid flow rate through each of the liquid collecting regions was measured and recorded. This was done by weighting the amount of liquid collected within a certain period of time. After the liquid flow rate from each collecting region was measured, the radial liquid flow pattern (distribution) was constructed based on these measured local liquid flow rates.

The effects of liquid distributor design, operating condition, packed bed height, and liquid physical properties on the liquid distribution were determined.

Liquid distributor. Two different liquid distributors were used in this study. The first of these is a standard commercial ladder-type distributor. It had six branches and 31 drip points as shown in Figure 3.4 (a). The liquid distributor is usually quantified in terms of drip point density, defined as

38

$$Drip\ point\ density = \frac{Number\ of\ drip\ points}{Cross\ sectional\ area\ of\ column} \qquad (3\text{-}2)$$

Based on the above definition, this distributor had a drip point density of 110 points per square meter. A distributor with this high drip point density is considered to distribute liquid uniformly over the top of the packing (Olujic and de Graauw, 1989; Perry et al., 1990; Klemas and Bonilla, 1995). Therefore, in the following discussion, we will refer to this distributor as a uniform liquid distributor. The other liquid distributor was a modification of the first one. We plugged the most outside 15 holes and left the inside 16 holes open (see Figure 3.4 (b)). In this way, this distributor could only supply liquid to the central part of the column, which occupied about 43% of column cross sectional area. The drip point density of this modified distributor was 57 points per square meter. In the later discussion, this distributor will be referred to as a center inlet liquid distributor.

Operating conditions. Three liquid flow rates were used in this study, that is, 2.91, 4.78 and 6.66 $kg/m^2 s$. The gas flow rates were varied from 0 (single liquid phase flow) to 3.0 $kg/m^2 s$.

Packed bed height. The packed bed height was varied from 0.9 m to 3.5 m. In most of the test runs, three different packed bed heights were employed: 0.9 m, 1.8 m, and 3.0 m. The position of liquid distributor was adjusted accordingly with variation of the packed bed height.

Liquid physical properties. To study the effect of liquid physical properties such as surface tension and viscosity on liquid distribution, three different systems were used in this study: water/air, aqueous detergent solution/air, and Isopar/air. These three systems

39

were chosen because they had relatively large differences in liquid viscosity and surface tension. The relevant physical properties of the three liquids are listed in Table 3.4.

3.5 Results and Discussion

3.5.1 Reliability of the Experiments

The reliability of experimental data was confirmed as follows:

Performance of liquid distributor. A quality liquid distributor should distribute the liquid uniformly over the top of the packing. The quality of the uniform liquid distributor used in this study has been checked as follows:

(1) the number of drip (distribution) points. The drip point density of approximately 65 to 100 is required for a liquid distributor to perform satisfactorily in large diameter columns (Olujic and de Graauw, 1989).

(2) the difference between liquid flow rates from each drip point. Ideally, the flow rate from each of the drip points should be equal.

The uniform liquid distributor used in this study had 110 points/m^2. Thus it met the first criterion. To test the second criterion, the liquid flow rate from each drip point was individually measured at different total liquid flow rates. Figure 3.5 shows that this liquid distributor provided almost uniform drip flow rates. The average standard deviation is 1.576×10^{-3}.

Reproducibility. Reproducibility tests were carried out for the water/air system at a packed bed height of 0.9 m with both the uniform liquid distributor and center inlet liquid distributor. The liquid flow rate was selected to be 4.78 kg/m^{2}s. The gas flow rate was varied form 0 to 1.57 kg/m^{2}s. Typical results are shown in Figures 3.6 to 3.9 with

40

error bars (the method of calculating uncertainties is given in Appendix A). The data is plotted in terms of the liquid relative velocity against the radial position. The liquid relative velocity (u_{rel}) is defined as the ratio of the local liquid velocity (u_{loc}) to the average liquid velocity (u_{av}) over the empty column cross section, that is

$$u_{rel} = \frac{u_{loc}}{u_{av}}$$ (3-3)

From the measurement of the local liquid flow rate for each collecting region, the local liquid velocity can thus be calculated as

$$u_{loc} = \frac{f_{loc}}{\rho_L A_{region}}$$ (3-4)

where f_{loc} is the local liquid flow rate in kg/s and A_{region} is the cross sectional area of each collecting region.

Figures 3.6 to 3.9 present two runs that were conducted on different days. As can be seen, the liquid profiles of the two runs are very similar. The largest difference between the two runs is 10.6%. This difference, in our opinion, is within acceptable error limits for these large scale experiments.

Effect of redumping of the packing. It is of interest to see how the liquid flow distribution changes after the packing is redumped. To investigate this effect, the packing was redumped four times at a fixed packed bed of 0.9 m. The corresponding liquid flow distribution for each dumping was measured. Figure 3.10 shows the variation of the liquid velocity profile. These liquid velocity profiles show that the largest deviation of the liquid relative velocity from the average value is 10.3%.

41

From the above discussion, we can conclude that the experimental apparatus can be used reliably to measure the liquid distribution in a packed column.

3.5.2 Flooding Point and Loading Point

Flooding is the upper limit of the packed column operation. At the flooding point, the frothy liquid fills up the voids within the packing elements. The gas phase can only bubble up through the column, thus resulting a very high pressure drop.

There are several different indications that show flooding occurring in a packed column. The most obvious one of these is when the liquid can no longer drain freely through the column but is held back by the upward flow of gas. When flooding occurs, an appreciable amount of liquid droplet is entrained by the gas and sprayed violently back to the top of the column. When plotted on a log-log plot against the gas velocity at the fixed liquid flow rate, the pressure drop shows a very steep rise (almost vertically) with a slight increase in the gas velocity. It is obvious that at the flooding point, the column can no longer perform satisfactorily as a liquid and gas contacting device.

The loading point is defined as the gas flow rate at which the gas phase begins to interact with the liquid phase to generate a high pressure drop. The loading point is considered to occurs at about 70% of the flooding point (Kister, 1992; Billet, 1995).

To determine the flooding point and loading point for the experimental column, the pressure drops for both water/air and Isopar/air systems were measured. Figure 3.11 shows a plot of the pressure drop for the water/air and the Isopar/air systems. In the range of the liquid flow rates from 2.91 to 6.66 kg/m^2s, the flooding point for the water/air system occurs at $G=2.9\sim3.3$ kg/m^2s, and the loading point occurs at $G=2.0\sim2.3$ kg/m^2s.

42

For the Isopar/air system, the flooding point occurs at $G=2.2\sim2.5$ kg/m^{2}s, and the loading point occurs at $G=1.5\sim1.7$ kg/m^{2}s.

3.5.3 Effect of Liquid Distributor Design on Liquid Distribution

The liquid distribution was measured for the two liquid distributors: uniform liquid distributor and center inlet liquid distributor. Figures 3.12 and 3.13 present the typical effect of liquid distributor design on liquid distribution. Figure 3.12 shows a comparison of the liquid velocity profiles obtained with these two liquid distributors at different packed bed height in the absence of gas flow. The working fluid was water, and its flow rate was kept constant at 4.78 kg/m^{2}s. As can be seen from Figure 3.12, the resultant liquid velocity profiles are quite different. For the uniform liquid distributor, the liquid velocity profile is nearly flat in the bulk region of the packed bed throughout the whole bed height. At the bed height of 0.9 m, some liquid can be seen to build up on the column wall, which will be referred to as "liquid wall flow" in the later discussion. As the liquid flows down, more liquid moves towards the column wall, as can be see from the increase of liquid velocity in the wall region. As shown in Figure 3.12 near the top part of the column, the build up of liquid wall flow is relatively fast, however, after a bed height of 1.8 m from the top of the packing, the build up speed is significantly reduced. Comparing the liquid velocity profiles at the bed height of 1.8 m and 3.0 m for the case of the uniform liquid distributor, the average difference between these two profiles is less than 10% for all the corresponding points. This means that at the bed height of 1.8 m, the liquid flow distribution is fully developed. This stable liquid flow pattern, which is an inherent characteristic of the packing, is also referred to as the liquid natural flow

43

(Albright, 1984; Hoek et al., 1986). The formation of the liquid wall flow is one of the most important characteristics associated with all of randomly packed columns. In the wall region, the void fraction is higher than that in the bulk region. As a result, the flow resistance is lower in the wall region, thus causing more liquid to flow along the wall region.

For the case of center inlet liquid distributor, the liquid can only be introduced into the column through the central region, which is corresponding to the 43% of the total column cross sectional area. As can be seen from Figure 3.12, the liquid relative velocity in the central region is much greater than the mean value based on the column cross section. At the bed height of 0.9 m, the relative liquid wall flow is still less than the mean value. At the packed height of 1.8 m, the liquid flow distribution is still very different from that resulting from the uniform liquid distributor. In the center region, the liquid velocity with the center inlet liquid distributor is about 70% higher than that with the uniform liquid distributor, and the corresponding liquid wall flow is about 50% lower. At the packed height of 3.0 m, the difference still exists but is smaller. For this case, the liquid distribution is still far from a fully developed flow pattern even at a bed height of 3.0 m.

As illustrated in Figure 3.12, the difference between the two liquid velocity profiles obtained with the two different liquid distributors becomes smaller as the liquid flows downwards. In other words, the non-uniform liquid distribution over the top layer of the packing generated by the center inlet liquid distributor is smoothed out gradually as the bed height is increased. This indicates that the packing has the ability to spread the

vertical liquid flow radially. The liquid tends to move from the high flow rate region to the low flow rate region due to the liquid radial spreading.

Figure 3.13 illustrates the effect of liquid distributor design on the liquid wall flow development along the packed bed height at different gas and liquid flow rates. It can be seen that the liquid wall flow tends to increase with the bed height for both liquid distributors. However, for the uniform liquid distributor, the liquid wall flow approaches its fully developed value after the bed height of 1.8 m for the case of two-phase flow. For the center inlet liquid distributor, the liquid wall flow continues to increase even at the bed height of 3.5 m, indicating that fully developed wall flow has not been reached. The effect of gas and liquid flow rates on the liquid flow distribution will be discussed in the following sections.

The above experimental results would indicate that the design of the liquid distributor is crucial for the liquid distribution and proper operation of randomly packed columns (Perry, et al., 1990). Poor inlet liquid distribution, resulting from a poor liquid distributor design, will require additional bed height to reach a natural flow pattern. From visual observations of the experimental phenomena during the test runs, the liquid did not reach the column wall until 0.5~0.6 m from the top of the packing when the liquid was introduced in the central 43% of the column cross section. This simply means that part of the packing is only partially used when such a non-uniform initial liquid distribution occurs in a packed distillation column, because the dry packing cannot take part in the mass transfer process. Baker et al. (1935) also found that in a 0.3 m diameter column packed with spheres and saddles, at least 3.0 m of the bed height was needed for the

45

liquid to reach its fully developed state when the liquid was introduced at the center of the column as a point source.

3.5.4 Effect of Gas Flow Rate on Liquid Distribution

The effect of gas flow rate on liquid distribution is shown in Figures 3.14 and 3.15. These figures present data for the uniform liquid distributor at different bed heights and liquid flow rates for the system water/air. The data emphasis the interaction between the gas and liquid phases and the effect of gas flow rate on the liquid wall flow.

Figure 3.14 shows a comparison of liquid velocity profiles measured at different gas flow rates at the bed height of 0.9 m. The liquid flow rate was kept constant at 2.91 kg/m^2s. It can be seen that in the bulk region of the packed bed the liquid velocity profile becomes flatter with the increase of gas flow rate. The net result is that increased gas flow enhances the liquid radial spreading and reduces the liquid maldistribution in the bulk region of the packed bed. This effect of gas flow on the liquid distribution over the bulk bed has also been observed by Dutkai and Ruckenstein (1970), and Kouri and Soulo (1987, 1996).

The effect of gas flow rate on the liquid wall flow is shown in Figure 3.15. In this figure, the liquid relative wall flow is plotted against gas flow rate at different bed heights of 0.9 m, 1.8 m and 3.0 m. As can be seen, the effect of gas flow rate on the liquid wall flow is insignificant at the low gas loadings (gas flow rate less than about 2.1 kg/m^2s). This is due to the fact that the interaction between the gas phase and liquid phase is very small under these conditions. However, at the higher gas loadings (especially above the loading point), the liquid wall flow increases significantly with the gas flow rate. Above

46

the loading point, the interaction between the gas phase and liquid phase is significant (caused by the increase of the interface drag force between the gas phase and liquid phase). Due to the more significant increase of the liquid flow resistance in the packing than in the wall region, where the void fraction is relatively higher and the flow resistance is relatively lower, more liquid is forced to the wall region.

Based on the experimental results, one can conclude that the effect of gas flow rate on liquid distribution is insignificant below the loading point. Above the loading point, the effect is significant, especially for the liquid wall flow. The general trend is that the liquid distribution in the bulk region becomes flatter, and the liquid wall flow increases significantly with an increase in the gas flow rate.

3.5.5 Effect of Liquid Flow Rate on Liquid Distribution

The effect of liquid flow rate on the liquid distribution is illustrated in Figures 3.16 and 3.17 for the bed height of 3.0 m and 0.9 m, respectively. The results shown in these figures were obtained using the uniform liquid distributor. It was found that the effect of liquid flow rate on liquid distribution in the bulk region is insignificant when the liquid flow rate was varied from 2.91 to 6.66 kg/m^{2}s. The liquid relative wall flow reduced somewhat with the increase of liquid flow rate at low gas loadings. This observation is in agreement with the findings reported by Porter and Templeman (1968) and Kouri and Sohlo (1987, 1996). When the packing in the column is well wetted, an increase in liquid flow rate will increase the thickness of liquid film on the packing surface, and the liquid holdup will increase accordingly (Kister, 1992). It is believed that this increase in the liquid film thickness with the increase of liquid flow rate will occur

47

uniformly within the packing, thus the liquid distribution will not be affected too much in the bulk region. The increase of liquid holdup with the liquid flow rate can be clearly seen from the following empirical correlation (Kister, 1992)

$$h_L = \frac{0.4184}{\varepsilon_p}\left(\frac{\mu_L}{\rho_L}\right)^{\frac{1}{6}}\left(u_L a_p\right)^{0.5} \tag{3-5}$$

where the liquid holdup is proportional to the square root of the liquid superficial velocity.

As for the liquid wall flow, because the thickness of the liquid film increases with the increase of the liquid loading, more liquid is held within the packings. Thus, the relative liquid wall flow is reduced accordingly.

The effect of liquid flow rate on the liquid wall flow development can be seen in Figure 3.13. This figure shows a comparison of liquid relative wall flows for two different liquid flow rates of 2.91 and 6.66 kg/m^{2}s, respectively. It can be seen that the liquid wall flow reaches its fully developed state sooner at the higher liquid flow rates than at the lower liquid flow rates for the uniform liquid distributor.

3.5.6 Effect of Liquid Surface Tension on Liquid Distribution

To investigate the effect of liquid surface tension on liquid distribution, a low foaming detergent (dishwasher detergent, Electra sol^{TM}) was selected and added to the water to form a low surface tension solution. This solution had the same density and viscosity as water, but its surface tension was half that of pure water. Its physical properties are given in Table 3.4.

48

Figures 3.18 to 3.20 show a comparison of the results obtained with these two systems: water/air and detergent solution/air. Figure 3.18 presents the data for the single liquid phase flow at a bed height of 0.9 m. Figure 3.19 shows the data for the two-phase flow with a gas loading of 1.57 kg/m²s at a bed height of 1.8 m. Figure 3.20 presents the data for the two-phase flow with a higher gas loading (3.0 kg/m²s) at a bed height of 3.0 m. All the results shown in Figures 3.18, 3.19 and 3.20 were taken at a liquid flow rate of 6.66 kg/m²s. The experimental data show that the two velocity profiles are very close for all the cases presented here. The effect of liquid surface tension on liquid distribution is further demonstrated in Figure 3.21 plotted in terms of the liquid relative wall flow against the gas flow rate. For all the gas flow rates studied, the difference between the wall flows obtained for these two different systems is less than 6%. Based on these studies, it can be concluded that there is little or no effect of liquid surface tension on liquid distribution in the large scale packed columns. The same conclusion was reached by Bemer and Zuiderweg (1978) based on their measurements for a 0.2 m diameter column filled with glass Raschig rings (10 mm diameter and larger) in the absence of gas flow. However, Onda et al. (1973) found that the liquid spreading increases with the increase of liquid surface tension. It should be pointed out that their results were obtained in a 0.15 m diameter column packed with 4 mm ceramic Raschig rings.

To investigate the reasons why the liquid surface tension shows different effects on the liquid distribution in the small size packings and large size packings, a number of small scale experiments were carried out with a 0.1 m diameter glass column packed with 8 mm ceramic Raschig rings. The systems examined were: water, detergent solution and methanol/isopropanol mixture. It was found that liquid tended to foam easily in the small

49

size packings. The amount of gas bubbles formed inside the rings and within the interstices between the rings depended on the liquid surface tension, the lower the liquid surface tension, the greater the number of gas bubbles that were formed. The entrapment of gas bubbles within the liquid would certainly affect the liquid distribution. On the other hand, in the large diameter column packed with large size flow-through packings, the void fraction is much higher. This physical situation reduces the tendency for liquid foaming, as was confirmed during the test runs with the 0.6 m diameter column packed with 25.4 mm Pall rings. Thus the effect of liquid surface tension is insignificant in the large size packing.

Hence it can be concluded that liquid surface tension is a physical property that does not significantly affect the liquid distribution in the large diameter columns packed with large size packings.

3.5.7 Effect of Liquid Viscosity on Liquid Distribution

The effect of liquid viscosity on liquid distribution was studied with the Isopar/air system. The viscosity of Isopar is about two times greater than that of water. Its relevant physical properties are listed in Table 3.4.

The measurements of liquid flow distribution with this system were made at different bed heights, gas and liquid flow rates using the uniform liquid distributor. The results are presented in Figures 3.22 to 3.26. Figures 3.22 and 3.23 illustrate the comparison of the liquid flow distributions for water and Isopar without gas flow at the bed heights of 0.9 m and 3.0 m, respectively. Figures 3.24 to 3.26 show the comparison of the liquid flow distribution and relative wall flow for the water/air system and

50

Isopar/air system at varying gas and liquid flow rates. It can be seen from Figures 3.22 to 3.25 that the relative velocity of Isopar is higher than that of water in the central region of the bed. However, the liquid wall flow with Isopar is lower than that with water at all bed heights. The data would suggest that the higher liquid viscosity tends to retard the liquid radial spreading at low gas flow rates. This can be explained as follows. The higher liquid viscosity means a thicker liquid film on the packing surface, thus more liquid is held within the packing (Strigle, 1987), thereby reducing the liquid wall flow. This effect of liquid viscosity on liquid holdup can also be seen from Equation (3-5). Second, the liquid radial spreading is due in part to the unstable turbulent flow within the packing. Evidently, the turbulent motion of liquid will enhance the liquid spreading. With the increase of the liquid viscosity, the turbulence intensity is reduced compared with that of liquid with lower viscosity at the same flow rate. Subsequently, the liquid radial spreading is reduced. At higher gas flow rates, however, as shown in Figure 3.26, the liquid wall flow with the Isopar/air system is higher than that with the water/air system, because the Isopar/air system has a lower column loading point due to the high viscosity of Isopar (see Section 3.5.2). At the same gas flow rate, the Isopar/air system is closer to the loading point than the water/air system. In the loading region, as demonstrated in Section 3.5.4, the liquid wall flow shows a significant increase with the increase of the gas flow rate.

It should be noted that the surface tension and density of Isopar were also different from that of water. However, it has been shown in Section 3.5.6 that surface tension does not affect the liquid distribution. At the present time, it is not clear what the effect of

51

liquid density on liquid distribution for the Pall rings would be, as there are no published studies available in literature.

3.6 Conclusions

Liquid flow distribution in a 0.6 m diameter column randomly packed with 25.4 mm stainless steel Pall rings has been measured under various conditions. The important factors affecting the liquid distribution have been determined. These factors include the liquid distributor design, the packed bed height, the gas and liquid flow rate, and liquid physical properties (surface tension and viscosity). The most significant conclusions are summarized as follows.

1. The liquid distribution in a randomly packed column is always far from uniform. Even if the liquid is uniformly introduced into the column, the liquid will tend to move towards the column wall, and forms a higher wall flow.

2. Distributor design is crucial for the liquid distribution in randomly packed columns. More bed height is required for the liquid distribution to reach its natural flow pattern if the liquid is non-uniformly introduced into the column.

3. With the increase of liquid flow rate, the liquid relative wall flow is reduced somewhat at low gas loadings. The bed height required for the liquid to reach its fully developed state is also reduced.

4. In the preloading region, the effect of gas flow rate on liquid distribution is insignificant. Above the loading point, however, the liquid wall flow increases rapidly with increasing gas flow rate.

52

5. The liquid surface tension has little or no effect on liquid distribution in the large scale packed columns.

6. Liquid viscosity tends to reduce the liquid radial spreading. The higher the liquid viscosity, the lower the liquid wall flow.

The experimental measurements not only offer a deeper understanding of the liquid flow distribution phenomena encountered in randomly packed columns, but also provide necessary data for evaluating models that can be used to simulate the liquid flow distribution in randomly packed columns.

53

3.7 Nomenclature

A   Cross Sectional Area of Liquid Collecting Region, m^2

a_p Total Surface Area of Packings Per Unit Volume, m^{-1}

F_{pd} Packing factor, m^{-1}

f   Local Liquid Flow Rate, $kg\ s^{-1}$

G   Gas Flow Rate, $kg\ m^{-2}\ s^{-1}$

H   Packed Bed Height, m

h   Liquid Holdup

L   Liquid Flow Rate, $kg\ m^{-2}\ s^{-1}$

N_p Number of Packing particles per Unit Volume, m^{-3}

n   Number of Gas Rising Tubes in Each of Liquid Collecting Regions

q   Gas Flow Rate Passing through Each of the Gas Rising Tubes, $m^3\ s^{-1}$

u   Liquid Superficial Velocity, $m\ s^{-1}$

v   Average Gas Velocity over Each of the Liquid Collecting Region, $m\ s^{-1}$

Greek Symbol

ε_p Void Fraction

μ Viscosity, $kg\ m^{-1}\ s^{-1}$

ρ Liquid Density, $kg\ m^{-3}$

Subscripts

av   Average

i   Index of Liquid Collecting Region

L   Liquid Phase

loc   Local

rel   Relative

3.8 References

Albright, M. A., (1984) Packed Tower Distributors Tested. *Hydrocarbon Processing* Sept., 173-177.

Baker, T., Chilton, T. H. and Vernon, H. C., (1935) The Course of Liquor Flow in Packed Towers. *Trans. AIChE.* **31**, 296-313.

Bemer, G. G. and Zuiderweg, F. J., (1978) Radial Liquid Spread and Maldistribution in Packed Columns under Different Wetting Conditions. *Chem. Eng. Sci.* **33**, 1637-1643.

Billet, R., (1995) Packed Towers in Processing and Environmental Technology, VCH Publishers, Weinheim, Germany.

Dutkai, E. and Ruckenstein, E., (1970) New Experiments Concerning the Distribution of a Liquid in a Packed Column. *Chem. Eng. Sci.* **25**, 483-488.

Eckert, J. S., Foote, E. H. and Huntington, R. L., (1958) Pall Rings — New Type of Tower Packing. *Chem. Eng. Prog.* **54**, 70-75.

Hoek, P. J., Wesselingh, J. A. and Zuiderweg, F. J., (1986) Small Scale and Large Scale Liquid Maldistribution in Packed Columns. *Chem. Eng. Res. Des.* **64**, 431-449.

Gunn D. J., (1978) Liquid Distribution and Redistribution in Packed Columns-I: Theoretical. *Chem.Eng.Sci.* **33**, 1211-1219.

Jameson, G. J., (1966) A Model for Liquid Distribution in Packed Columns and Trickle-Bed Reactors. *Trans. Inst. Chem. Engrs.* **44**, 198-206.

Kister, H. Z., (1992) *Distillation Design*, McGraw-Hill, New York.

Klemas, L. and Bonilla, J. A., (1995) Accurately Assess Packed-Column Efficiency. *Chem. Eng. Prog.* **July**, 27-44.

Kouri, R. J. and Sohlo, J., (1987) Liquid and Gas Flow Patterns in Random and Structured Packings. *I. Chem. E. Symp. Ser.* No. 104, B193-B211.

Kouri, R. J. and Sohlo, J., (1996) Liquid and Gas Flow Patterns in Random Packings. *Chem. Eng. J.* **61**, 95-105.

Olujic, Z. and de Graauw, J., (1989) Appearance of Maldistribution in Distillation Columns Equipped with High Performance Packings. *Chem. Biochem. Eng.* **Q3 (4)**, 181-196.

Onda, K., Takeuchi, H., Maeda, Y. and Takeuchi, N., (1973) Liquid Distribution in a Packed Column. *Chem. Eng. Sci.* **28**, 1677-1683.

Perry, D., Nutter, D. E. and Hale, A., (1990) Liquid Distribution for a Optimum Packing Performance. *Chem. Eng. prog.* **January**, 30-35.

Porter, K. E. and Templeman, J. J., (1968) Liquid Flow in Packed Columns. Part III: Wall Flow. *Trans. Inst. Chem. Engrs.* **46**, T86-T94.

Strigle, R. F., Jr., (1987) Random Packings and Packed Towers: Design and Applications. Gulf Publishing Company, Houston.

Templeman, J. J. and Porter, K. E., (1965) Experimental Determination of Wall Flow in Packed Columns. *Chem. Eng. Sci.* **20**, 1139-1140.

Table3.1 The Characteristics of Raschig Rings and Pall Rings

Packing type	Material	Nominal size mm	N_p $1/m^3$	a_p m^2/m^3	ε_P	F_{pd} $1/m$
Pall ring	Stainless steel	25.4	49,441	207	0.94	174
Raschig ring	Metal	25.4	49,794	203	0.92	492

57

Table 3.2 Areas of Liquid Collecting Regions

Collecting region	Outside radius, mm	Area m^2	Relative area %	Cumulative area, %
I	100.0	0.0314	11.22	11.22
II	150.0	0.0393	14.04	25.26
III	200.0	0.0550	19.64	44.90
IV	250.0	0.0707	25.25	70.15
V	293.8	0.0748	26.71	96.86
Wall	298.5	0.00875	3.12	100.00

Table 3.3 Arrangement of Gas Rising Tubes and Liquid Drain Tubes

Region number	I	II	III	IV	V	Wall
Numbers of gas rising tubes	8	10	14	18	22	0
Numbers of liquid drain tubes	1	2	2	2	2	2
Diameter of liquid drain tube (mm)	32.0	25.9	25.9	25.9	25.9	15.2

59

Table 3.4 System Physical Properties

System	Density kg/m^3	Viscosity Pas	Surface tension N/m
Water	1000	0.001	0.072
Detergent solution	1000	0.001	0.033
Isopar	788	0.00246	0.028
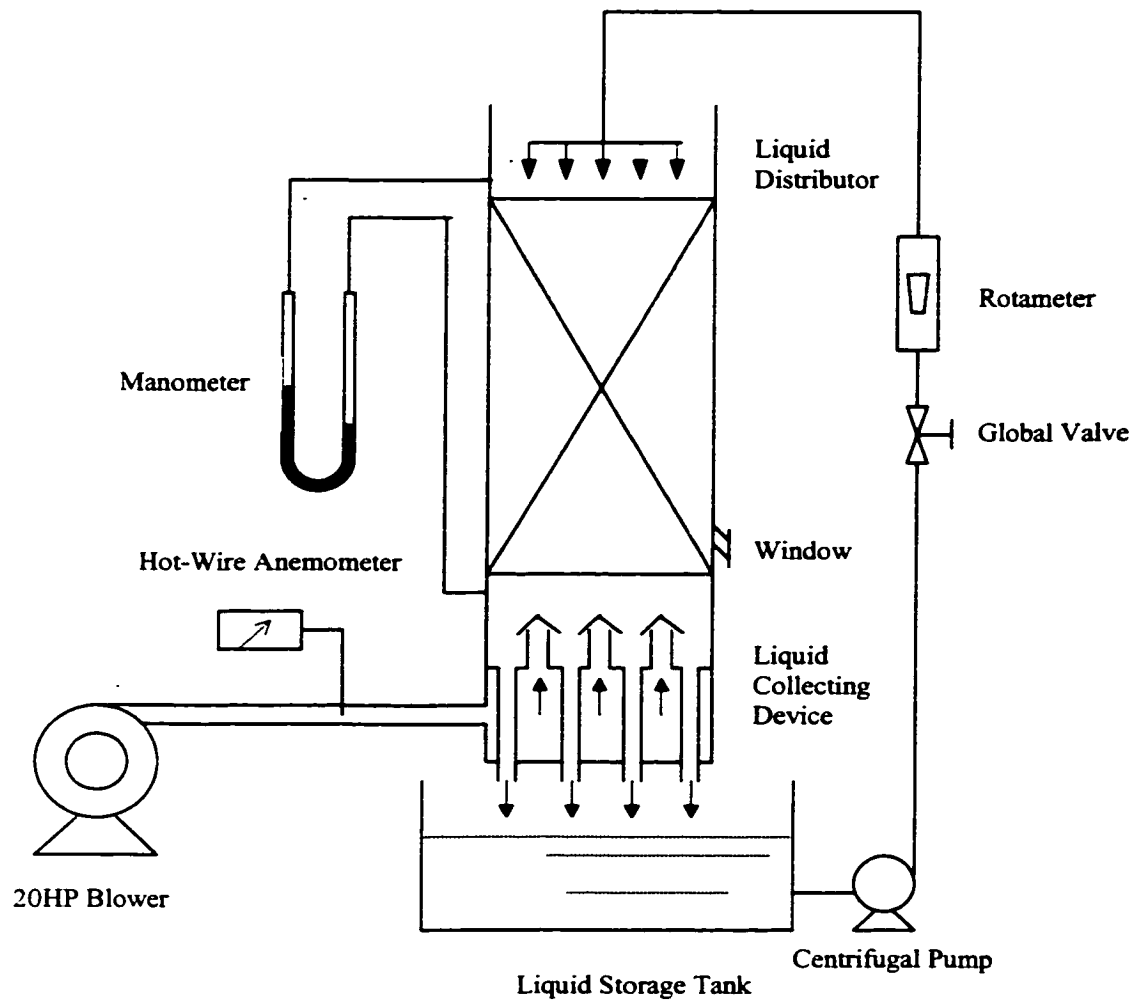
Figure 3.1. Experimental set-up for measuring liquid distribution
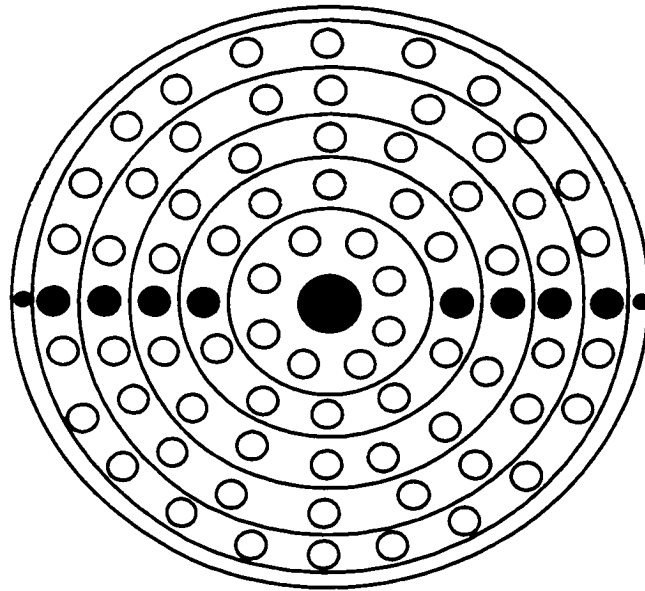
● Liquid Drain Tube

○ Gas Rising Tube

Figure 3.2. Design of liquid collector (top view)

Column Center   Column Wall
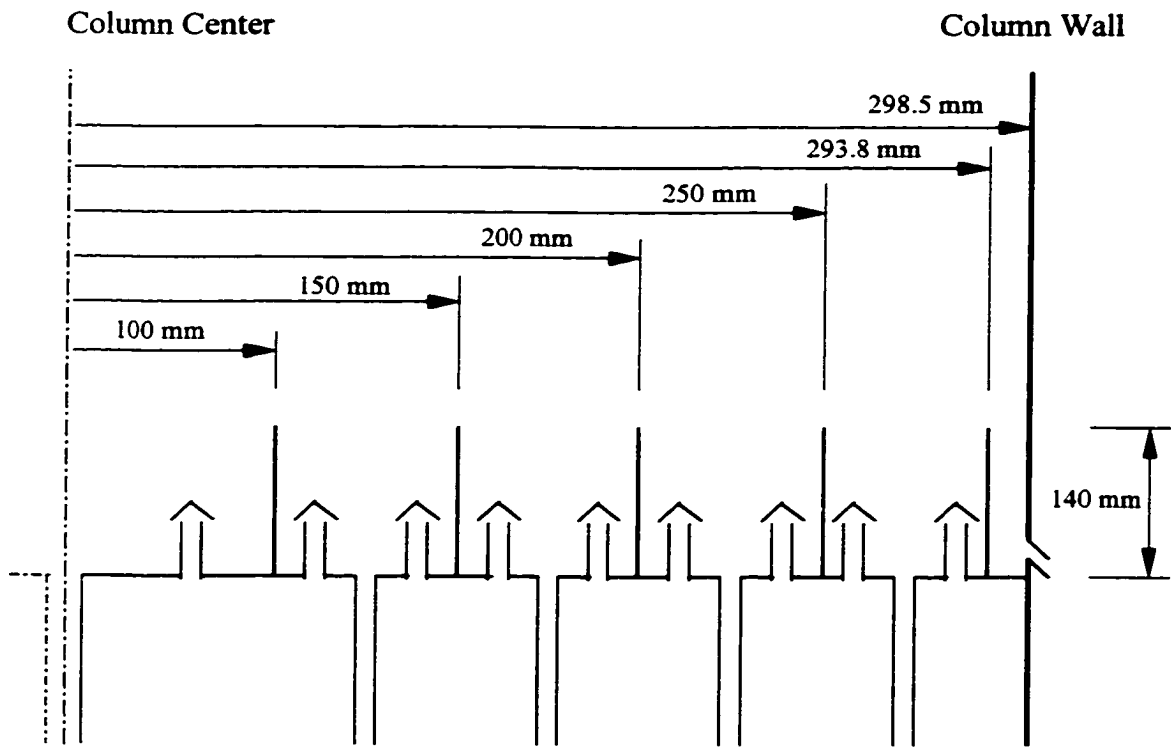
Figure 3.3. Design of liquid collector (side view)
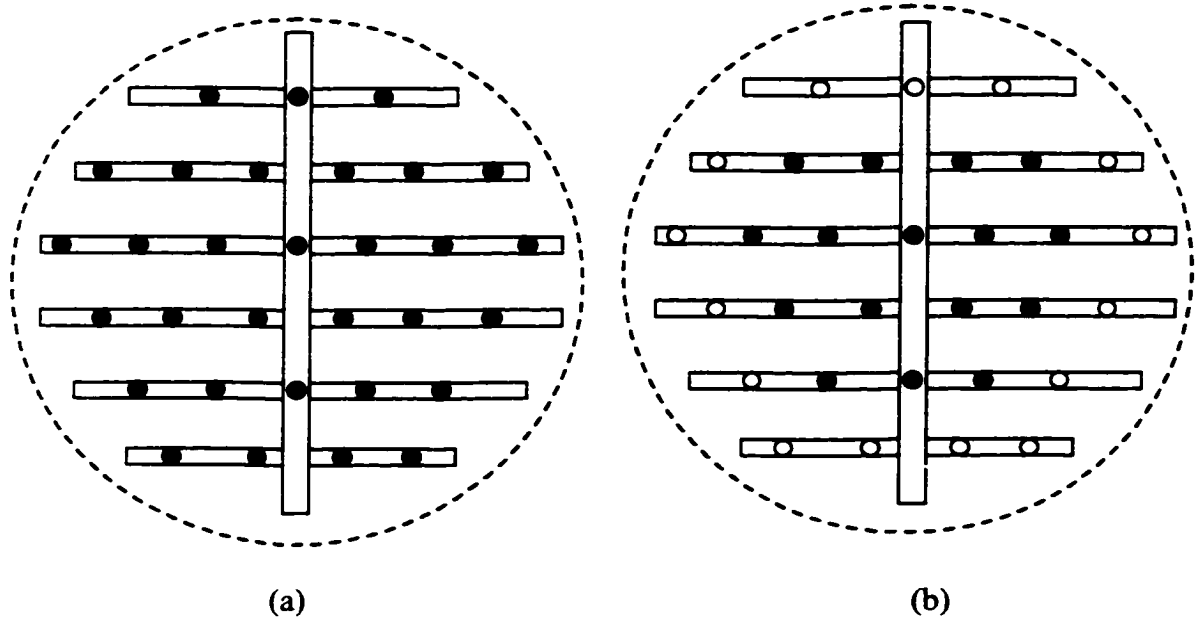
Figure 3.4. (a) Uniform liquid distributor; (b) Center inlet liquid distributor
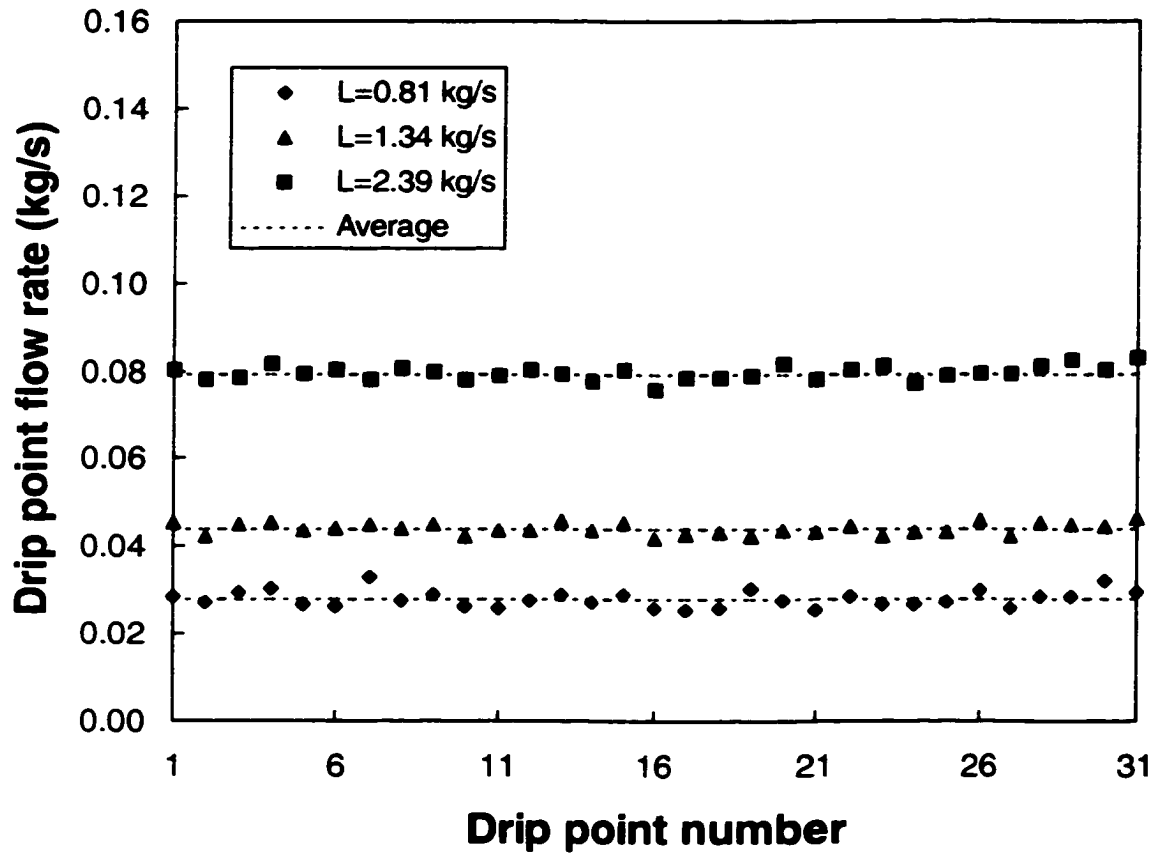
Figure 3.5. Distributor test with uniform liquid distributor.

65
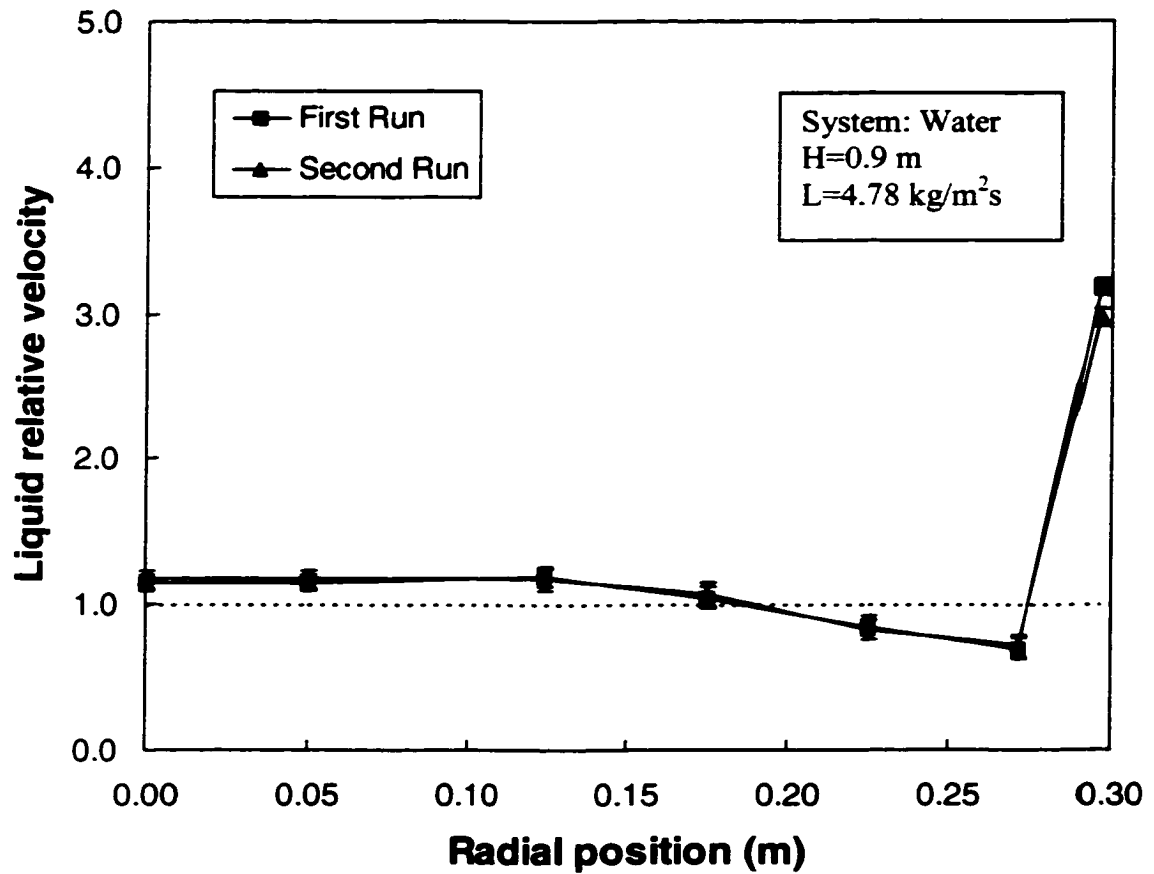
Figure 3.6. Reproducibility test for the uniform liquid distributor.
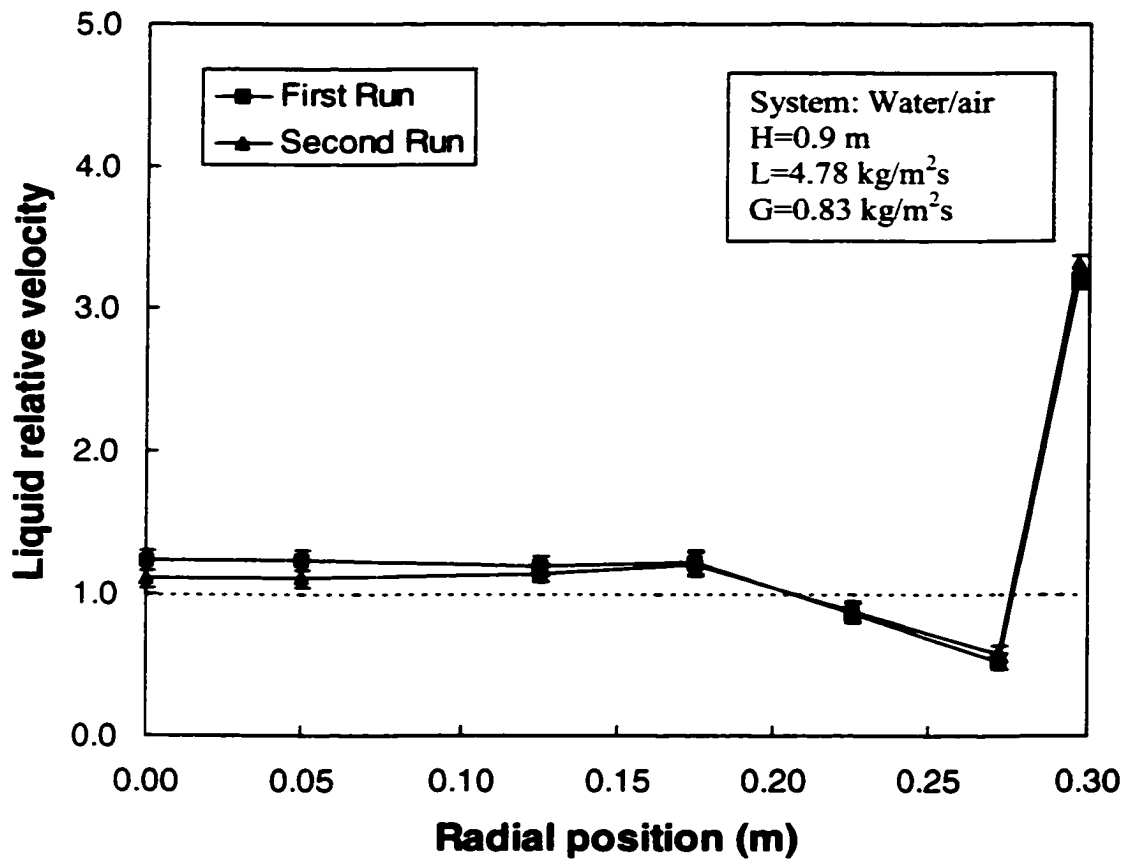
Figure 3.7. Reproducibility test for the uniform liquid distributor.
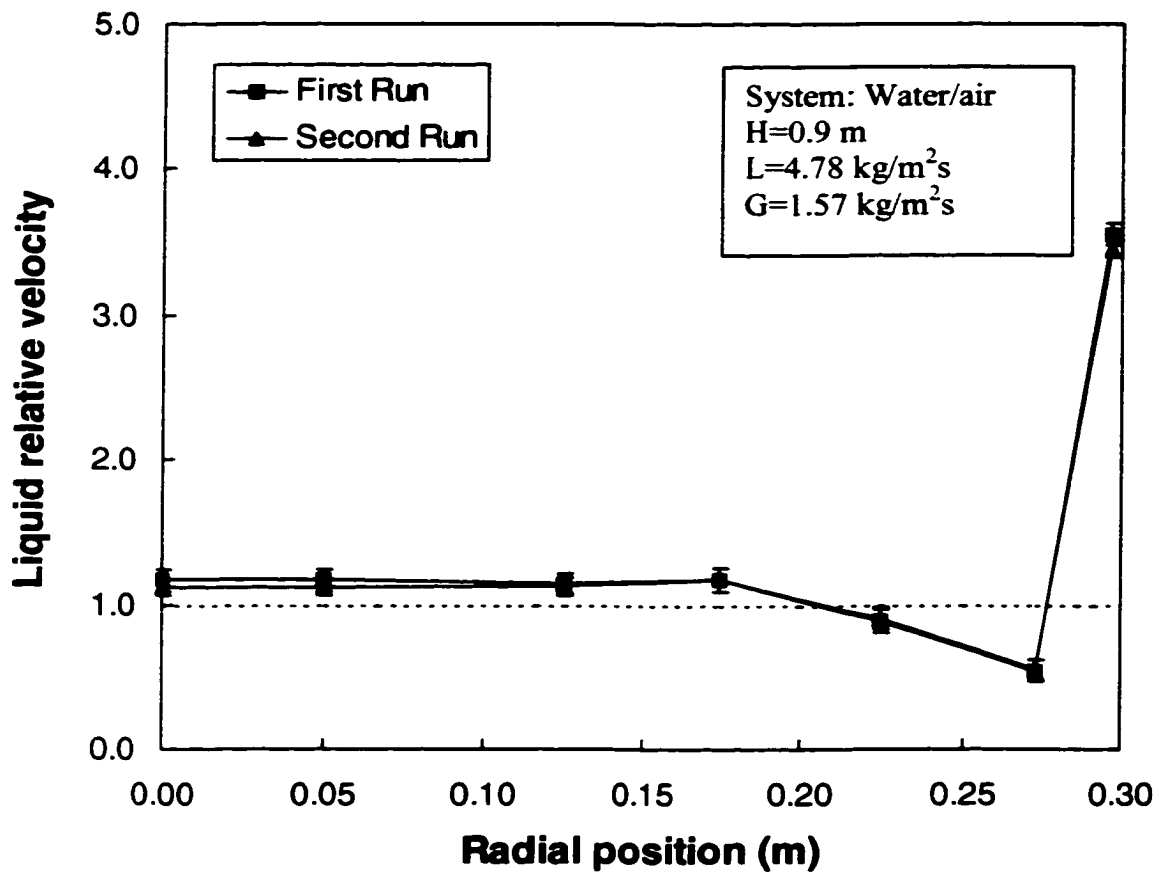
Figure 3.8. Reproducibility test for the uniform liquid distributor.
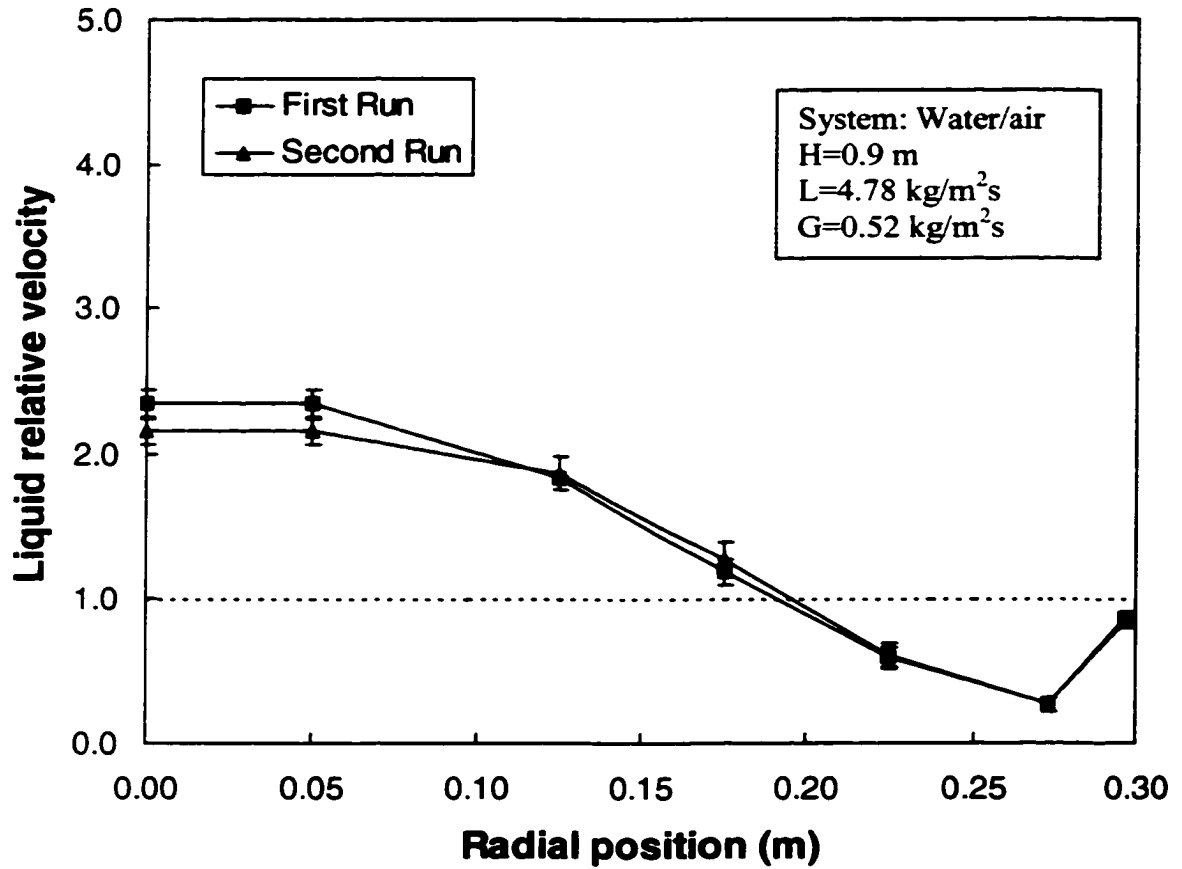
Figure 3.9. Reproducibility test for the center inlet distributor.
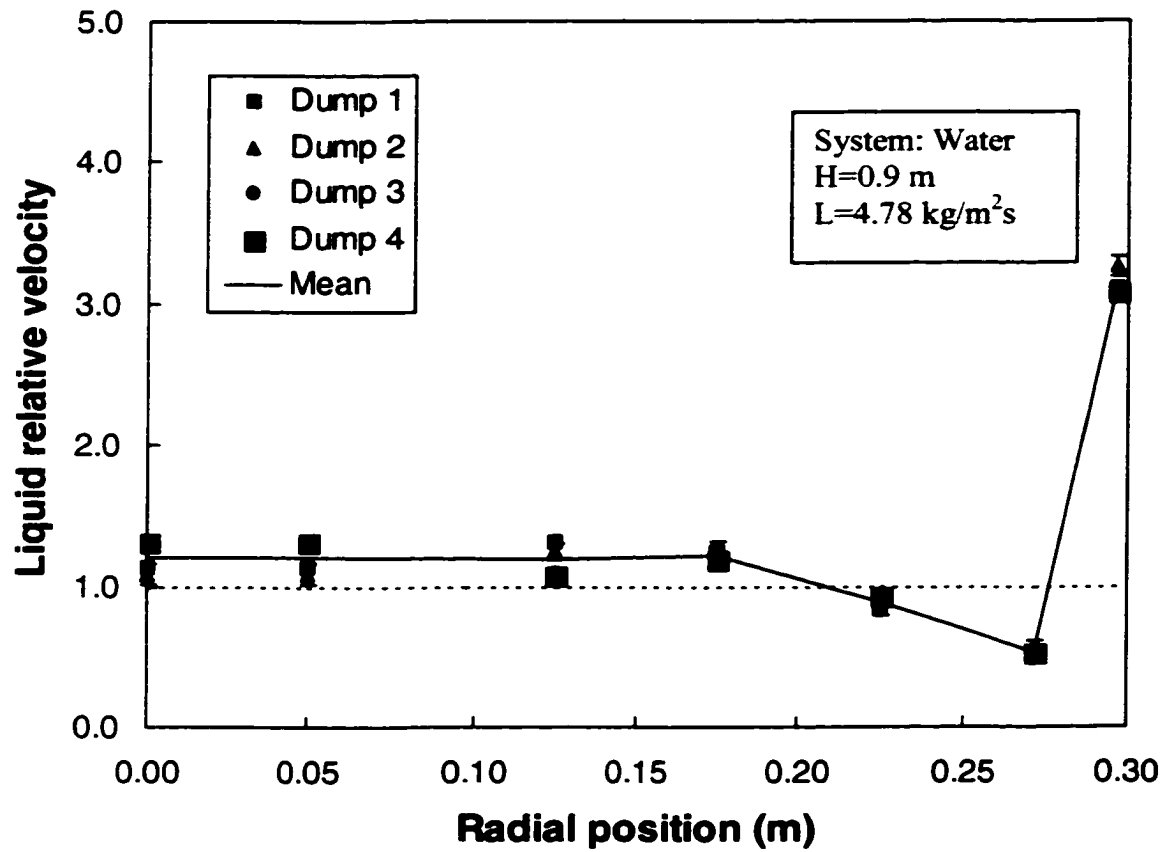
Figure 3.10. Effect of redumping on liquid distribution.
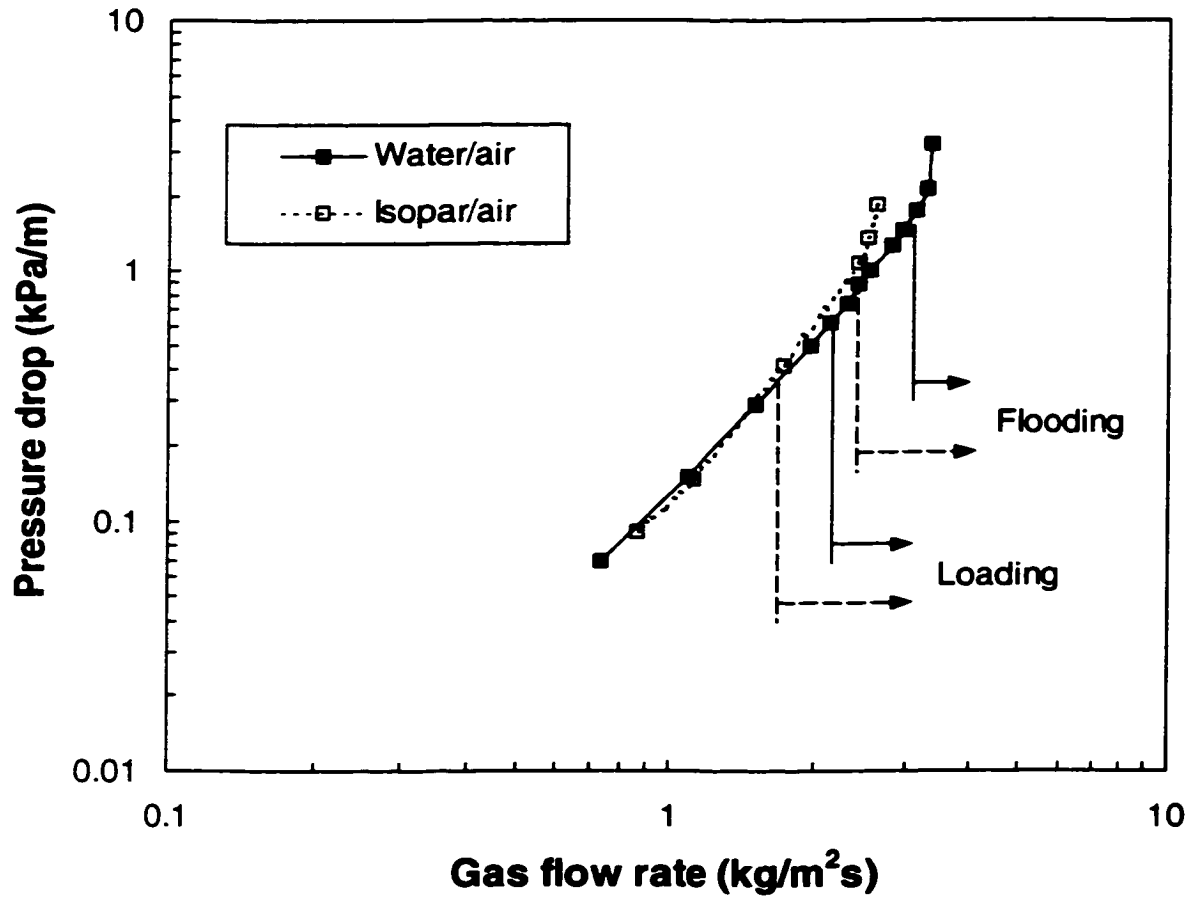
Figure 3.11. Pressure drop vs. gas flow rate for water/air and Isopar/air systems, L=4.78kg/m²s.

Uniform distributor   **Packed bed height**   **Center inlet distributor**
0.0m

0.9m

1.8m

3.0m
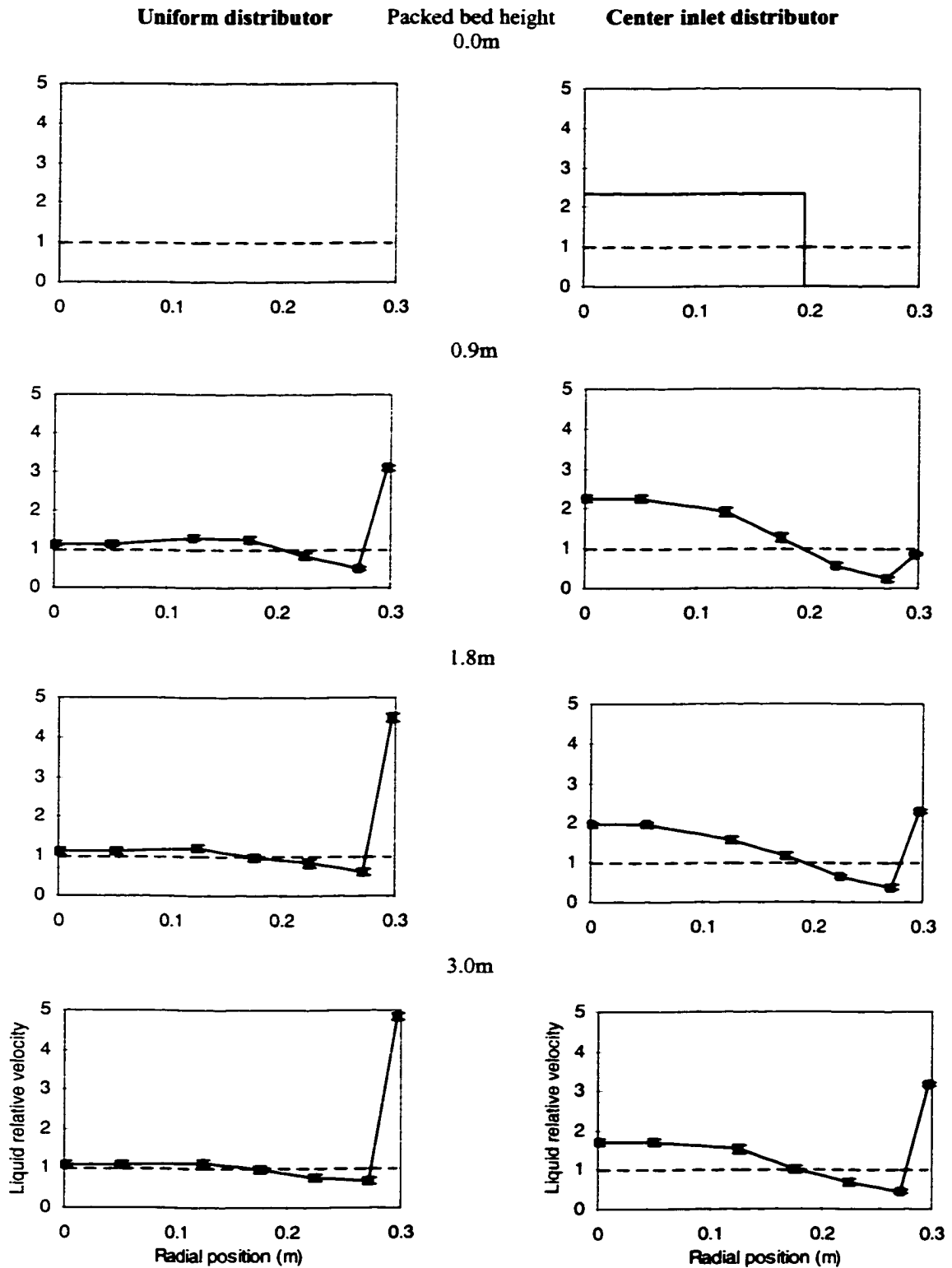
Figure 3.12. Development of liquid flow pattern along bed height (L=4.78 kg/m^{2}s).

72

Uniform distributor **Center inlet distributor**

Gas flow rate = 0

Gas flow rate = 0.75 kg/m²s

Gas flow rate = 1.57 kg/m²s
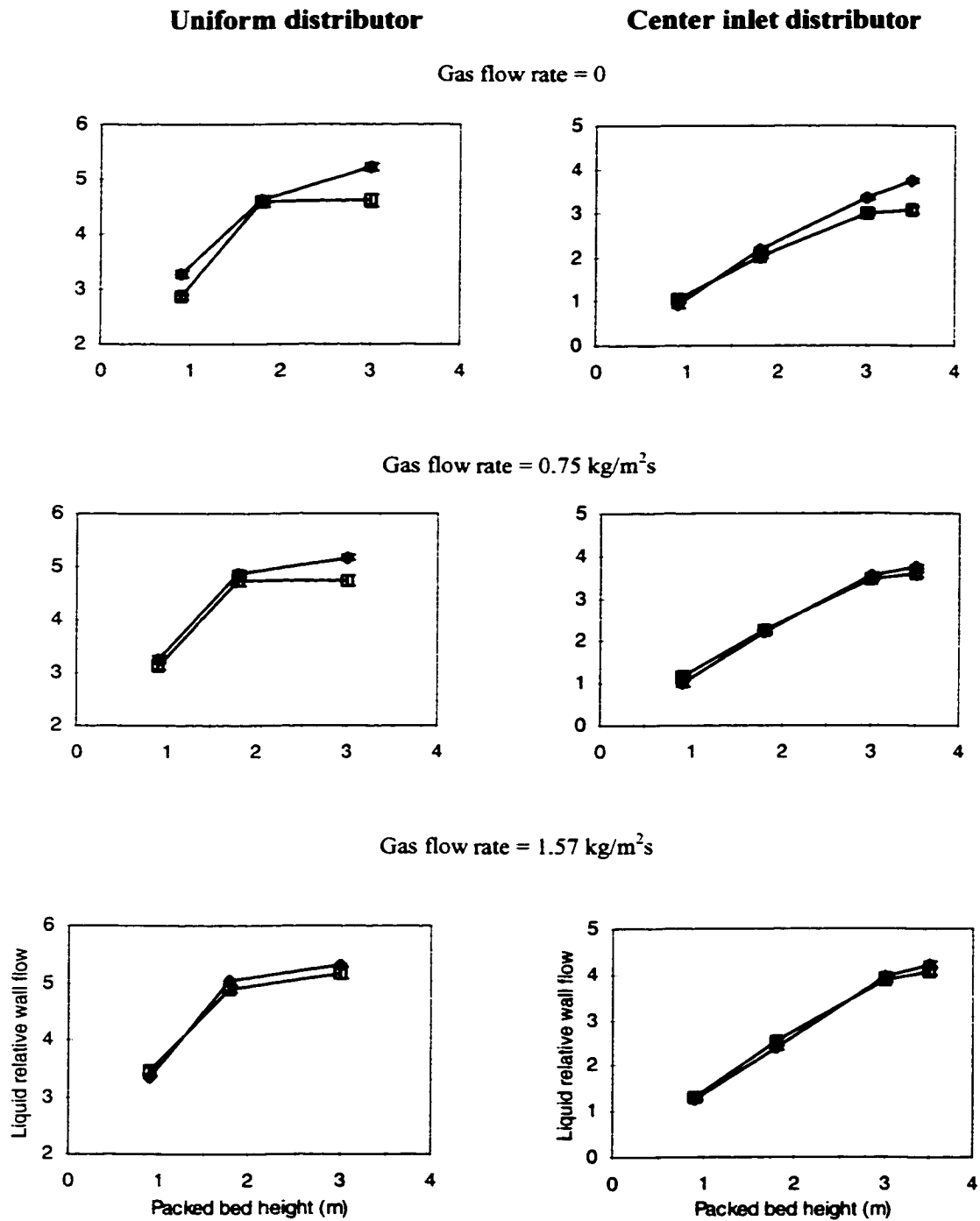
Figure 3.13. Development of liquid relative wall flow along bed height, -♦- L= 2.91 kg/m²s; -□- L= 6.66 kg/m²s.

73
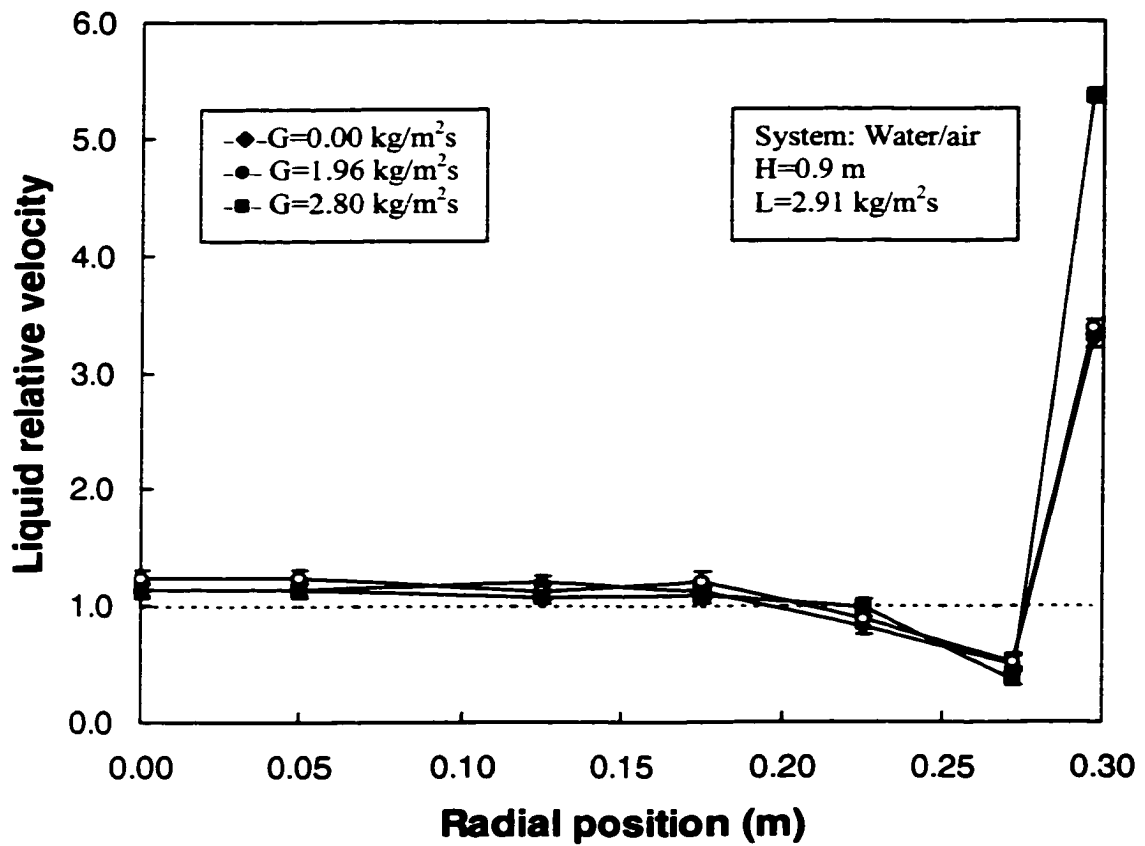
Figure 3.14. Effect of gas flow rate on liquid distribution for the uniform liquid distributor.
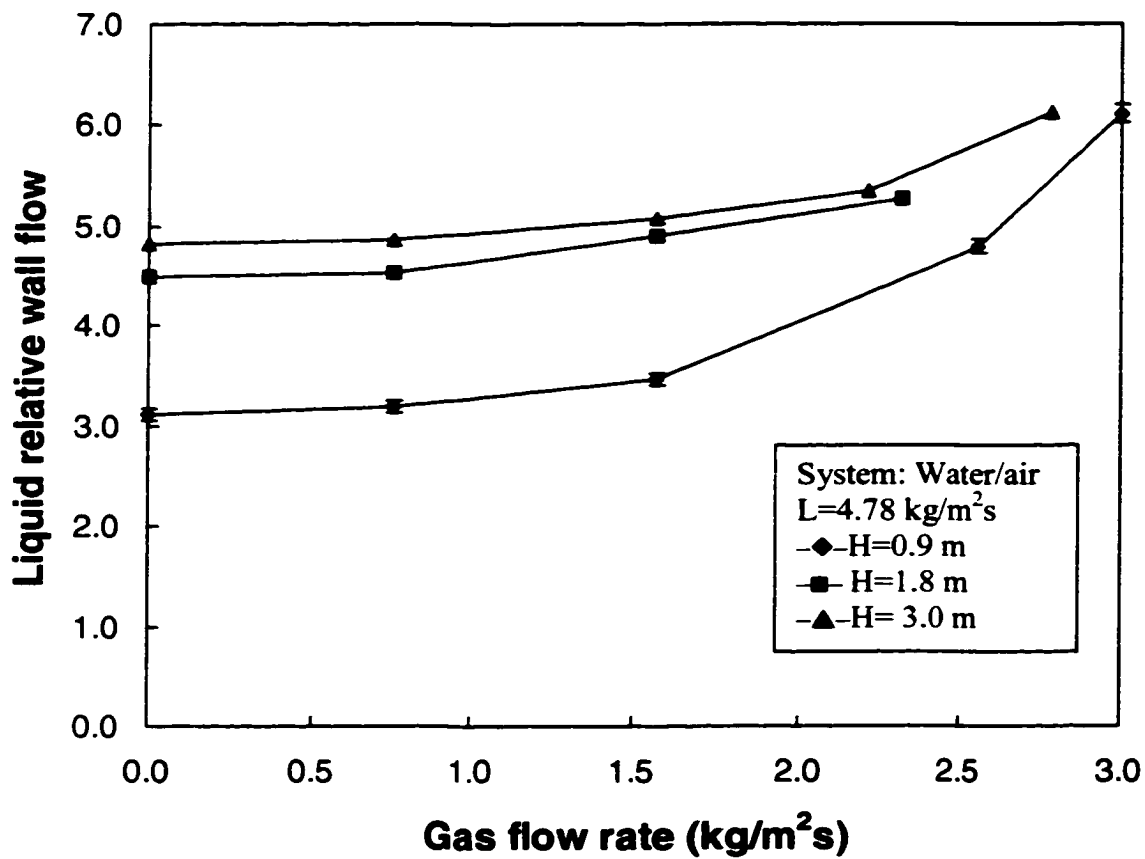
Figure 3.15. Effect of gas flow rate on liquid wall flow for the uniform liquid distributor.

75
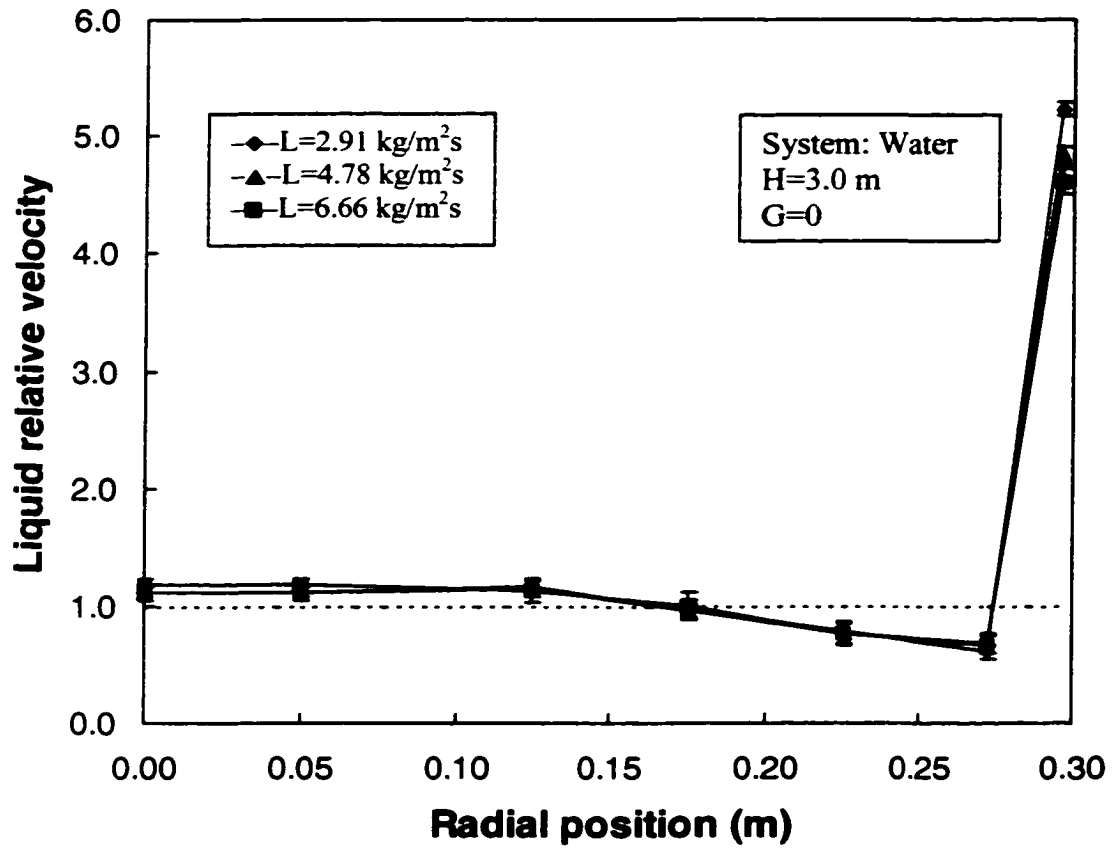
Figure 3.16. Effect of liquid flow rate on liquid distribution for the uniform liquid distributor.
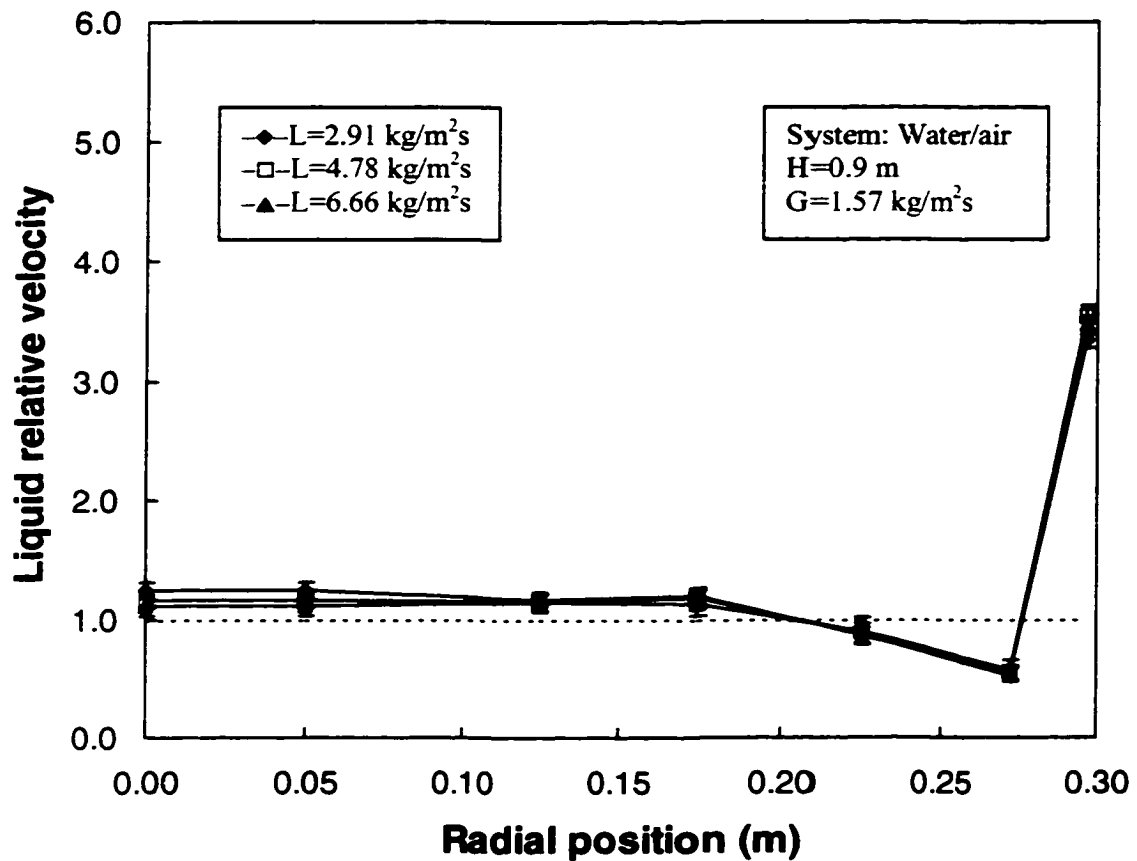
Figure 3.17. Effect of liquid flow rate on liquid distribution for the uniform liquid distributor.
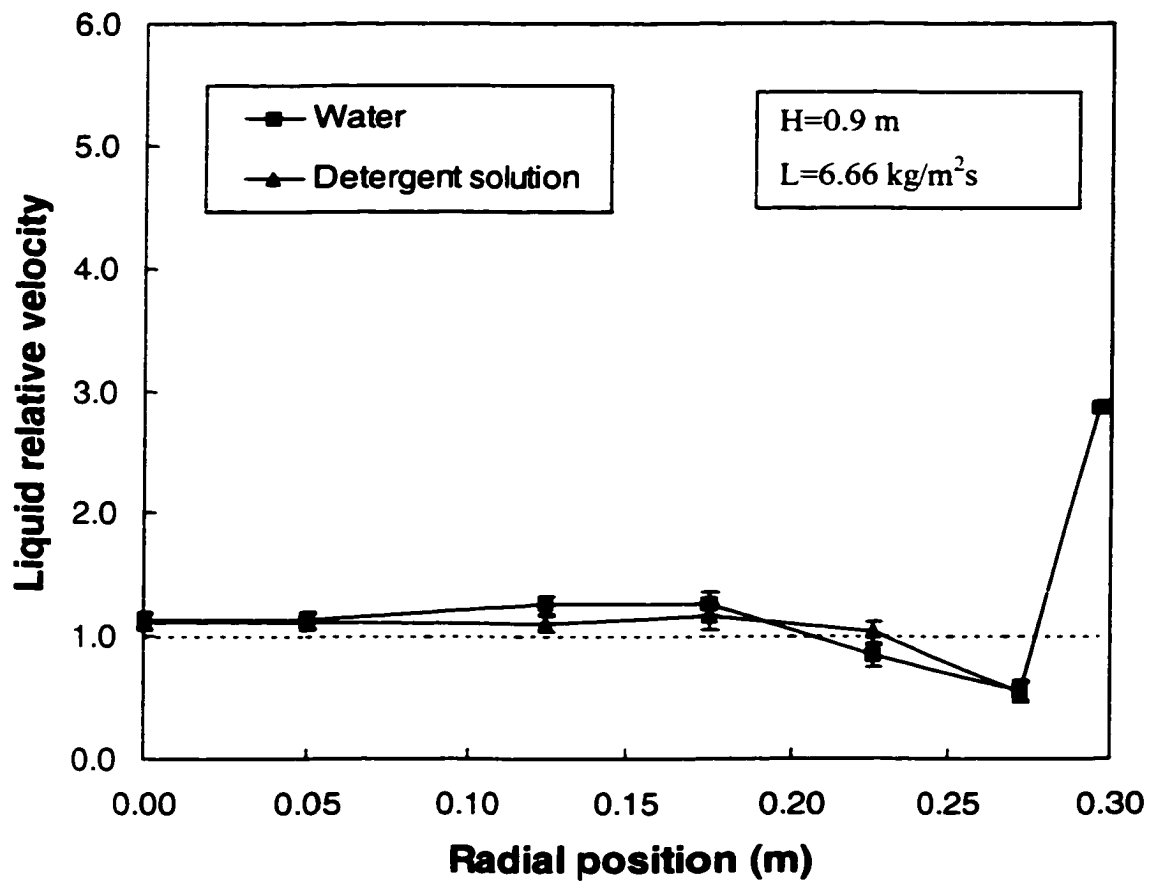
Figure 3.18. Effect of liquid surface tension on liquid distribution for the uniform liquid distributor.
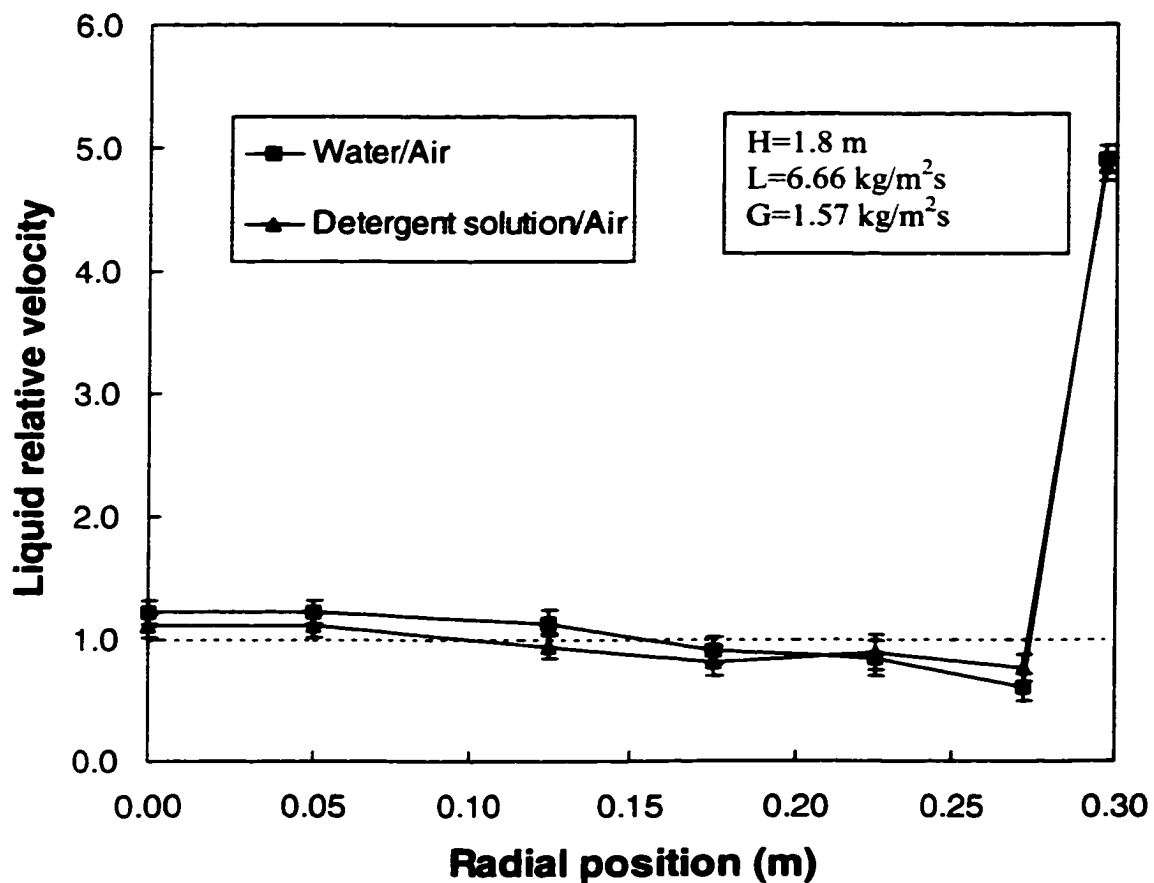
Figure 3.19. Effect of liquid surface tension on liquid distribution for the uniform liquid distributor.
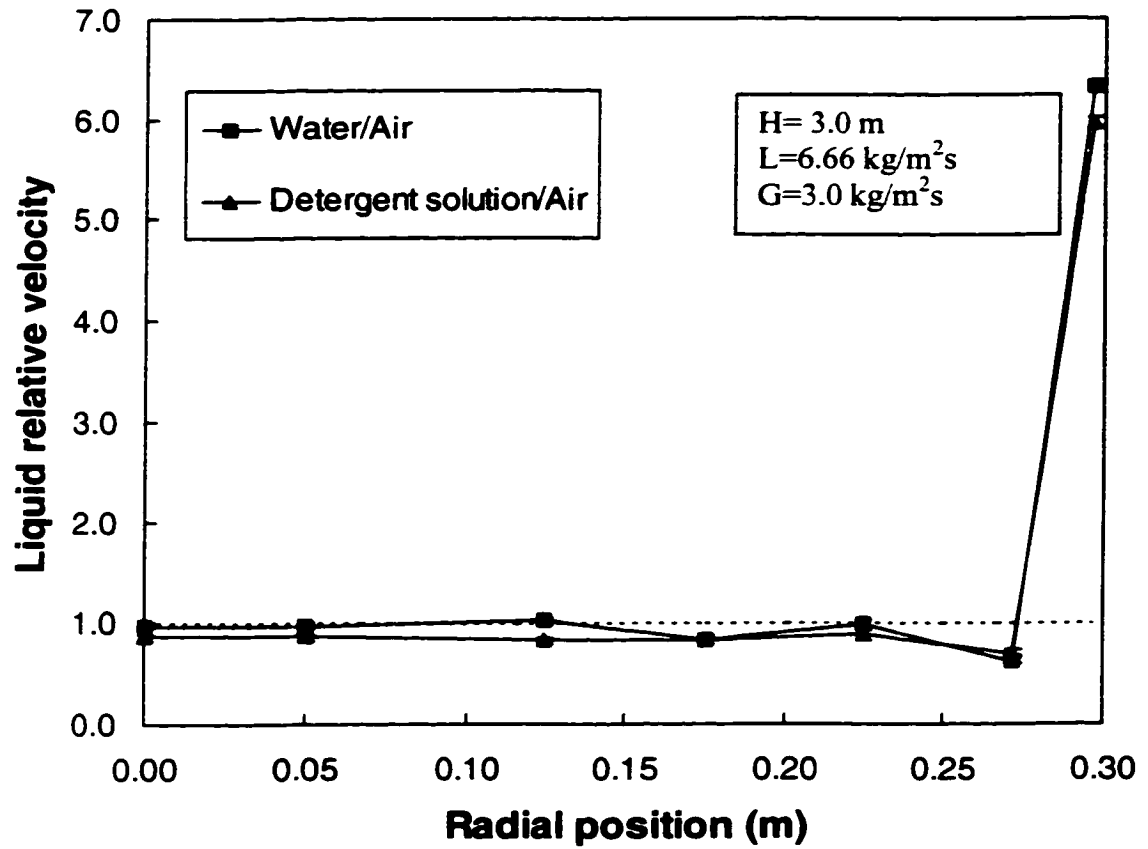
Figure 3.20. Effect of liquid surface tension on liquid distribution for the uniform liquid distributor.
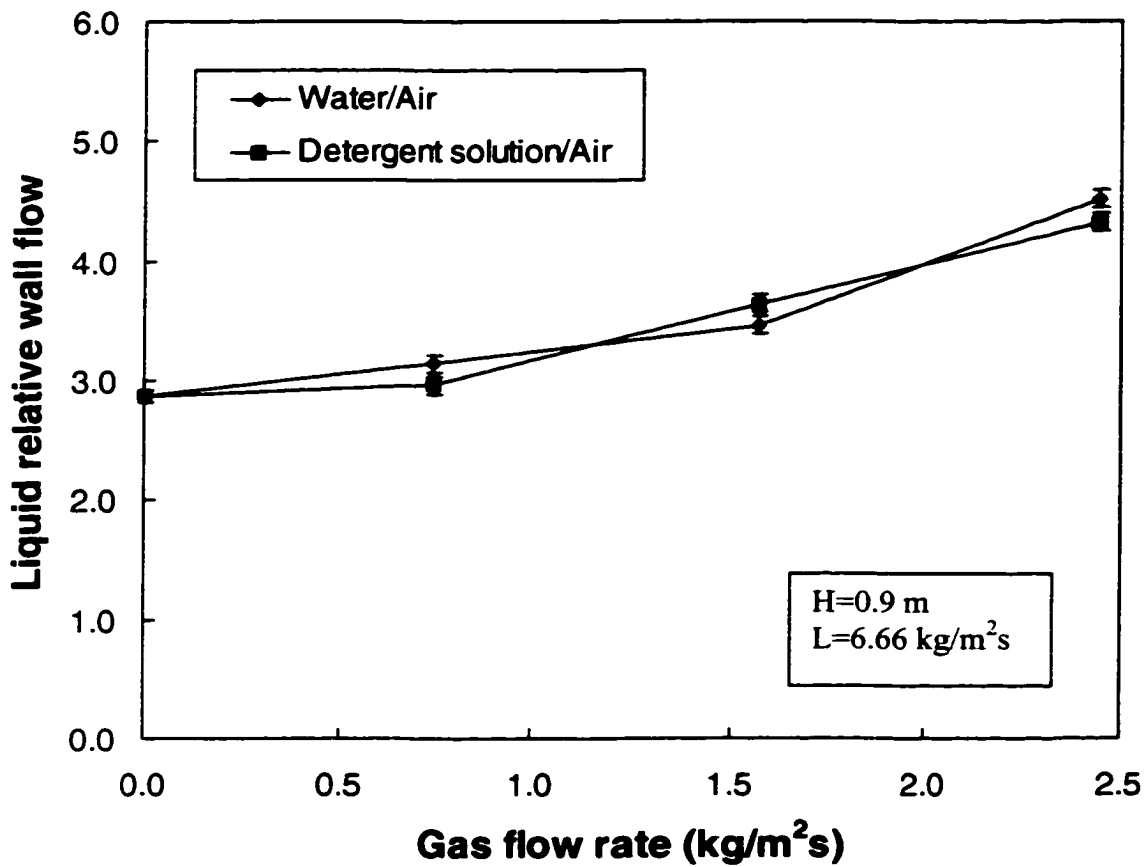
Figure 3.21. Effect of liquid surface tension on liquid wall flow for the uniform liquid distributor.
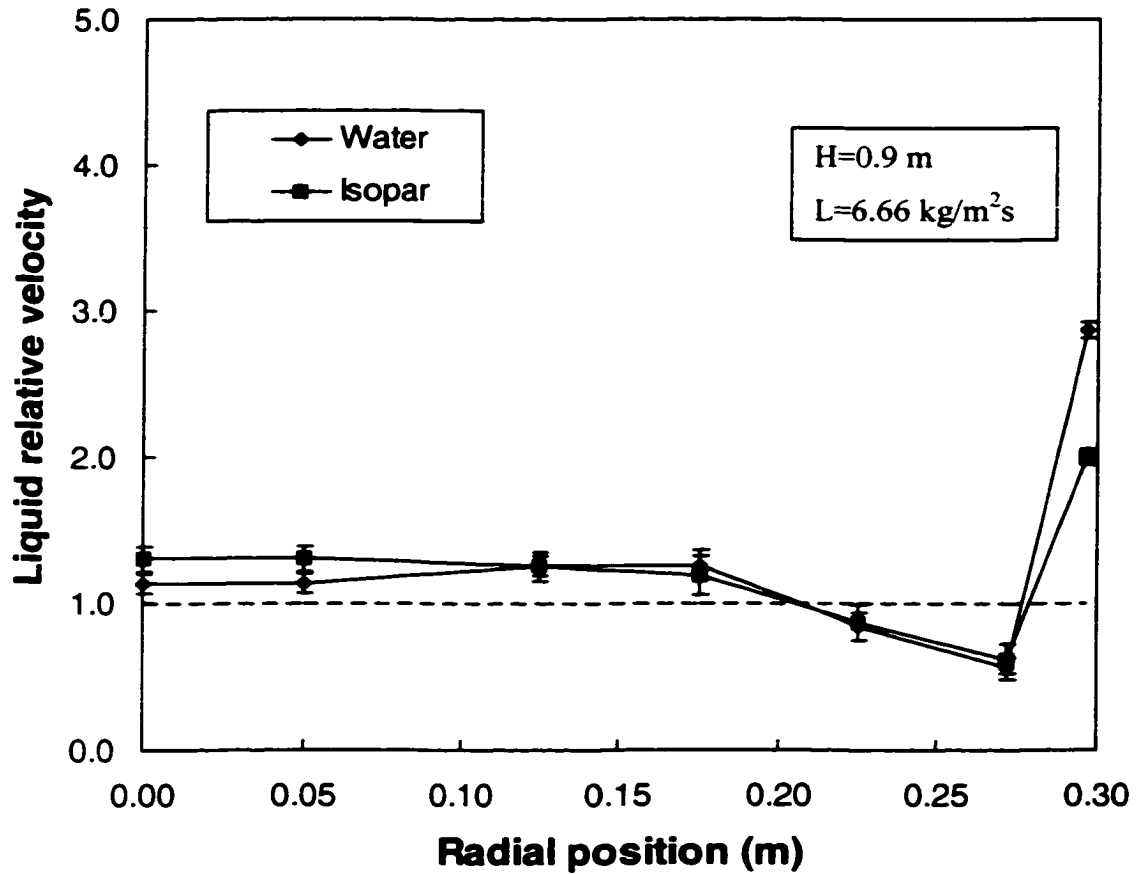
Figure 3.22. Effect of liquid viscosity on liquid distribution for the uniform liquid distributor.
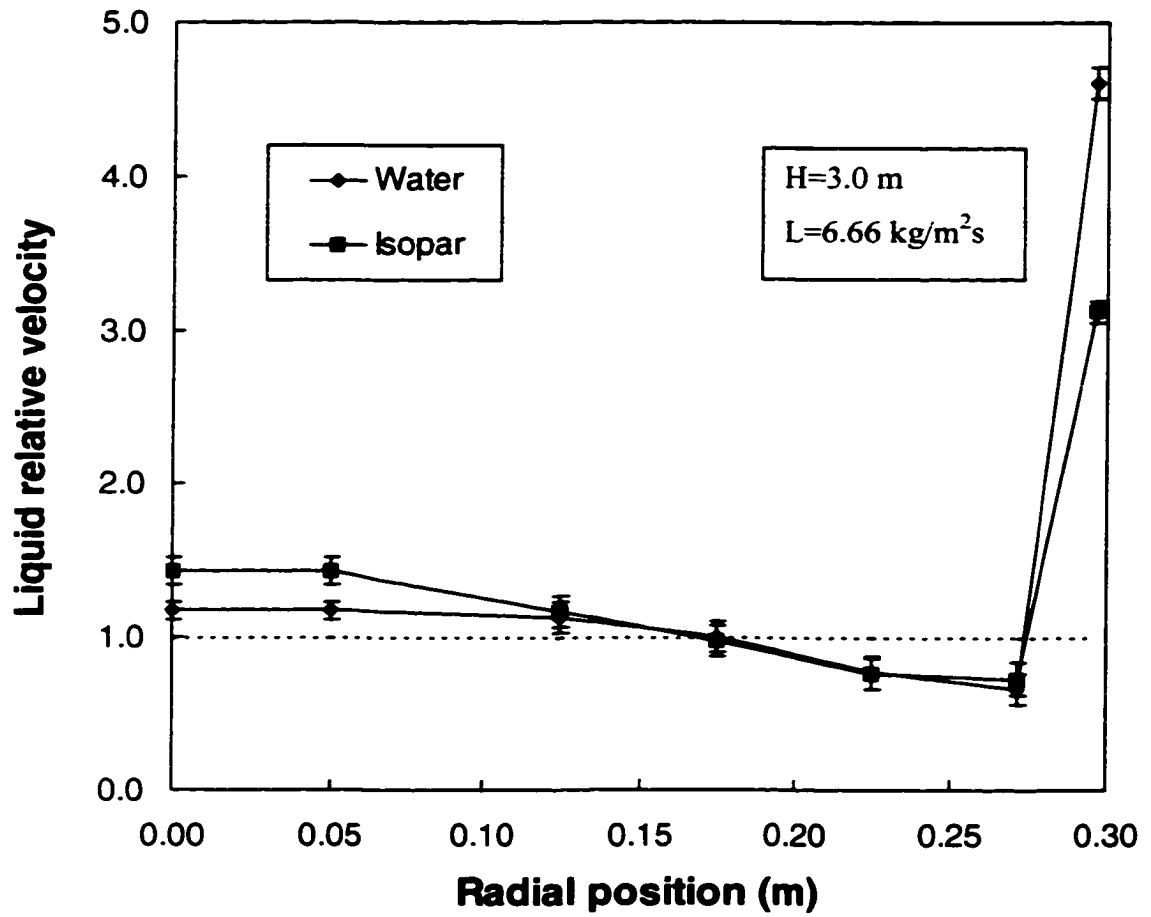
Figure 3.23. Effect of liquid viscosity on liquid distribution for the uniform liquid distributor.
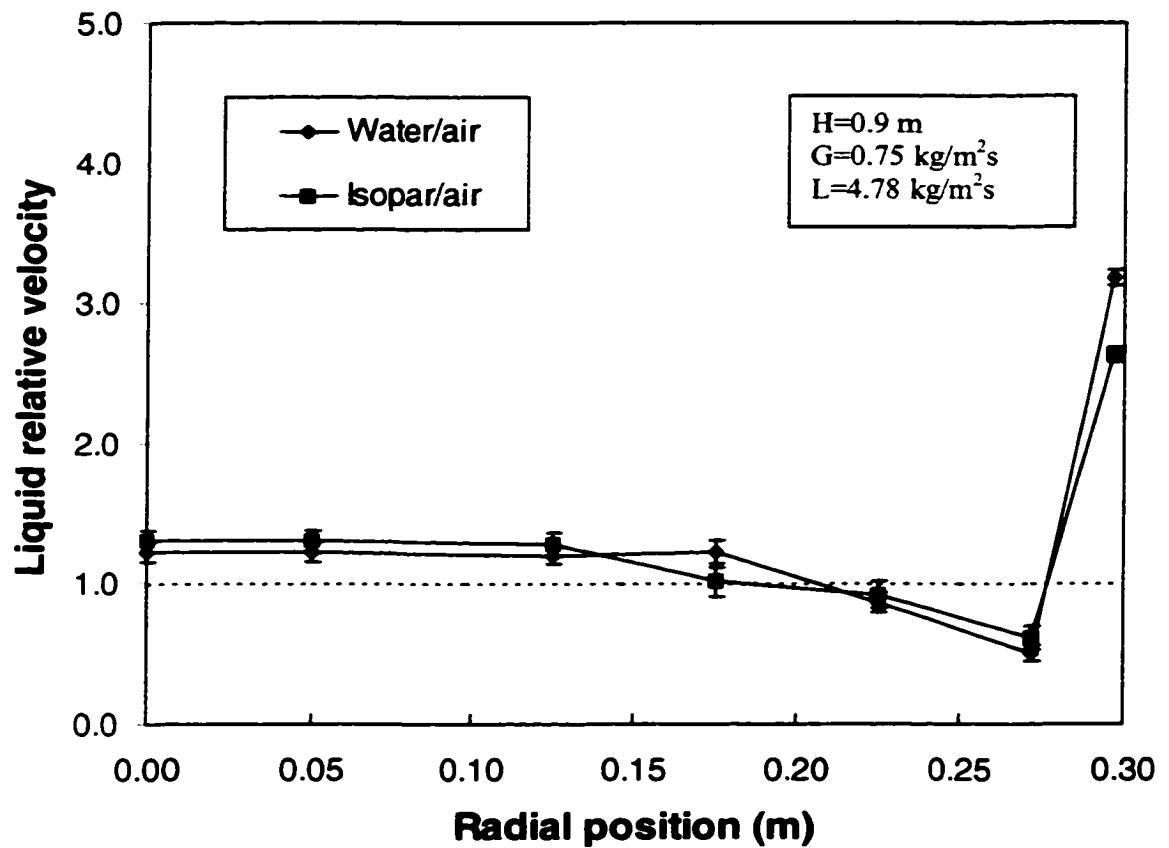
Figure 3.24. Effect of liquid viscosity on liquid distribution for the uniform liquid distributor.
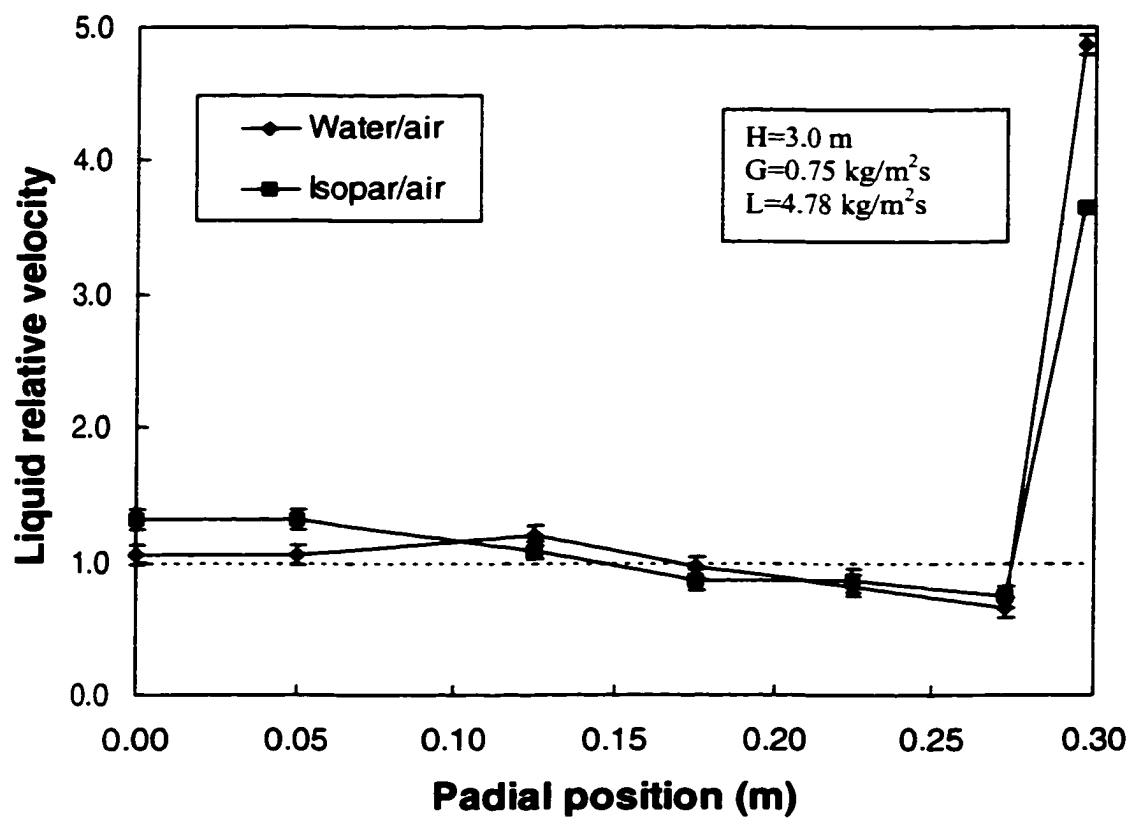
Figure 3.25. Effect of liquid viscosity on liquid distribution for the uniform liquid distributor.
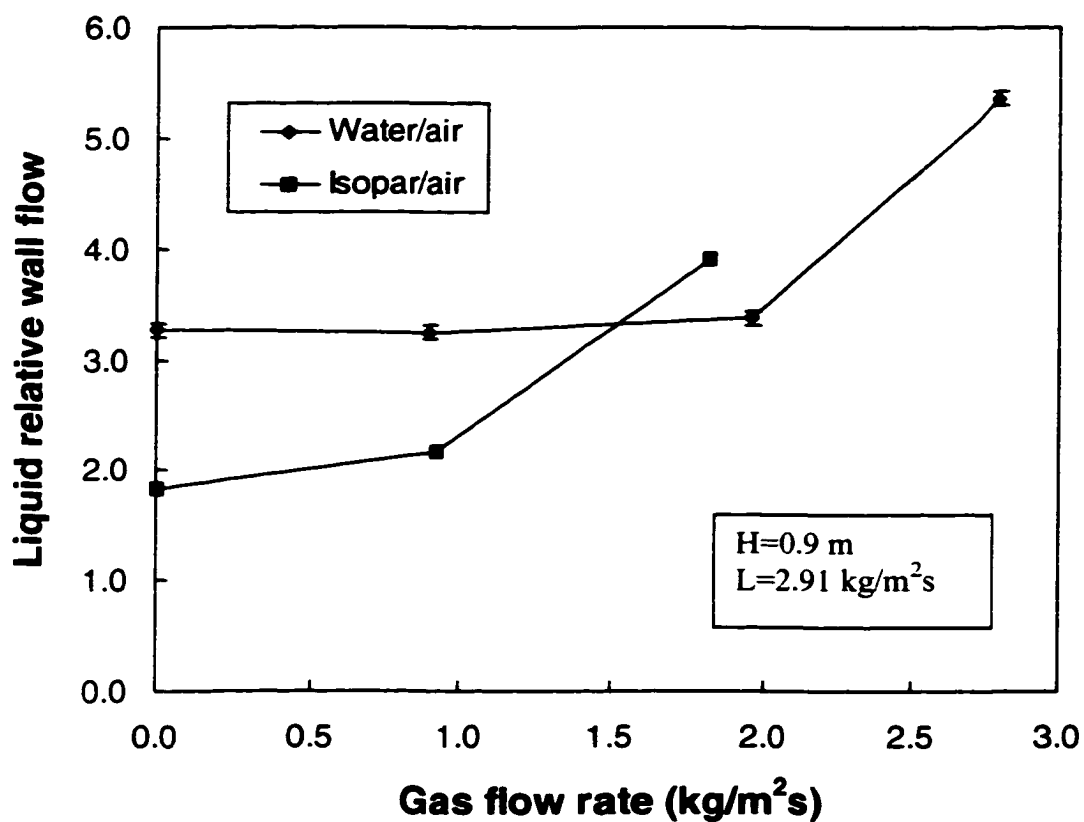
Figure 3.26. Comparison of liquid relative wall flow for the water/air system and Isopar/air system for the uniform liquid distributor.

Chapter 4

HYDRODYNAMICS SIMULATIONS-MODELS

4.1 Introduction

It is recognized that the application of large diameter packed columns is limited due to the uncertainty in design procedures (Olujic and de Graauw, 1989, Kister, 1992). Traditionally, both the liquid phase and the gas phase are assumed to be in the plug flow for the design purposes. However, it has been demonstrated that the liquid flow distribution is far from uniform. Although some simple models have been proposed in the literature to try to predict the liquid flow distribution in randomly packed columns, they are purely empirical and fail to work well as pointed out in the literature survey. Therefore, theoretical models based on the principles of fluid dynamics for the modeling of flow distribution are badly needed.

It is one of the purposes of this study to establish a rigorous approach to model the flow distribution patterns in randomly packed columns based on the volume-averaged Navier-Stokes equations (CFD based models). A major advantage of this approach is that the model equations derived from the conservation laws will remain valid on any scale, from laboratory to industrial size. Therefore they can be used as the basic tools for the more rigorous design and scale up of packed columns. CFD based models, however, require the specification of a number of closure models to capture the information lost during the averaging process. These closure models should describe (a) the flow resistance offered by the packing elements, (b) the interface drag force of two-phase

87

flow, (c) the volume fraction dispersion in the packed bed, (d) turbulent flow, and (e) the void fraction variation within the bed.

In this chapter, we present the models used to close the volume averaged Navier-Stokes equations, the boundary conditions and the numerical methodology used to solve these equations.

4.2 Introduction to the Volume Averaging Concept

A packed bed can be considered as a porous media that is partially filled with solid material (packing). Random packings are fixed in position during operation. While the liquid phase trickles down the bed by means of gravity, the gas phase passes up through the bed by means of the pressure drop, thus forming the countercurrent operation mode. The motion in each phase is governed by the Navier-Stokes equations. However, if we apply the Navier-Stokes equations directly to the porous media flow, we will find that it is almost impossible to specify the boundary conditions owing to the very complex and dynamic nature of the interfaces. Such problems can be addressed more effectively if some form of averaging procedures are used.

Figure 4.1 shows a planar sketch of the Representative Elementary Volume (*REV*) in porous medium. The concept of *REV* is very important in porous medium studies and has been used by various researchers such as Whitaker (1966), Slattery (1969), Bear (1972) and Liu and Masliyah (1996). A *REV* is defined as a minimum volume within which measurable variables (velocity, concentration, density, etc.) become continuum quantities inside a porous medium. In the sketch shown in Figure 4.1, *S* stands for a solid

phase, L stands for a liquid phase, and G stands for a gas phase, respectively. The solid phase here represents the packing material.

The *REV*, as shown in Figure 4.1, consists of two parts, the solid part with the volume V_S and the void part with the volume V_0. The void fraction or the porosity is defined as

$$\varepsilon_p = \frac{V_0}{V} \tag{4-1}$$

where V is the total volume of the *REV*.

For two-phase (liquid and gas) flow, the local liquid phase and gas phase holdups can be defined as

$$h_L = \frac{V_L}{V} \tag{4-2}$$

$$h_G = \frac{V_G}{V} \tag{4-3}$$

where V_L and V_G are the volumes occupied by the liquid phase and gas phase within the *REV*, respectively.

From the above definitions, we can obtain

$$\varepsilon_p = h_L + h_G \tag{4-4}$$

If we assume that ϕ^* stands for the point variable associated with a fluid, then the volume average of this variable can be defined as

$$\phi = \frac{1}{V} \int_V \phi^* dV \tag{4-5}$$

89

where the average is taken over the entire *REV*. In the volume averaging approach, the volume averaged quantity ϕ is used to represent the value of this variable within the *REV*.

The volume average can also be taken over the partial volume of the individual phase itself as follows

$$\phi_{\alpha\varepsilon} = \frac{1}{V_\alpha} \int_{V_\alpha} \phi^* dV \qquad (4\text{-}6)$$

where V_α can be V_L or V_G. $\phi_{\alpha\varepsilon}$ is then referred to as the intrinsic phase average.

$\phi_{\alpha\varepsilon}$ and ϕ are related as

$$\phi = h_\alpha \phi_{\alpha\varepsilon} \qquad (4\text{-}7)$$

For example, the liquid superficial velocity can be determined from its interstitial velocity as

$$u = h_L u_{L\varepsilon} \qquad (4\text{-}8)$$

In the volume averaged approach, the phases are treated as interpenetrating continua, that is, at every point in the porous medium, there is a volume averaged value assigned to all the fluid variables for each of the phases. The volume averaged equations describing the volume averaged variables are still expressed in the traditional form containing convection and diffusion terms and some extra terms to account for the information that is lost in the averaging process.

4.3 The Volume Averaged Equations

The detailed flow field for the two-phase flow through a packed column can be determined by solving the volume averaged fluid dynamic equations given by

90

Continuity equations

$$\frac{\partial}{\partial t}(\gamma_\alpha \rho_\alpha) + \nabla \cdot (\gamma_\alpha \rho_\alpha \mathbf{U}_\alpha - \Gamma_\alpha \nabla \gamma_\alpha) = 0 \qquad \alpha = L, G \qquad (4\text{-}9)$$

Momentum equations

$$\frac{\partial}{\partial t}(\gamma_\alpha \rho_\alpha \mathbf{U}_\alpha) + \nabla \cdot \left\{ \gamma_\alpha \left[\rho_\alpha \mathbf{U}_\alpha \mathbf{U}_\alpha - \mu_{e\alpha} \left(\nabla \mathbf{U}_\alpha + (\nabla \mathbf{U}_\alpha)^T \right) \right] \right\} = \gamma_\alpha (\mathbf{B}_\alpha - \nabla p) + \mathbf{F}_\alpha \qquad (4\text{-}10)$$

$$\alpha = L, G$$

where γ stands for the volume fraction occupied by each phase, ρ is the fluid density, μ_e the effective viscosity including the contribution from turbulent stress, $\mathbf{U}$ the interstitial velocity vector, $\mathbf{B}$ the body force (including the gravity and the flow resistance offered by the packing elements), p the pressure, $\mathbf{F}$ the interface drag force, Γ the volume fraction dispersion coefficient, and α the phase index.

The volume fraction γ is defined as

$$\gamma_L = \frac{V_L}{V_L + V_G} \qquad (4\text{-}11)$$

$$\gamma_G = \frac{V_G}{V_L + V_G} \qquad (4\text{-}12)$$

Thus the volume fraction must sum to unity

$$\gamma_L + \gamma_G = 1 \qquad (4\text{-}13)$$

Comparing Equations (4-2), (4-3), (4-11) and (4-12), results in

$$h_L = \varepsilon_p \gamma_L \qquad (4\text{-}14)$$

$$h_G = \varepsilon_p \gamma_G \qquad (4\text{-}15)$$

91

4.4 The Closure Models

Equations (4-9) and (4-10) do not form a closed system, until the quantities like **B**, **F**, μ_e and Γ are specified through closure models. In this study, they are adopted and developed from existing empirical correlations. Many of these empirical correlations have been developed from experiments conducted on a macroscopic (or equipment) scale – i.e. based only on observations of input/output quantities. Use of these correlations in a local sense is akin to the use of Darcy's theory on a microscale, which is based initially on macroscopic observations of flow rates vs. pressure drop data for packed beds.

There is clearly room for further refinement of these closure models, as more refined experimental data on flow and concentration distributions become available. The clear advantage of the CFD models is in their natural ability to track inhomogenieties within the column, provided the closure models remain valid at the pore scale and the inhomogenieties are caused by the packed bed structure or by poor distributor designs.

4.4.1 Interface Drag Force F

The interface drag force between the gas and liquid phases is modeled by

$$\mathbf{F}_G = C_{GL}(\mathbf{U}_L - \mathbf{U}_G) \tag{4-16}$$

$$\mathbf{F}_L = C_{LG}(\mathbf{U}_G - \mathbf{U}_L) \tag{4-17}$$

$$\mathbf{F}_L = -\mathbf{F}_G \tag{4-18}$$

where C_{GL} or C_{LG} is the interface drag coefficient. In the model equations, C_{GL} or C_{LG} is prescribed in a way that incorporates experimentally measured correlations for pressure drops in countercurrent two-phase flow through packed columns.

92

There are several correlations available in the literature that predict pressure drop for two-phase flow through a randomly packed column, such as the Leva correlation (Leva, 1954; 1992) and the Robbins correlation (Robbins, 1991). The Leva correlation states that the total pressure drop is proportional to the square of the gas velocity

$$\frac{\Delta p}{z} = \alpha_1 \frac{G^2}{\rho_G} 10^{\alpha_2 \psi L} \tag{4-19}$$

This is applicable in the low range of gas loading. However when the liquid load is high, the interaction between the two phases will be substantial. Robbins (1991) modified the Leva equation and proposed the following correlation to predict the pressure drop across the packed column

$$\frac{\Delta p}{z} = C_1 G_f^2 10^{C_2 L_f} + 0.774 \left(\frac{L_f}{20000}\right)^{0.1} \left(C_1 G_f^2 10^{C_2 L_f}\right)^4 \tag{4-20}$$

where $C_1 = 4.002 \times 10^{-2}$, and $C_2 = 1.99 \times 10^{-2}$. G_f and L_f are the gas and liquid loading factors and can be calculated as

$$G_f = \begin{cases} G\left[\dfrac{1.2}{\rho_G}\right]^{0.5}\left[\dfrac{F_{pd}}{65.62}\right]^{0.5} & \text{for } P \leq 1atm \\[3em] G\left[\dfrac{1.2}{\rho_G}\right]^{0.5}\left[\dfrac{F_{pd}}{65.62}\right]^{0.5} 10^{0.0187\rho_G} & \text{for } P > 1atm \end{cases} \tag{4-21}$$

$$L_f = \begin{cases} L\left[\dfrac{1000}{\rho_L}\right]\left[\dfrac{F_{pd}}{65.62}\right]^{0.5}\mu_L^{0.1} & \text{for } F_{pd} \geq 15 \\[3em] L\left[\dfrac{1000}{\rho_L}\right]\left[\dfrac{65.62}{F_{pd}}\right]^{0.5}\mu_L^{0.1} & \text{for } F_{pd} < 15 \end{cases} \tag{4-22}$$

93

Equation (4-20) can be considered to consist of two parts. The first part, $C_1 G_f^2 10^{C_2 L_f}$,

allows for the estimation of pressure drop through the packings in the preloading region,

while the second part, $0.774 \left(\dfrac{L_f}{20000} \right)^{0.1} \left(C_1 G_f^2 10^{C_2 L_f} \right)^4$, takes into account the increase of

the pressure drop due to the stronger interaction between gas and liquid phases in the

loading regime. The presence of liquid in the packings will reduce the free flow space of

the gas phase, thus leading to a higher pressure drop. The parameter F_{pd}, also called the

packing factor, represents the effect of packing size and shape on the pressure drop and

has been documented for almost all the commonly used random packings. For instance,

F_{pd} equals 174 m^{-1} for 25.4 mm metal Pall rings, and 79 m^{-1} for 50.8 mm metal Pall rings

(Kister, 1992). The larger the packing factor, the higher the pressure drop.

If we consider that the total pressure drop can be expressed as

$$\frac{\Delta p}{z} = \left(\frac{\Delta p}{z} \right)_{dry} + \left(\frac{\Delta p}{z} \right)_{wet} \tag{4-23}$$

then

$$\left(\frac{\Delta p}{z} \right)_{dry} = C_1 G_f^2 \tag{4-24}$$

and

$$\left(\frac{\Delta p}{z} \right)_{wet} = \left(C_1 G_f^2 - 1 \right) 10^{C_2 L_f} + 0.774 \left(\frac{L_f}{20000} \right)^{0.1} \left(C_1 G_f^2 10^{C_2 L_f} \right)^4 \tag{4-25}$$

The wet pressure drop across the packed column represents the energy loss due to the

interaction between gas phase and liquid phase. From this pressure drop, one can

determine the interface drag coefficient as follows

$$C_{GL} = \frac{\left(\dfrac{\Delta p}{z}\right)_{wet}}{|\mathbf{U}_L - \mathbf{U}_G|} \qquad (4\text{-}26)$$

where $|\mathbf{U}_L - \mathbf{U}_G|$ is the slip velocity, defined as

$$|\mathbf{U}_L - \mathbf{U}_G| = \sqrt{(U_L - U_G)^2 + (V_L - V_G)^2 + (W_L - W_G)^2} \qquad (4\text{-}27)$$

for three-dimensional flow. U, V and W are the three velocity components. In cylindrical coordinates, as shown in Figure 4.2, U is the axial velocity component in the z-direction, V is the radial velocity component in the r-direction, and W is circumferential velocity component in the θ-direction. For the two-dimensional flow, $W=0$, the slip velocity reduces to

$$|\mathbf{U}_L - \mathbf{U}_G| = \sqrt{(U_L - U_G)^2 + (V_L - V_G)^2} \qquad (4\text{-}28)$$

G and L in the above equations are the superficial gas and liquid flow rates, respectively. They are related to the gas and liquid interstitial velocities as

$$G = \varepsilon_p \rho_G \gamma_G |\mathbf{U}_G| \qquad (4\text{-}29)$$

$$L = \varepsilon_p \rho_L \gamma_L |\mathbf{U}_L| \qquad (4\text{-}30)$$

$|\mathbf{U}|$ is the absolute magnitude of the interstitial velocity, and defined as

$$|\mathbf{U}| = \sqrt{U^2 + V^2 + W^2} \qquad (4\text{-}31)$$

for three-dimensional flow. For two-dimensional flow, $W=0$, and Equation (4-31) can be simplified.

95

4.4.2 Body Force B

In addition to the gravitational body force, the increased resistance to flow due to the presence of the packing particles is also treated as a body force and can be modeled as follows

$$\mathbf{B}_\alpha = \rho_\alpha \mathbf{g} + \mathbf{R}_\alpha \cdot \mathbf{U}_\alpha \tag{4-32}$$

where $\mathbf{g}$ is the acceleration vector due to gravity, and $\mathbf{R}$ is the resistance tensor, representing the flow resistance offered by the porous medium to the liquid and gas phase (that is, the liquid-solid and gas-solid interactions).

From Darcy's theory

$$\mathbf{U}_\alpha = -\mathbf{R}_\alpha^{-1} \cdot \nabla p \tag{4-33}$$

where $\mathbf{R}_\alpha^{-1}$ is the inverse tensor of $\mathbf{R}_\alpha$ and is related to the permeability of the porous medium. ∇p is the gradient of pressure. Hence it is possible to estimate $\mathbf{R}_\alpha$ from the measured pressure drop data.

For the gas phase, the flow resistance offered by the solid packing elements can be modeled utilizing the dry pressure drop part of the Robbins equation. Rewriting Equation (4-24) in tensor form with the aid of the Equation (4-29) and substituting the resulting expression into the Equation (4-33) leads to

$$\mathbf{R}_G = \begin{cases} C_1 \varepsilon_p^2 \rho_G^2 \gamma_G^2 \left[\dfrac{1.2}{\rho_G}\right]\left[\dfrac{F_{pd}}{65.12}\right]|\mathbf{U}_G|\,\mathbf{I} & \text{for } p \le 1atm \\[3ex] C_1 \varepsilon_p^2 \rho_G^2 \gamma_G^2 \left[\dfrac{1.2}{\rho_G}\right]\left[\dfrac{F_{pd}}{65.12}\right]\left[10^{0.0374\rho_G}\right]|\mathbf{U}_G|\,\mathbf{I} & \text{for } p > 1atm \end{cases} \tag{4-34}$$

where $\mathbf{I}$ is the second order unit tensor.

96

For the liquid phase, the well-known Ergun equation can be used to model the flow resistance term (Ergun, 1952). The Ergun equation accounts for viscous and inertial resistance losses and relates them to the dynamic variable and the structure of the packed bed, as characterized by the bed mean void fraction and the equivalent diameter of the packing particles. For the maldistributed flows, it is necessary to write the Ergun equation in the vector form. This form has been used by various researchers to study the flow distribution in the packed bed (Stanek and Szekely, 1972, 1974; Parsons and Porter, 1992).

$$gradP + \left(f_1 + f_2 |\mathbf{U}| \right)\mathbf{U} = 0 \tag{4-35}$$

where

$$f_1 = \frac{150(1-\varepsilon_p)^2 \mu}{d_{eq}^2 \varepsilon_p^2} \tag{4-36}$$

$$f_2 = \frac{1.75(1-\varepsilon_p)\rho}{d_{eq}\varepsilon_p} \tag{4-37}$$

Here the term $f_1\mathbf{U}$ represents the viscous resistance and the term $f_2|\mathbf{U}|\mathbf{U}$ represents the inertial resistance. The equivalent diameter, d_{eq}, of the packing element is defined as

$$d_{eq} = \frac{6(1-\varepsilon_p)}{a_p} \tag{4-38}$$

where a_p is the total surface area of a packing element per unit volume.

The flow resistance $\mathbf{R}_L$ can then be calculated as

$$\mathbf{R}_L = f_1 + f_2 |\mathbf{U}_L| \mathbf{I} \tag{4-39}$$

4.4.3 Dispersion Coefficient Γ

Liquid spreading apart from a vertical flow in packed columns is due in part to spatial variation in flow resistance. This implies that if a certain flow channel formed within a packed bed offers less resistance to flow than other channels of equal cross sectional area, liquid will tend to move towards this channel, where the flow resistance is lower, thus causing a higher liquid holdup (or volume fraction) in this channel. Spatial variation of the flow resistance is generated mainly from two sources: the spatial variation of void fraction, and the non-uniform liquid distribution. The main cause of void fraction variation in a randomly packed column is the wall effect. In the wall region, the void fraction is generally higher than that in the bulk region. The non-uniform liquid distribution can be formed, even in a homogeneous bed, if the fluid passing through the system is introduced in a form of a non-uniform initial distribution such as shortage of liquid near the column wall, discontinuities or zonal flow, caused by malperformance of a liquid distributor.

In this study, the dispersion coefficient for volume fraction is assumed to be linearly proportional to the negative gradient of the resistance along the direction of liquid main flow (i.e., the axial direction of the packed column). Mathematically, this relation can be expressed as

$$\Gamma = -K_c \nabla R_z \tag{4-40}$$

where K_c is a proportionality constant and can be determined by fitting experimental data.

The liquid flow resistance offered by the packing elements along the direction of main flow is given by Equation (4-35). This equation relates the pressure drop to two

98

terms, the viscous resistance and inertial resistance. Normally the inertial component provides the major resistance to flow in the packed columns under the normal operating conditions. Thus, taking the inertial term of the Ergun equation as R_z and differentiating it, results in

$$\Gamma = 1.75 K_c \frac{\rho \, U^2}{d_{eq}\varepsilon_p^{\,2}} \nabla \varepsilon_p - 3.5 K_c \frac{(1-\varepsilon_p)\rho U}{\varepsilon_p \, d_{eq}} \nabla U \qquad (4\text{-}41)$$

The first term on the right side of Equation (4-41) represents the effect of the bed structure (i.e., the spatial void fraction variation) on liquid spreading, and the second term implies the fact that even for homogeneous packed beds the liquid spreading can occur if the liquid distribution is non-uniform.

Another important cause for the liquid spreading is the unstable turbulent flow encountered under the normal operating conditions in packed columns. The momentum exchange between the fluid elements in turbulent flow can be expected to be much greater than that in laminar flow. In order to account for this effect, an additional term, Γ_T, is introduced to the right side of Equation (4-41). Γ_T represents the turbulent dispersion coefficient and can be calculated based on the eddy viscosity hypothesis as

$$\Gamma_T = \frac{\mu_T}{\sigma_t} \qquad (4\text{-}42)$$

where μ_T is the turbulent viscosity of the liquid phase and σ_t if the turbulent Prandtl number (AEA Technology plc, 1997).

The spreading of gas is a much faster process than that of liquid. This has been substantiated experimentally by Kouri and Sohlo (1987, 1996), Stikkelman and Wesselingh (1987), Stikkelman et al. (1989), Stoter et al. (1992), and Suess (1992). One

99

may conclude based on these experimental results that under normal operating conditions (i.e., in the preloading region), the gas flow pattern and its spreading mainly depend upon the liquid flow behavior. On the other hand, compared with the liquid phase, the turbulence intensity is much higher in the gas phase due to its lower viscosity. Thus one may assume that the spreading of gas phase is dominated by the turbulent dispersion. The turbulent dispersion coefficient of gas phase is defined in the same manner as Equation (4-42), except μ_T represents the gas turbulent viscosity.

4.4.4 Void Fraction Variation in Radial Direction

Due to the presence of the column wall, the void fraction in the near wall region is greater than that in the bulk region, thus leading to a non-uniform distribution in the radial direction. Void fraction radial variation is one of the most important characteristics of randomly packed columns because this renders the non-uniform flow resistance on fluids passing through the columns. The literature abounds with studies on the void fraction distribution for spheres, cylindrical particles, and Berl saddles (Roblee et al., 1958; Benenati and Brosilow, 1962; Beavers et al., 1973; Dixon, et al., 1984; Govindaro and Froment, 1986; Dixon, 1988; Kufner and Hofmann, 1990; Foumeny and Roshani, 1991; Zou and Yu, 1996). The experimental data generally show that the most significant variation in the void fraction occurs in the region near the column wall. Especially for the packings of highly irregular shapes such as Berl saddles the void fraction increases regularly from the mean void fraction at about 1 particle diameter from the wall to unity at the wall (Roblee et al., 1958).

100

For modern, commercially important packings such as Pall rings, Hiflow rings and Intalox saddles, the studies on the radial void fraction distribution seem to be very limited. A recent experimental study by Toye et al. (1998) using a 0.6 m diameter column packed with 44 mm Cascade Mini-Ring 1A packing reported a radial void fraction profile quite similar to that of Berl saddles (Roblee et al., 1958). Note, modern packings normally have a very complex structure and irregular shape. These structural characteristics are especially significant, because they contribute to the collection of liquid in the wall region and lead to the so-called large scale liquid maldistribution. For modeling the void fraction variation in the radial direction for packed beds of spheres, Vortmeyer and Schuster (1983) used an exponentially decaying function. The similar form was used in this study to represent the void fraction variation for packed beds of Pall rings

$$\varepsilon_p = 1 - \left(1 - \varepsilon_{pb}\right)\left\{1 - \exp\left[-2\left(\frac{R-r}{d_p}\right)^2\right]\right\} \qquad (4\text{-}43)$$

where R is the radius of the packed column, d_p is the nominal diameter of packing particles and ε_{pb} is the bulk void fraction. For 25.4 mm stainless steel Pall rings, ε_{pb}=0.94 (Kister, 1992).

The radial void fraction profile for the 25.4 mm stainless steel Pall rings predicted by Equation (4-43) is shown in Figure 4.3. From this figure, it can be seen that the void fraction variation is mainly confined to within one packing element diameter from the wall and in the bulk region the void fraction is almost constant. This is in agreement with the experimental findings of Roblee et al. (1958) and Toye et al. (1998).

101

4.4.5 Turbulence Model

Modern random packings have some common features, such as complex geometric structure, large specific area and high void fraction (generally, larger than 0.9). These characteristics not only ensure a large gas-liquid contact area but also intensify the two phase mixing due to the continually changed flow direction and interruption of the fluids over the packing surface. For the flow through a packed column, the Reynolds number can be calculated as (Billet, 1995)

$$\text{Re}_L = \frac{L}{a_p \mu_L} \tag{4-44}$$

$$\text{Re}_G = \frac{G}{a_p \mu_G} \tag{4-45}$$

Based on numerous experimental measurements on some 50 different types of packings, Billet (1995) found that the critical Reynolds number for the flow region transition from laminar to turbulent is about 10. In this study, the Reynolds numbers for most of cases were normally much greater than that value, i.e. the flows were in the turbulent region. Since the high capacity operation is the main objective in the design and operation of packed columns, the condition of $\text{Re}_{L,cr} < 10$ is rarely encountered in practice.

Turbulent flows are extremely complex, time dependent flows. The traditional method to model turbulent flow is to separate the flow variables into their mean and fluctuating parts. The mean value can be calculated from the time-averaged Navier-Stokes equations. These time-averaged equations have the same form as the governing equations for laminar flow, but with some extra terms, which are solely functions of the

fluctuating quantities, such as the so-called Reynolds stresses or Reynolds flux. Hence, turbulence models provide a means for computing Reynolds stresses or Reynolds flux. There are mainly two types of turbulence models: eddy viscosity models (such as k-ε model) and second order closure models (such as differential stress model (DSM) and algebraic stress model (ASM)) (AEA Technology plc, 1997). While eddy viscosity models model the Reynolds stresses or Reynolds flux algebraically in terms of known mean quantities, the second order closure models solve differential transport equations for the turbulent flux. Among these models, the k-ε model is generally believed to be the simplest model to give useful predictions of the general turbulent flows (Hamill, 1996). For most engineering problems, the k-ε model has been used with significant success (Patankar, 1981; Taulbee, 1989).

The k-ε model uses an eddy viscosity hypothesis for the turbulence. In this model, the effective viscosity is defined as

$$\mu_{e\alpha} = \mu_\alpha + \mu_{T\alpha} \qquad (4\text{-}46)$$

where μ is the molecular viscosity. μ_T is the turbulent viscosity and can be calculated as

$$\mu_{T\alpha} = C_\mu \rho_\alpha \frac{k_\alpha^2}{\varepsilon_\alpha} \qquad (4\text{-}47)$$

where C_μ is an empirical constant, k is the turbulence kinetic energy and ε is the turbulence dissipation rate.

The transport equations for the turbulence kinetic energy k and turbulence dissipation rate ε have the same form as the generic advection-diffusion equation and can be solved along with the momentum equations. The effective viscosity required in the momentum equations can then be determined from Equations (4-46) and (4-47).

103

The modeling of turbulent features in multiphase flow is not as well developed. The applicability of the k-ε model for incompressible turbulent flow in porous media has been examined by Antohe and Lage (1997). For high void fraction packings, such as those found in packed columns, the study was inconclusive.

4.5 Boundary Conditions

The flow computational domain is isolated from its surroundings through the definition of the boundaries. The boundary conditions are information specified on boundary surface. There are several different boundaries such as flow boundary, wall boundary, and symmetry boundary that must be considered. The flow boundary is such a boundary that it is used to define the conditions at the entrance and/or exit of the flow domain. At the inlet of the flow domain, the flow boundary is known as the inlet boundary, and at the outlet (exit) of the flow domain, mass flow boundary can be used. For countercurrent multi-phase flow, it is possible to have flows that enter and leave the same flow boundary simultaneously. Therefore special treatment is required at these boundaries.

4.5.1 Inlet Boundary Condition

An inlet boundary is mathematically referred to as Dirichlet boundary. The reason to choose this boundary in this study is because it is easy to define different liquid inlet profiles. At this boundary all the variables (such as velocity, volume fraction, mass fraction, etc.) must be specified. However, for incompressible flow, the specified inlet pressure value will not be used, its value will be extrapolated from downstream. At the

inlet boundary, both inlet flow and outlet flow can be defined. For the inlet flow, a positive value should be specified for the velocity, and for the outlet flow, a negative value should be assigned to the velocity component perpendicular to the inlet. This way the outlet flow is defined to have a direction that is pointing away from the computational domain. For turbulent flow, the inlet boundary conditions also need to be specified for the turbulence quantities. When using the two-equation k-ε model, the inlet values for k and ε can be calculated based on the mean flow characteristics (AEA Technology plc, 1997).

$$k_{inl} = c_{p1} u_{inl}^2 \tag{4-48}$$

$$\varepsilon_{inl} = \frac{k_{inl}^{1.5}}{c_{p2} D_H} \tag{4-49}$$

where c_{p1} and c_{p2} are empirical constants and was set to c_{p1}=0.002 and c_{p2}=0.3. u_{inl} is the mean inlet velocity. D_H is the hydraulic diameter, given by

$$D_H = \frac{4A_f}{P_w} \tag{4-50}$$

where A_f is the cross sectional area available for flow and P_w is the wetted perimeter of the flow domain, respectively. For the flow through porous media, the hydraulic diameter can be related to void fraction ε_p and wetted surface area a_p per unit volume of the bed as (Bird et al., 1960)

$$D_H = \frac{4\varepsilon_p}{a_p} \tag{4-51}$$

The detailed specifications of inlet boundary conditions used in the simulations are given in Section 4.5.3.

105

4.5.2 Mass Flow Boundary

Mass flow boundaries are used to specify the inflow and outflow boundaries where the total mass flow rate into or out of the domain is known, but the detailed velocity profile is not. At mass flow boundary Neumann boundary conditions are imposed on all transported variables, that is, the variable gradients are specified, rather than their values. It is assumed that at the mass flow boundary, the flow is fully developed. If the flow goes into the flow domain at the mass flow boundary instead of going out, it is necessary to specify Dirichlet boundary conditions to certain variables such as mass fractions, while other variables are still specified using Neumann conditions. Section 4.5.3 gives examples that show how to define the mass flow boundary conditions.

4.5.3 Examples of Boundary Condition Specifications

In packed column operation, the liquid is introduced at the top of the column via a liquid distributor while the gas is fed into the column at the bottom. Hence the inlet conditions for both the liquid and gas are usually known from the process operating conditions. Figure 4.4 shows the sketch of the computational domain and identifies the boundaries used in the simulations. To predict the flow fields of liquid phase and gas phase within the flow domain, four different boundary conditions are specified, that is, at the top, bottom, wall and the axis of the packed bed. For a typical simulation with the liquid flow rate L and gas flow rate G, the boundary conditions are specified as follows:

(1) At the top of the column, the 'inlet' boundary is specified. At this boundary the appropriate values for velocity components, volume fractions, turbulence quantities, etc. must be specified for both the liquid phase and gas phase. For the liquid phase, the flow enters the flow domain, and the velocity components are specified as follows:

$U_L = \dfrac{L}{\rho_L \gamma_L \varepsilon_p}$; $V_L = 0$; $W_L = 0$. For the gas phase, the flow leaves the flow domain, the z-

component of velocity must be assign a negative value, that is, $U_G = -\dfrac{G}{\rho_G \gamma_G \varepsilon_p}$; $V_G = 0$;

$W_G = 0$. The inlet volume fraction of liquid is difficult to specify since there is no measured value available. However, it can be estimated from the liquid holdup based on the liquid flow rate as follows (Kister, 1992)

$$h_L = \frac{0.4184}{\varepsilon_p}\left(\frac{\mu_L}{\rho_L}\right)^{\frac{1}{6}}\left(u_L a_p\right)^{0.5} \qquad (4\text{-}52)$$

$$\gamma_L = \frac{h_L}{\varepsilon_p} \qquad (4\text{-}53)$$

where u_L is the liquid superficial velocity.

The volume fraction of gas phase can then be determined as

$$\gamma_G = 1 - \gamma_L \qquad (4\text{-}54)$$

The values of turbulence kinetic energy k and turbulence dissipation rate ε can be calculated from Equations (4-48) and (4-49).

(2) At the bottom of the column, the mass flow boundary is used to specify the total mass flow rates of both the liquid and gas phases. For the liquid phase, the positive value is

107

assigned to indicate that it leaves the flow domain, that is, $m_L = L \times A$. For the gas phase, the negative value is used to indicate that it enters the flow domain, that is, $m_G = -G \times A$. The Neumann boundary conditions are used for all other variables in both the liquid phase and the gas phase.

(3) At the column wall, the 'non-slip' boundary condition is specified to the velocities of both the liquid phase and the gas phase. For other variables, such as volume fractions, and mass fractions, no flux conditions are specified. Turbulence kinetic energy and turbulence dissipation rate are calculated using the logarithmic wall functions.

(4) At the column axis all variables are mathematically symmetric and no diffusion occurs across this boundary for two-dimensional simulation. Therefore, an axisymmetry boundary condition is imposed on all variables at the column axis ($r=0$).

4.6 Numerical Methodology

First the computational domain of interest is divided into a number of control volumes, also called computational cells. For two-phase flow through the cylindrical packed columns, the most significant variations in the flow field are expected to appear in the top region, bottom region and wall region of the packed column. In these regions, sufficiently fine grids should be utilized to give an accurate prediction. In this study a geometric progression (G.P.) was used to generate a grid structure in the radial direction with the smallest cell size of about 1/8 of a packing diameter being adjacent to the column wall. In the axial direction a symmetric geometric progression (SYM G.P.) was

used to generate a grid structure in which the smallest cell size was about 1/2 a packing diameter in the top and the bottom of the packed column.

Since the liquid is often introduced into the column with radial symmetry, it can be assumed that the flow in the column is two-dimensional. To test the validity of this assumption, some three-dimensional simulations have also been carried out. For two-dimensional simulations, there is only one grid cell needed in the circumferential direction. The computational grid used with a resolution of 80 (axial)×25 (radial) is shown in Figure 4.5. The result for the grid independent study is shown in Figure 4.6.

The governing equations are solved numerically by means of a finite volume method, using the CFD package CFX 4.2. The variables needed to be calculated were the velocity components (U, V, W), pressure (p), turbulence kinetic energy (k), turbulence energy dissipation rate (ε) (if it is turbulent flow), volume fractions (γ_L, γ_G) (if it is multi-phase flow), and mass fractions (if it is multi-component flow). The governing equations relating these variables are of the following general form (AEA Technology plc, 1997)

$$Convection - Diffusion = Sources - Sinks \qquad (4\text{-}55)$$

Each equation is integrated over each control volume (computational cell) to obtain a linearised discrete equation that connects the variable at the center of the control volume with its neighbors. Each linearised equation can thus be regarded as belonging to a particular variable and to a particular control volume.

The convection terms in the governing equations are discretised using a hybrid differencing method and all other terms are discretised using second-order central differencing scheme. Hybrid differencing is a modification of the upwind differencing. In this scheme, the central differencing is used if the mesh Peclet number is less that 2, and

upwind differencing is used if the mesh Peclet number is greater than 2, but ignoring diffusion. The name hybrid is indicative of a combination of the upwind scheme and central difference scheme. The hybrid scheme is still first-order accurate, but is slightly better than the upwind scheme.

The well-known SIMPLEC algorithm (Van Doormal and Raithby, 1984) is employed to solve the pressure-velocity coupling in the momentum equations.

4.7 Summary

The model for describing the liquid volume fraction dispersion coefficient was developed based on the non-uniform distribution of liquid flow resistance. The closure models for modeling the hydrodynamics in randomly packed columns, the boundary conditions and the numerical methodology used in the simulation were presented and discussed.

4.8 Nomenclature

A   Cross Sectional Area of Column, m^2

A_f Cross Sectional Area Available for Flow, m^2

a_p Total Surface Area of Packings Per Unit Volume, m^{-1}

B   Body Force, $N\ m^{-3}$

C   Inter-Phase Drag Coefficient

C_1 Constants in Robbins's Correlation

C_2 Constants in Robbins's Correlation

c_{p1} Parameter in Equation (4-48)

c_{p2} Parameter in Equation (4-49)

C_μ Parameter in Equation (4-47)

D_H Hydraulic Diameter, m

d_{eq} Equivalent Diameter of Packing, m

d_p Nominal Diameter of Packing, m

F   Interface Drag Force, $N\ m^{-3}$

f_1 Defined in Equation (4-36)

f_2 Defined in Equation (4-37)

F_{pd} Packing Factor, m^{-1}

G   Gas Superficial Flow Rate per Unit Cross sectional Area, $kg\ m^{-2}\ s^{-1}$

G_f Gas Loading Factor, $kg\ m^{-2}\ s^{-1}$

g   Gravitational Vector, $m\ s^{-2}$

h   Holdup

I   Second Order Unit Tensor

k   Turbulence Kinetic Energy, $m^2\ s^{-2}$

K_c Parameter in Equation (4-40), $m^2\ s$

L   Liquid Superficial Flow Rate per Unit Cross sectional Area, $kg\ m^{-2}\ s^{-1}$

111

L_f	Liquid Loading Factor, kg m^{-2} s^{-1}
m	Flow Rate, kg s^{-1}
P	Pressure, Pa
P_w	Wetted Perimeter of the Flow Domain, m
Δp	Pressure drop, Pa m^{-1}
R	Resistance Tensor, kg m^{-3} s^{-1}
R	Radius of the Column, m
R_z	Axial Resistance Component, N m^{-3}
Re	Reynolds Number
Re_{cr}	Critical Reynolds Number
r	Radial Coordinate, m
t	Time, s
U	Interstitial Velocity Vector, m s^{-1}
U	Interstitial Axial Velocity, m s^{-1}
u	Liquid Superficial Velocity, m s^{-1}
$u_{L\varepsilon}$	Liquid Intrinsic Phase Averaged Velocity, m s^{-1}
V	Interstitial Radial Velocity, m s^{-1}, or Volume, m^3
W	Interstitial Angular Velocity, m s^{-1}
z	Packed Bed Height, m

Greek Symbols

α_1	Parameter in Equation (4-19)
α_2	Parameter in Equation (4-19)
ε	Turbulence Dissipation Rate, m^2 s^{-3}
ε_p	Void Fraction or Porosity

112

γ	Volume Fraction
μ	Viscosity, $kg\ m^{-1}\ s^{-1}$
μ_e	Effective Viscosity, $kg\ m^{-1}\ s^{-1}$
ρ	Density, $kg\ m^{-3}$
Γ	Dispersion Coefficient for Volume Fraction, $kg\ m^{-1}\ s^{-1}$
ψ	Ratio of Water density to Liquid Density
ϕ	Volume Averaged Variable
$\phi^{\bullet}$	Point Variable
ϕ_{ε}	Intrinsic Phase Averaged Variable
σ_t	Turbulent Prandtl Number
θ	Angular Coordinate

Subscripts

0	Void Space
b	Bulk Region of Packed Bed
G	Gas Phase
inl	Inlet
L	Liquid Phase
l	Local
S	Solid Phase
T	Turbulent Flow
z	Outlet
α	Phase Index

4.9 References

AEA Technology plc, (1997) *CFX-4.2: Solver.* Oxfordshire OX11 ORA, United Kingdom.

Antohe, B. V. and Lage, J. L., (1997) A General Two-Equation Macroscopic Turbulence Model for Incompressible Flow in Porous Media. *Int. J. Heat Mass Transfer.* **40**, 3013-3024.

Bear, J., (1972) Dynamics of Fluids in Porous Media. Elsevier, New York.

Beavers, G. S., Sparrow, E. M. and Rodenz, D. E., (1973) Influence of Bed Size on the Flow Characteristics and Porosity of Randomly Packed Beds of Sphere. *Trans. ASME. J. App. Mech.* **40**, 655-660.

Benenati, R. F. and Brosilow, C. B., (1962) Void Fraction Distribution in Beds of Spheres. *AIChE J.* **8**, 359-361.

Billet, R., (1995) Packed Towers in Processing and Environmental Technology, VCH Publishers, Weinheim, Germany.

Bird, R. B., Stewart, W. E., and Lightfoot E. N., (1960) Transport Phenomena. John Wiley & Sons, Inc.

Dixon, A. G., (1988) Correlations for Wall and Particle Shape Effects on Fixed Bed Bulk Voidage. *Can. J. Chem. Eng.* **66**, 705-708.

Dixon, A. G., DiCostanzo, M. A. and Soucy, B. A., (1984) Fluid-Phase Radial Transport in Packed Beds of Low Tube-to-Particle Diameter Ratio. *Int. J. Heat Mass Transfer.* **27**, 1701-1713.

Ergun, S., (1952) Fluid Flow through Packed Columns. *Chem. Eng. Prog.* **48**, 89-94.

Foumeny, E. A. and Roshani, S., (1991) Mean Voidage of Packed Beds of Cylindrical Particles. *Chem. Eng. Sci.* **46**, 2363-2363.

Govindaro, V. M. H. and Froment, G. F., (1986) Voidage Profiles in Packed Bed of Sphere. *Chem. Eng. Sci.* **41**, 533-539.

Hamill N., (1996) CFD Comes of Age in the CPI. *Chem. Eng.* **Dec.**, 68-72.

Kister, H. Z., (1992) Distillation Design, McGraw-Hill, New York.

Kouri, R. J. and Sohlo, J., (1987) Liquid and Gas Flow Patterns in Random and Structured Packings. *I. Chem. E. Symp. Ser.* No. 104, B193-B211.

Kouri, R. J. and Sohlo, J., (1996) Liquid and Gas Flow Patterns in Random Packings. *Chem. Eng. J.* **61**, 95-10

Kufner, K. and Hofmann, H., (1990) Implementation of Radial Porosity and Velocity Distribution in a Reactor Model for Heterogeneous Catalytic Gas Phase Reactions (TORUS-MODEL). *Chem. Eng. Sci.* **45**, 2141-2146.

Leva, M., (1954) Flow Through Irrigated Dumped Packings: Pressure Drop, Loading, Flooding. *Chem. Eng. Prog. Symp. Ser.* **50**, Nov., 51-62.

Leva, M., (1992) Reconsider Packed-Tower Pressure-Drop Correlations. *Chem. Eng. Prog.* **65**, 65-72.

Liu, S. J. and Masliyah, J. H., (1996) Single Fluid Flow in Porous Media. *Chem. Eng. Comm.* **148-150**, 653-732.

Olujic, Z. and de Graauw J., (1989) Appearance of Maldistribution in Distillation Columns Equipped with High Performance Packings. *Chem. Biochem. Eng.* **Q3 (4)**, 181-196.

Parsons, I. M. and Porter, K. E., (1992) Gas Flow Patterns in Packed Beds: A Computational Fluid Dynamics Model for Wholly Packed Domains. *Gas Separation & Purification.* **6**, 221-227.

Patankar, S. V., (1981) Numerical Heat Mass Transfer and Fluid Flow. McGraw-Hill Co., New York.

Robbins, L. A., (1991) Improve Pressure-Drop Prediction with a New Correlation. *Chem. Eng. Prog.* **87**, 87-91.

Roblee, L. H. S., Baird, R. M. and Tierney, J. M., (1958) Radial Porosity Variations in Packed Beds. *AIChE J.* **4**, 460-464.

Slattery, J. C., (1969) Single-Phase Flow through Porous Media. *AICHE J.*, **15**, 866-872.

Stanek, V. and Szekely, J., (1972) The Effect of Non-Uniform Porosity in Causing Flow Maldistributions in Isothermal Packed Beds. *Can. J. Chem. Eng.* **50**, 9-14.

Stanek, V. and Szekely, J., (1974) Three-Dimensional Flow of Fluids through Nonuniform Packed Beds. *AICHE J.* **20**, 974-980.

Stikkelman, R. M. and Wesselingh, J. A., (1987) Liquid and Gas Flow Patterns in Packed Columns. *I. Chem. E. Symp. Ser.* No. 104, B155-B164.

Stikkelman, R. M., de Graauw, J., Olujic, Z., Teeuw, H. and Wesselingh, J. A., (1989) A Study of Gas and Liquid Distributions in Structured Packings. *Chem. Eng. Technol.* **12**, 445-449.

Stoter, F., Olujic, Z. and de Graauw, J., (1992) Modelling of Hydraulic and Separation Performance of Large Diameter Columns Containing Structured Packed. *I. Chem. E. Symp. Ser.* No. 128, A201-A210.

Suess, Ph., (1992) Analysis of Gas Entries of Packed Columns for Two Phase Flow. *I. Chem. E. Symp. Ser.* No. 128, A369-A383.

Taulbee, D. B., (1989) Engineering Turbulence Models, in *Advances in Turbulence*, Eds. W. K. George and R. Arndt, Hemisphere Publishing, NY, 75-125.

Toye, D., Marchot, M. C., Pelsser, A.-M. and L'Homme, G., (1998) Local Measurements of Void Fraction and Liquid Holdup in Packed Columns Using X-ray Computed Tomography. *Chem. Eng. and Progressing.* **37**, 511-520.

Van Doormal, J. P. and Raithby, G. D., (1984) Enhancements of the SIMPLE Method for Predicting Incompressible Fluid Flows. *Numerical Heat Transfer.* **7**, 147-163.

Vortmeyer, D. and Schuster, J., (1983) Evaluation of Steady Flow Profiles in Rectangular and Circular Packed Beds by a Variational Method. *Chem. Emg .Sci.* **38**, 1691-1699.

Whitaker, S., (1966) The Equations of Motion in Porous Media. *Chem. Eng. Sci.* **21**, 291-300.

Zou, R. P. and Yu, A. B., (1996) Wall Effect on the Packing of Cylindrical Particles. *Chem. Eng. Sci.* **51**, 1177-1180.
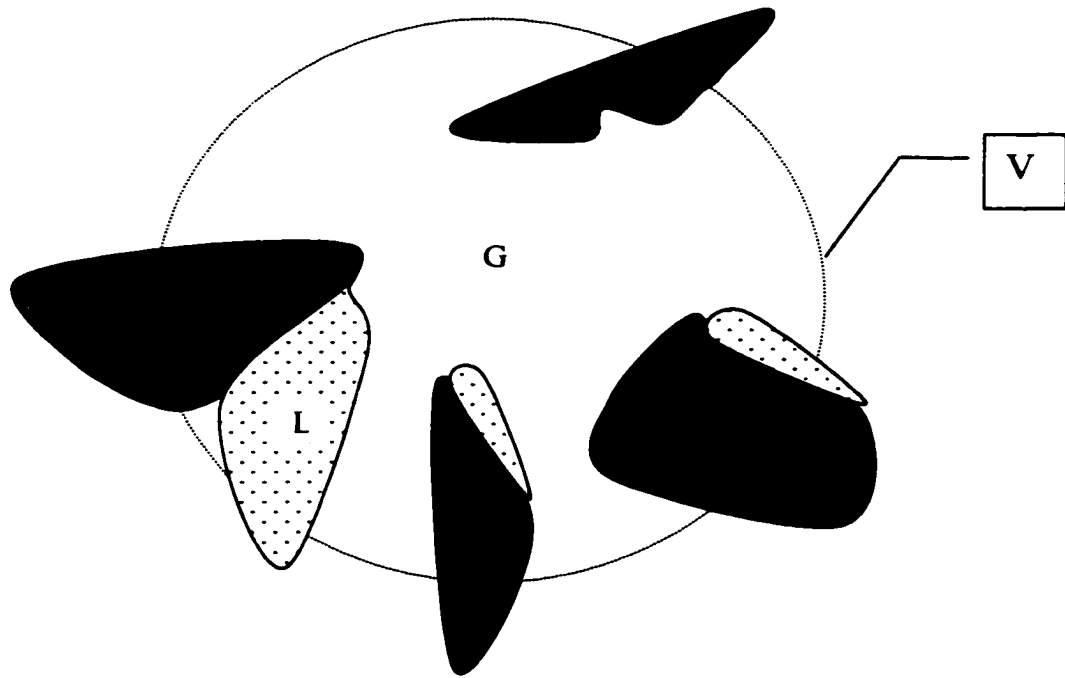
Figure 4.1. A planar sketch of Representative Elementary Volume,
S-solid phase; L-liquid phase; G-gas phase; V-volume of REV
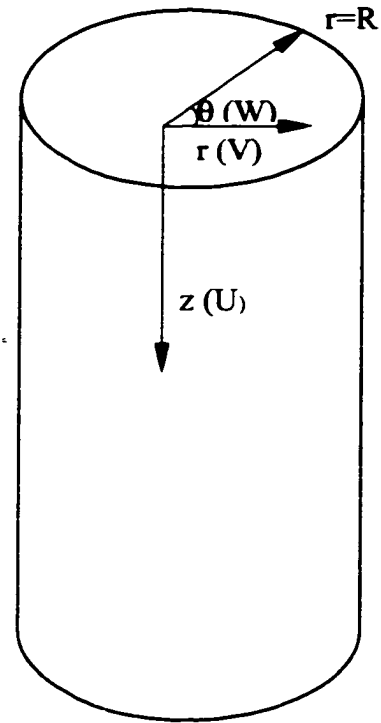
Figure 4.2. A cylindrical coordinate system
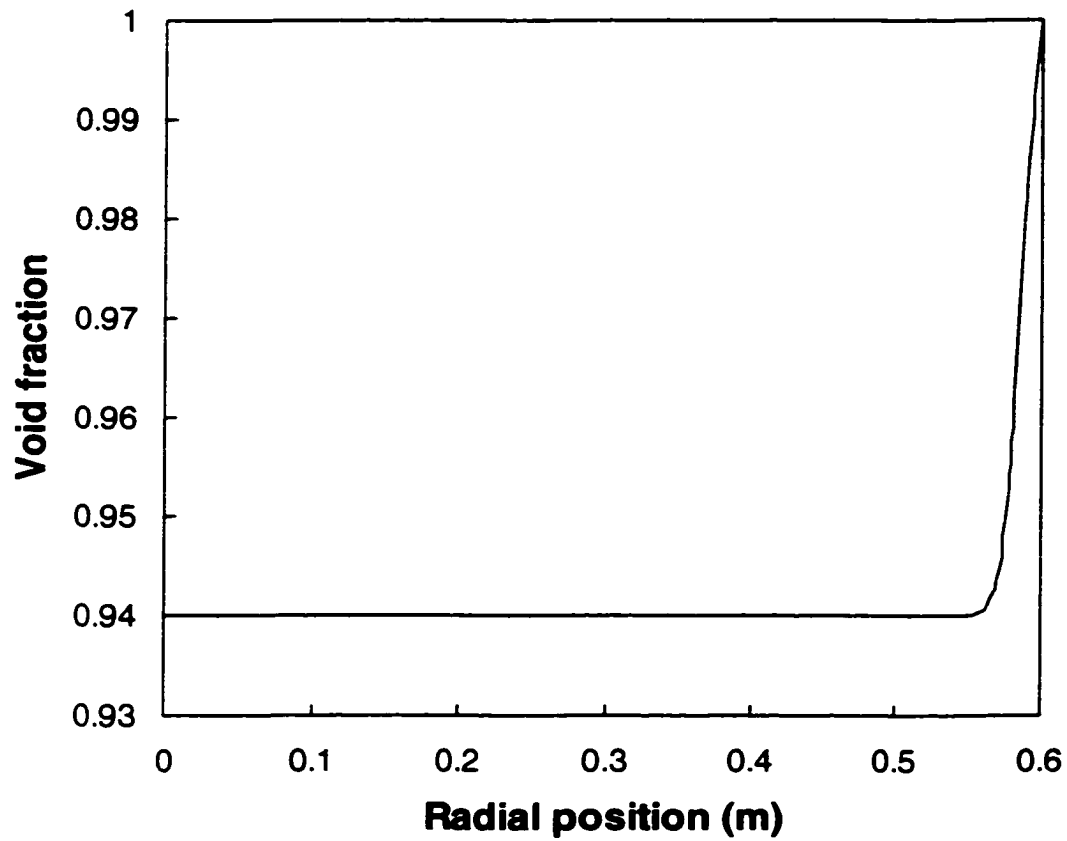
Figure 4.3. Void fraction radial variation for 25.4 mm metal Pall rings as predicted by Equation (4-43).
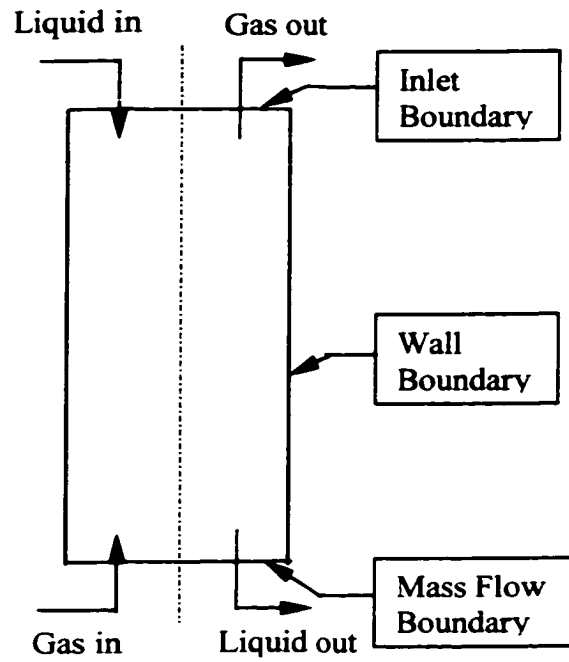
Figure 4.4. Boundary conditions
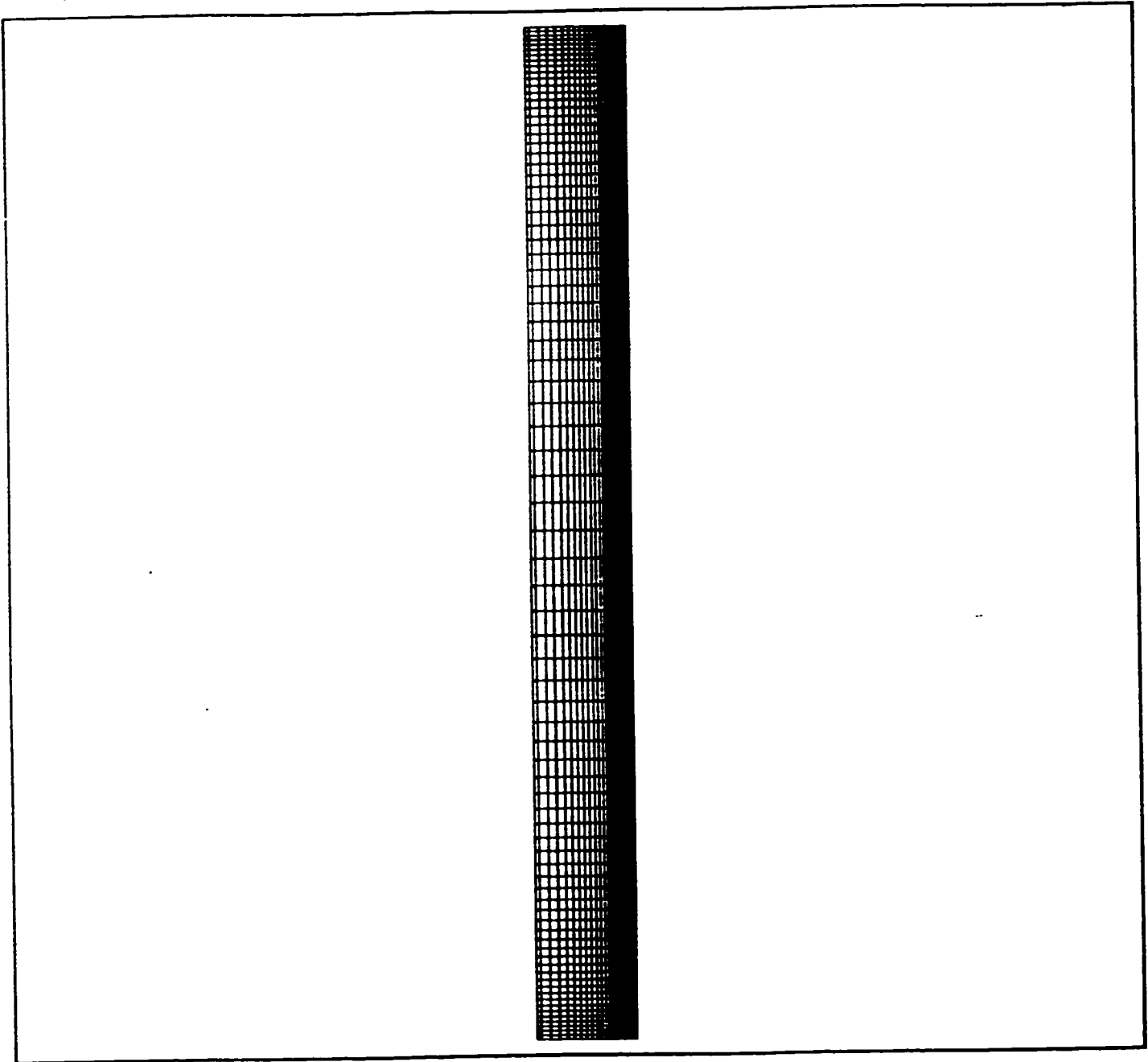
Figure 4.5. A computational grid in z-plane
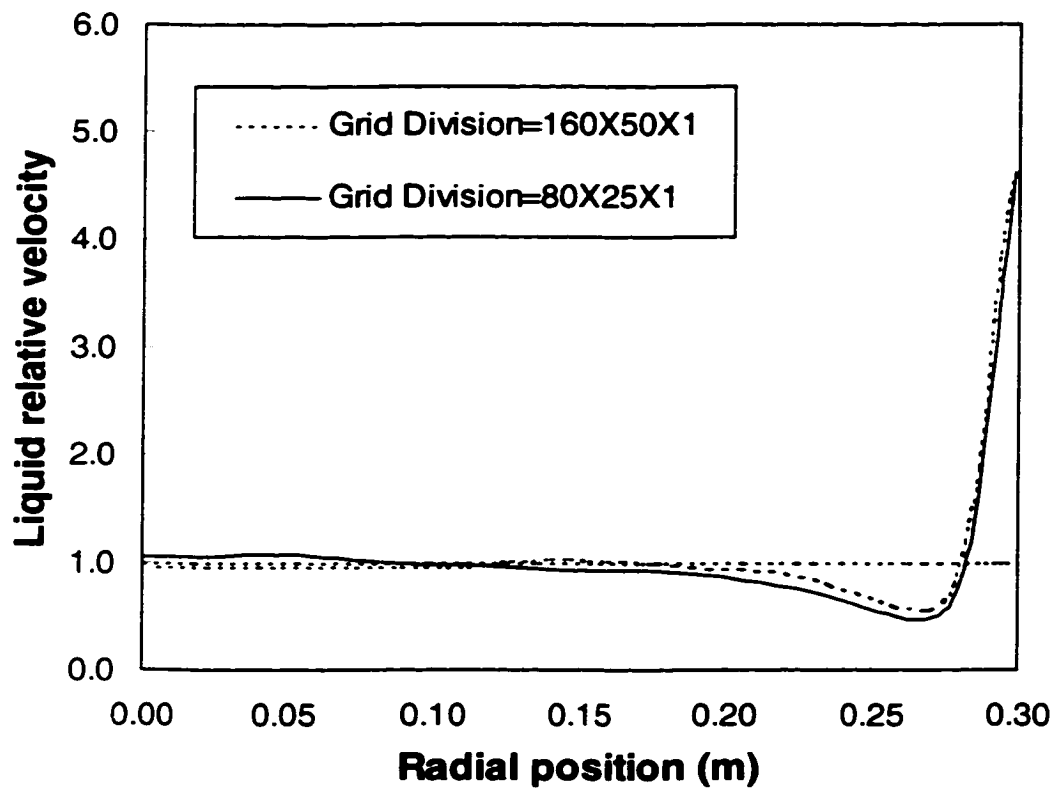
Figure 4.6. Grid independent study

Chapter 5

HYDRODYNAMICS SIMULATIONS–VERIFICATIONS AND PREDICTIONS

5.1 Introduction

This chapter presents the simulation results based on the models proposed in Chapter 4. These simulation results will first be compared with the experimental data, and then the predicted liquid flow distribution will be shown and discussed.

5.2 Simulation Systems and Conditions

To evaluate the models developed in Chapter 4, the simulation results were compared with the experimental data presented in Chapter 3. Both of the liquid distributors used in the experiment were simulated in order to test the ability of the models to capture the liquid spreading characteristics in randomly packed columns. Also, the simulations were carried out with three different systems, namely, water/air, Isopar/air, and cyclohexane/n-heptane (C_6/C_7). The simulation conditions used for water/air and Isopar/air systems are summarized in Table 5.1. The simulation conditions used for C_6/C_7 can be found in Chapter 6.

5.3 Simulation Results and Discussion

5.3.1 Comparison of Simulation with Experiment

Figures 5.1 to 5.3 show a comparison of predicted liquid velocity profiles with the experimental data (obtained with the uniform liquid distributor) for three different packed

124

bed heights: 0.9 m, 1.8 m, and 3.0 m. The simulation results were generated from the two-dimensional, axi-symmetric simulations. The system simulated was water/air. In the simulation a uniform inlet distribution (inlet velocity profile) was assumed for both the liquid phase and gas phase. In these figures, the liquid relative velocity as defined in Chapter 3 is plotted against the radial position. It can be seen that the predicted velocity profiles match the experimental data quite well for all three bed heights. These simulation results were obtained using K_c=2.9×10^{-3} and σ_t=0.01. These two parameters were introduced in the modeling of the dispersion coefficient for volume fraction (see Equations (4-41) and (4-42)). These values of K_c=2.9×10^{-3} and σ_t=0.01 were determined by minimizing the deviations between the predicted and measured liquid velocity profiles at different bed heights. The magnitudes of K_c and σ_t affect the liquid spreading rate. If K_c is too large and σ_t is too small, the predicted liquid wall will be greater than the measured wall flow. On the contrary, if K_c is too small and σ_t is too large, the predicted liquid wall will be smaller than the measured wall flow.

As demonstrated in Chapter 3, the design of liquid distributor is very important for the liquid distribution in packed columns. In the simulation, different liquid distributor designs can be simulated by specifying different liquid inlet distributions at the inlet boundary of the flow domain. For the center inlet liquid distributor used in the experiments, the liquid inlet distribution can be specified as follows: for the center inlet region, which occupied 43% of the column cross section, the liquid inlet velocity and volume fraction was calculated from the known liquid flow rate; for the remainder of the column cross section, a zero value was assigned to the liquid inlet velocity to ensure that there would be no liquid entering the flow domain through this region.

125

Figures 5.4 to 5.6 present the simulation results based on the liquid inlet distribution as described above for three different packed bed heights. The experimental data obtained with the center inlet liquid distributor are also given for comparison. Again it can be seen that there is a good agreement between the predictions and experimental measurements for all three bed heights. It should be pointed out that these simulation results were obtained with the same values of K_c and σ_t used for the case of uniform liquid distributor. This would indicate that these values of K_c and σ_t do give a reasonable account of the liquid spreading when used with the constitutive models proposed in Chapter 4.

Figure 5.7 shows comparisons of the fully developed liquid distributions for the two gas flow rates at the packed bed height of 3 m. The experimental data shown in the figure are based on the water/air system with the uniform liquid distributor. The prediction shows that the liquid flow profiles are almost identical for the two lower gas flow rates of G=0.47 kg/m²s and G=1.13 kg/m²s, indicating a weak dependence of the liquid flow distribution on the gas load in the lower range of gas flow rates. This is consistent with the published experimental data that state neither liquid holdup nor the liquid distribution is significantly influenced by the gas flow below the loading point (Dutkai and Rukenstein, 1970; Hoek et al., 1986; Olujic, Z. and de Graauw J., 1989; Kister, 1992; and Kouri and Sohlo, 1987, 1996).

The validity of the theoretical models is further evaluated through comparing the predicted and measured pressure drops at different gas and liquid loadings. The comparisons are illustrated in Figure 5.8 for two different systems: water/air and Isopar/air. In this figure, the pressure drop data are plotted as a function of the F-factor,

126

which is defined as $u_G \sqrt{\rho_G}$, where u_G is the superficial velocity of gas over the column cross section. The agreement between the theoretical prediction and experimental data is excellent for the water/air system. The relatively larger discrepancy for the Isopar/air system at the higher gas loading is mainly due to the fact that this system has a high viscosity and hence has a lower loading point. The models tend to under-predict the pressure drop for the Isopar/air system at higher gas loads, but the difference is within 12%. In general our models can give a reasonably good prediction of pressure drops.

It can be concluded from these simulation results that the theoretical models developed in this study can capture most of the important flow characteristics related to the large-scale liquid maldistribution in randomly packed columns.

5.3.2 Liquid Flow Distribution Development

After the liquid is introduced to the top of the packed column, uniformly or non-uniformly, it will redistribute as it flows downwards through the column due to the presence of packing. It is of great interest to see how the liquid flow distribution develops along the packed bed height, thus gaining some insight into the mechanism that determines the liquid flow distribution. This can be shown best by examining the case where the liquid was fed into the column only through the central region of the column cross section. Figure 5.9 shows this situation by plotting the predicted liquid flow distribution at different packed bed heights with the 43% liquid inlet distribution. In this figure, u is the liquid local superficial velocity and u_{av} is the liquid average superficial velocity over the column cross section. Thus u/u_{av} is still the liquid relative velocity. The abscissa r stands for the radial position. From this figure, it can be clearly seen that the

127

development of large-scale liquid flow behavior, i.e., the spreading of liquid towards the non-irrigated zone as well as the build up of liquid on the column wall. At the packed bed height of 0 m (the top of the packing), there is no liquid introduced into the peripheral zone (0.196<r<0.3) as shown in Figure 5.9. At the packed bed height of 0.25 m, some liquid can be seen to appear in the non-irrigated zone due to the liquid radial spreading, but the liquid still has not reached the column wall. At the packed bed height of 0.5 m, some liquid already appears on the column wall, and the build up of wall flow has started. As the liquid continues to flow down the column, more liquid moves towards the column wall, and liquid flow rate in the irrigated zone is reduced accordingly. This liquid redistributing process persists throughout the whole length of the packed column. It can be seen from the figure that even at the packed bed height of 3 m the liquid flow distribution is still far from fully developed. It is also worth noting that along with the formation of the liquid wall flow, the zone immediately adjacent to the column wall zone is relatively short of the liquid. Apparently, the accumulation of liquid along the column wall proceeds at the expense of taking liquid away from the region immediately adjacent to the wall region.

A better understanding of the large-scale liquid flow behavior shown in Figure 5.9 can be obtained from Equation (4-41). According to Equation (4-41), liquid spreading occurs when the liquid distribution is not uniform and there is a void fraction variation in radial direction. When the liquid is non-uniformly introduced at the top of the packed column, the liquid spreading initiates immediately from the liquid irrigated zone to the peripheral non-irrigated zone because a pronounced velocity gradient exists along the radial direction. Once the liquid moves into the wall region, the increase in the void

128

fraction along the radial direction induces further migration of liquid towards the column wall causing the increased liquid accumulation in the wall region. However, in the central core region of the packing the spreading rate of liquid appears to be slow because there is no void fraction variation and the radial velocity gradient is almost negligible in this region. This also implies that the turbulent dispersion in this region does not make a significant contribution to the liquid spreading. The simulation results show that the maximum liquid radial spreading velocity occurs in the region near the top of the column and its typical maximum value, expressed in terms of the radial interstitial velocity V, is of the order of 10^{-3} m/s.

From the simulation results shown in Figure 5.9, it can be seen that the non-uniform liquid inlet distribution, in the form of a shortage of liquid near the column wall, discontinuties or zonal flow caused by the poor design and/or the malperformance of liquid distributors, can have a serious effect on the liquid distribution in the packing. Therefore, the quality of the initial liquid distributions can be an important cause for packing efficiency loss found in practice.

As shown in Figure 5.10, the liquid flow pattern development along the packed bed height for the uniform inlet distribution is considerably different from that shown in Figure 5.9 with the 43% liquid inlet distribution. Liquid wall flow starts to build up immediately after the liquid is introduced into the top of the column. As the liquid flows downwards, the liquid wall flow continues increasing because of the spreading ability of liquid in the packed column. The build up of liquid wall flow shows to be a relatively rapid process, especially in the top part of the column. A relatively stable liquid distribution across the column cross section is achieved at the packed bed height of about

2 m, after that height only a small variation in the liquid velocity profile occurs. A similar variation in the liquid flow pattern with the packed bed height was also reported by Kouri and Sohlo (1987, 1996) based on their experimental observation. Note, the two simulations used to provide the data shown in Figures 5.9 and 5.10 used the same packing structure and the same gas and liquid flow rates, hence it would be expected that the fully developed flow patterns would be very similar regardless of the initial distribution at the top of the packing after enough long bed height. Our simulation results show that the packed bed height required for the flow to reach a fully developed state depends strongly on the design of liquid distributors.

The large-scale liquid flow behavior for the case of a uniform liquid inlet distribution is again dependent on the spreading features of liquid in the packed column. With the uniform liquid inlet distribution, i.e., the liquid is distributed evenly over the top layer of packing, the spreading of liquid starts immediately due to the void fraction variation in the wall region. The relatively lower flow resistance in the wall region causes more liquid to accumulate on the column wall. However, the build up of wall liquid in turn yields a reverse velocity gradient and hence induces an adverse driving force that hinders the liquid from further migration towards the wall region. This implies that the two effects corresponding to the two terms on the right hand side of Equation (4-41) will eventually balance each other to bring the flow distribution to the equilibrium (fully developed state). Hence, as can be seen form Figure 5.10, the speed of the liquid wall flow rate increase gradually decreases with the packed bed height until a relatively stable liquid flow pattern is reached at a packed bed height of about 2 m.

130

5.3.3 Quantification of Liquid Maldistribution

The liquid flow distributions in randomly packed columns can be further characterized by a maldistribution factor defined as (Kouri and Sohlo, 1987)

$$Mf = \left(\sum_i \frac{A_i}{A} \left(1 - \frac{u_i}{u_{av}} \right)^2 \right)^{0.5} \tag{5-1}$$

where A_i is the area of the ith cell perpendicular to the main flow direction of liquid, A is the area of the column cross section, u_i is the average liquid superficial velocity over the area A_i, and u_{av} is the superficial liquid velocity based on the column cross sectional area. Obviously, when the liquid has a uniform distribution over the column cross section, Mf equals zero. Higher value of Mf means higher degree of liquid maldistribution.

The calculated maldistribution factors based on the results shown in Figures 5.9 and 5.10 are presented in Figure 5.11. As can be seen, Mf increases with the packed bed height for the case of uniform inlet distribution and reaches a steady state value of about 0.67. For the 43% liquid inlet distribution, a very rapid decrease in Mf occurs in the region near the top of the column and at the packed bed height of 1.2 m Mf reaches its minimum value of 0.54. After that height the build up and development of liquid wall flow induce a gradual increase in Mf towards a finial steady state value.

The behavior of maldistribution factor for the uniform liquid inlet case can be explained as follows. At the top of the column, the value of Mf should be zero because there is no liquid maldistribution there. The increase in Mf along the packed bed height is due to the increase of the liquid wall flow. It can be seen that the increase of Mf value is

131

very fast near the top of the column due to the rapid build up of the liquid wall flow in that region. Since the liquid flow distribution reaches a fully developed state at the packed bed height of about 2 m, the value of Mf can be seen to approach a steady state value after that packed bed height.

For the case of the 43% liquid inlet distribution, the initial Mf value is expected to be very large because the liquid inlet velocity profile is highly maldistributed. The rapid decrease in the Mf value with the packed bed height in the top region of the column means that the large irregularities of the liquid flow distribution caused by the liquid distributor are smoothed out very quickly. After the packed bed height of 1.2 m, where the minimum value of Mf happens, the gradual increase in the liquid wall flow causes a gradual increase of Mf.

5.3.4 The Development of Liquid Wall Flow

Figure 5.12 shows the development of liquid wall flow with packed bed height for water/air system at two different liquid flow rates. The simulation results shown are for the case with the uniform liquid inlet distribution. As can be seen in Figure 5.12, an increase in the liquid flow rate results in a more rapid development of the liquid wall flow towards a steady state value. Furthermore, the relative liquid wall flow is reduced somewhat with the increase of the liquid flow rate. For example, for a liquid flow rate of 2.91 kg/m^{2}s, the relative liquid wall flow approaches a steady state value of about 5.1 at a packed bed height of 2.5 m. However, a steady state relative wall flow of about 4.5 is attained in a shorter packed bed height of about 1.6 m, at the higher liquid rate of 6.66 kg/m^{2}s. These predicted features are in agreement with the experimental observations and

132

published data reported by Templeman and Porter (1965) and Kouri and Sohlo (1996). These results would indicate that higher liquid flow rates tend to produce a relatively lower liquid wall flow and reduces the packed bed height required for the liquid to reach its fully developed state.

Figure 5.13 shows that the physical properties of the liquid phase can have a significant effect on the value of the liquid wall flow and the packed bed height required to reach a steady state value. This effect is attributed mainly to the larger difference in liquid viscosity between water and Isopar. With an increase of the liquid viscosity, the viscous resistance becomes more important, especially in the radial direction because the radial velocity component is generally about two orders of magnitude less than that axial velocity component. Obviously the relatively high radial viscous resistance will reduce the liquid spreading ability and hence leads to a slower development of liquid wall flow and a considerable decrease in the steady state value.

5.3.5 Three-Dimensional Simulation

From a practical point of view, uniform initial liquid distribution is virtually impossible to realize in any experiment, because practical distributors have a specific number of drip points, which are designed to distribute liquid as uniformly as possible. To test the validity of the two-dimensional simulations, three-dimensional simulations were also carried out with a uniform liquid distributor used in this study and a TDP distributor used in FRI (Shariat and Kunesh, 1995). In the three-dimensional simulations, the liquid inlet condition was specified in such a way that it exactly simulated the number of drip points, that is, there was liquid flow under the drip points, and there was no liquid

133

flow between the drip points. In the two-dimensional simulation, however, the liquid was assumed to be distributed uniformly across the column cross section.

The uniform liquid distributor used in this study had 31 drip points (drip point density=110 points/m^2). To simulate the design of this liquid distributor, 31 liquid drip points were distributed over the top of the bed in terms of their relative locations on the liquid distributor. The computational domain was divided into 80(axial)×28(radial)×48 (circumferential) control volumes. The diameter of the central drip point was 1/60 m, which was greater than the true diameter of drip points of the liquid distributor to account for the splashing of liquid on the top layer of the packing. Although the other holes (drip points) could not be designed in circular shape due to the size of the computational cell used, their radial lengths were specified in such a way that their drip areas were exactly the same as that of the central hole.

The three-dimensional simulation results are presented in Figures 5.14 to 5.17. The simulation conditions used are the same as those used in the two-dimensional simulation of the uniform inlet distribution (see Figure 5.10). It can be seen from these figures, that there exists an inlet region near the top of the packed bed in which the liquid flow behavior is significantly different from that predicted using the assumption of the uniform inlet distribution. As can be expected, the liquid velocity profile predicted using the three-dimensional simulation is irregular. The local high values in the velocity profile correspond to the drip points of the liquid distributor. As the liquid flows down the column, these local irregularities smooth out very rapidly, and the liquid streams from the drip points merge at a very short packed bed height (less than 0.04 m).

Figure 5.18 shows a comparison of the liquid velocity profiles generated from three-dimensional simulation (120×50×48) and two-dimensional simulation (120×50) using the TDP distributor for the C_6/C_7 system. This distributor had 121 drip points (drip point density=104 points/m^2). As can be seen, the two profiles are already very similar at a packed bed height of 0.5 m. It may be concluded from the simulation results that the liquid spreading in the top inlet region of a packed column is a very fast process. In the inlet region the liquid spreads both radially and circumferentially, which facilitates liquid to redistribute itself over the column cross section. However, further development of liquid flow pattern towards fully developed state depends mainly on the liquid spreading ability in the radial direction.

Generally the time consumed to run a three-dimensional simulation is very long compared with that required for the two-dimensional simulation. For 1000 iterations, a three-dimensional simulation needs about 20 hours on an IBM RS/6000 (43P Model 260), however, only about 0.4 hour is required for a two-dimensional simulation on the same machine. The two-dimensional simulation can be considered as a best comprise from the computational time required and reasonably good predictions obtained as presented in the plots

5.4 Conclusions

The validity of theoretical models presented in Chapter 4 is demonstrated by comparing the predicted liquid flow distributions with the experimental data obtained from a 0.6 m diameter column packed with 25.4 mm stainless steel Pall rings. The

135

simulation results showed that the theoretical models proposed in this study can capture the important flow characteristics resulting from the large-scale liquid maldistribution in randomly packed columns.

Simulations were carried out for the water/air and the Isopar/air systems for two initial liquid distributions. Based on these simulation results it can be concluded that the liquid spreading ability in a randomly packed column can have a significant effect on the build up of liquid wall flow and the development of the liquid flow pattern towards a fully developed state. The factors affecting the liquid spreading ability are shown to be the physical properties of liquid phase, radial void fraction variation, and liquid and gas flow rates. At higher liquid flow rates, the liquid spreading ability is improved and leads to a more rapid development of liquid wall flow. For a higher viscous liquid such as Isopar the liquid spreading ability is reduced due to the increase of the viscous resistance.

The large-scale liquid maldistribution caused by the 43% liquid inlet distribution indicates that the initial liquid distribution is an important factor affecting the performance of randomly packed columns. Moreover, the three-dimensional simulation results show that the assumption of the uniform initial liquid distribution (thus permitting the two-dimensional simulation) is applicable provided that a liquid distributor is designed with a sufficient high drip point density and the drip points are geometrical symmetric.

5.5 Nomenclature

A	Cross Sectional Area, m^2
F-factor	Defined as $u_G \sqrt{\rho_G}$, $(m/s)(kg/m^3)^{0.5}$
G	Gas Flow Rate, $kg\ m^{-2}\ s^{-1}$
H	Packed Bed Height, m
K_c	Parameter in Equation (4-40), m^2 s
L	Liquid Flow Rate, $kg\ m^{-2}\ s^{-1}$
Mf	Maldistribution Factor
r	Radial Coordinate, m
u	Superficial Velocity, $m\ s^{-1}$
V	Interstitial Velocity, $m\ s^{-1}$

Greek Symbol

ρ	Density, $kg\ m^{-3}$
σ_t	Turbulent Prandtl Number

Subscript

av	Average
G	Gas Phase
i	Index of Control Volume

137

5.6 References

Dutkai, E. and Ruckenstein, E., (1970) New Experiments Concerning the Distribution of a Liquid in a Packed Column. *Chem. Eng. Sci.* **25**, 483-488.

Kister, H. Z., (1992) *Distillation Design*, McGraw-Hill, New York.

Kouri, R. J. and Sohlo, J., (1987) Liquid and Gas Flow Patterns in Random and Structured Packings. *I. Chem. E. Symp. Ser.* No. 104, B193-B211.

Kouri, R. J. and Sohlo, J., (1996) Liquid and Gas Flow Patterns in Random Packings. *Chem. Eng. J.* **61**, 95-105.

Olujic, Z. and de Graauw J., (1989) Appearance of Maldistribution in Distillation Columns Equipped with High Performance Packings. *Chem. Biochem. Eng.* **Q3 (4)**, 181-196.

Shariat, A. and Kunesh, J. G., (1995) Packing Efficiency Testing on a Commercial Scale with Good (and Not So Good) Reflux Distribution. *Ind. Eng. Chem. Res.* **34**,1273-1279.

Templeman, J. J. and Porter, K. E., (1965) Experimental Determination of Wall Flow in Packed Columns *Chem. Eng. Sci.* **20**, 1139-1140.

Table 5.1 Detailed Simulation Conditions Used

Column diameter (m)	0.6
Column height (m)	0~3
Packing	25.4 mm S.S. Pall ring
Average void fraction	0.94
Packing factor (1/m)	174
Liquid density (water) (kg/m^3)	1000
Liquid density (Isopar) (kg/m^3)	788
Liquid viscosity (water) (Pas)	0.001
Liquid viscosity (Isopar) (Pas)	0.00246
Gas density (air) (kg/m^3)	1.2
Gas viscosity (air)(Pas)	0.00175

139
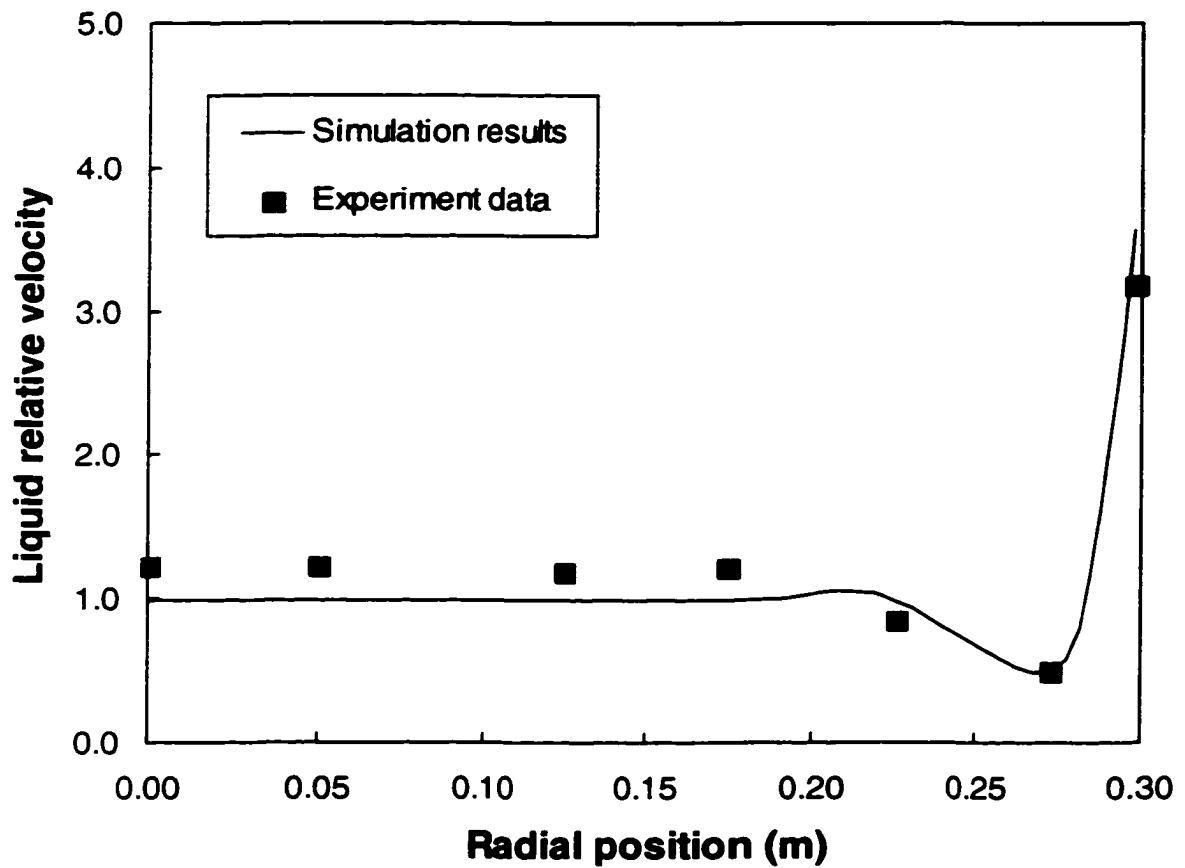
Figure 5.1. Comparison of liquid flow distribution between simulation and experiment for the uniform liquid inlet, water/air system; H= 0.9 m; L=4.78 kg/m²s; G=0.75 kg/m²s.
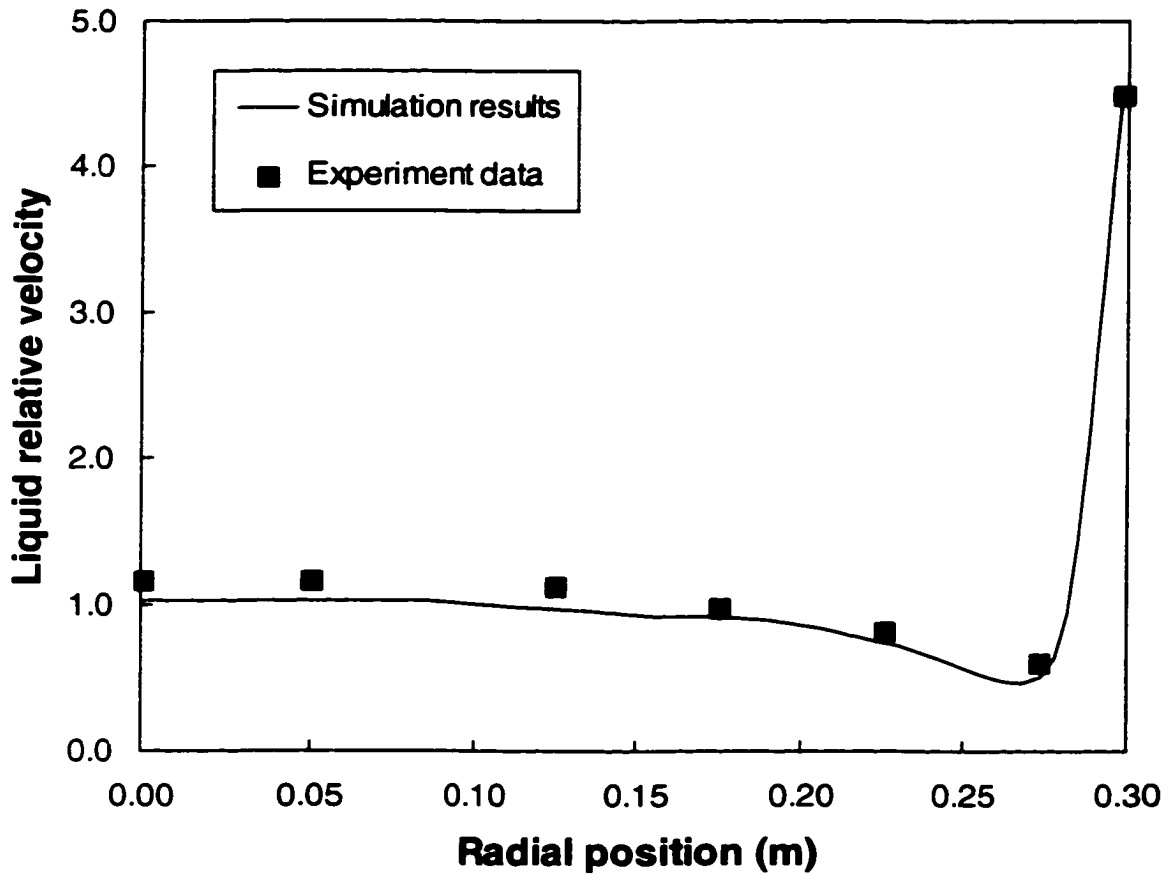
Figure 5.2. Comparison of liquid flow distribution between simulation and experiment for the uniform liquid inlet, water/air system; H= 1.8 m; L=4.78 kg/m²s; G=0.75 kg/m²s.

141
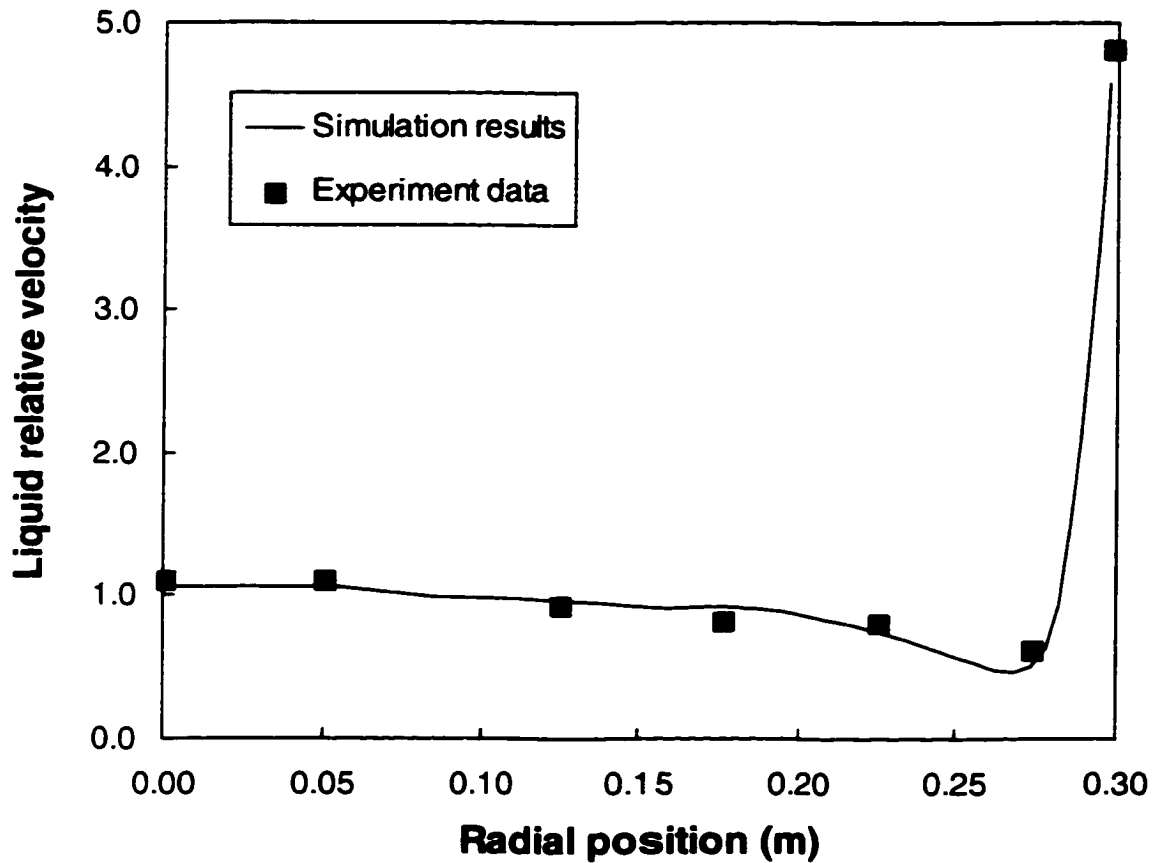
Figure 5.3. Comparison of liquid flow distribution between simulation and experiment for the uniform liquid inlet, water/air system; H= 3.0 m; L=4.78 kg/m^{2}s; G=0.75 kg/m^{2}s.
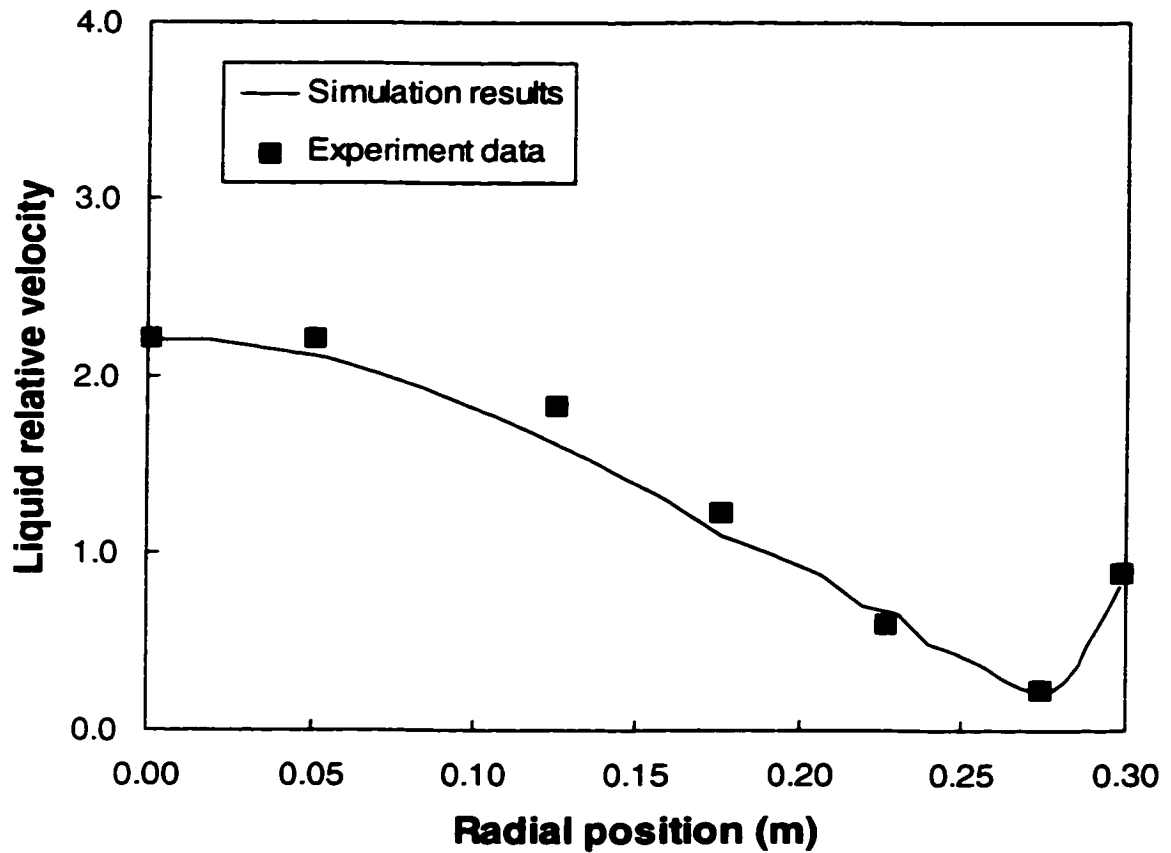
Figure 5.4. Comparison of liquid flow distribution between simulation and experiment for the 43% liquid inlet, water/air system; H= 0.9 m; L=4.78 kg/m^{2}s; G=0.75 kg/m^{2}s.
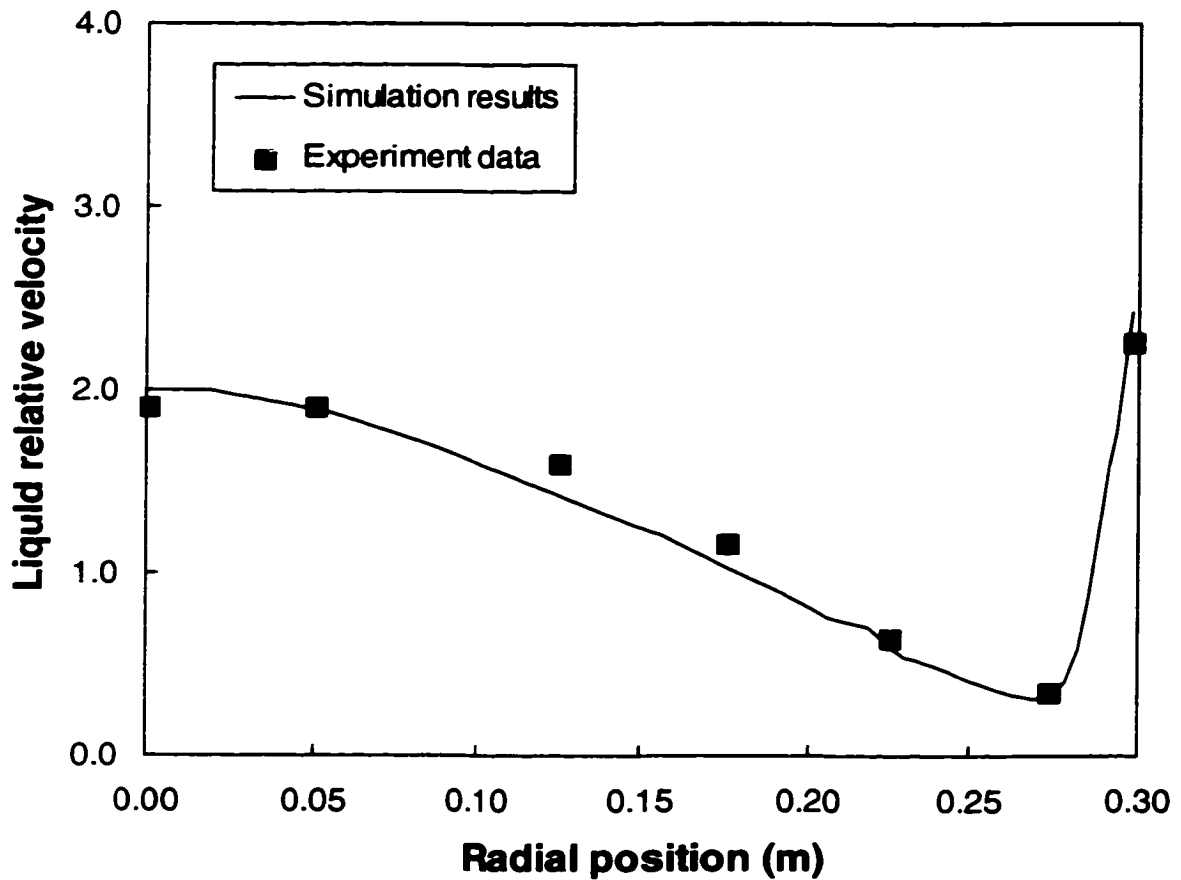
Figure 5.5. Comparison of liquid flow distribution between simulation and experiment for the 43% liquid inlet, water/air system; H= 1.8 m; L=4.78 kg/m^{2}s; G=0.75 kg/m^{2}s.

144
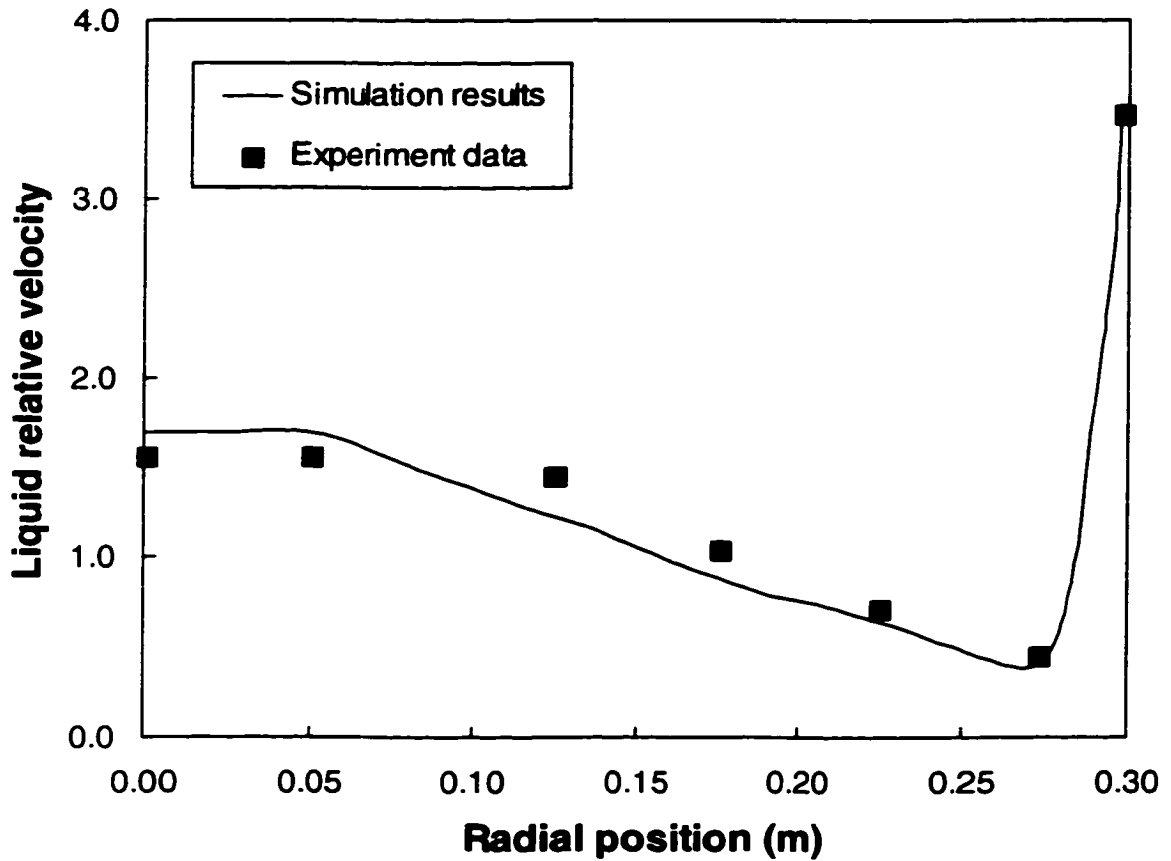
Figure 5.6. Comparison of liquid flow distribution between simulation and experiment for the 43% liquid inlet, water/air system; H= 3.0 m; L=4.78 kg/m²s; G=0.75 kg/m²s.
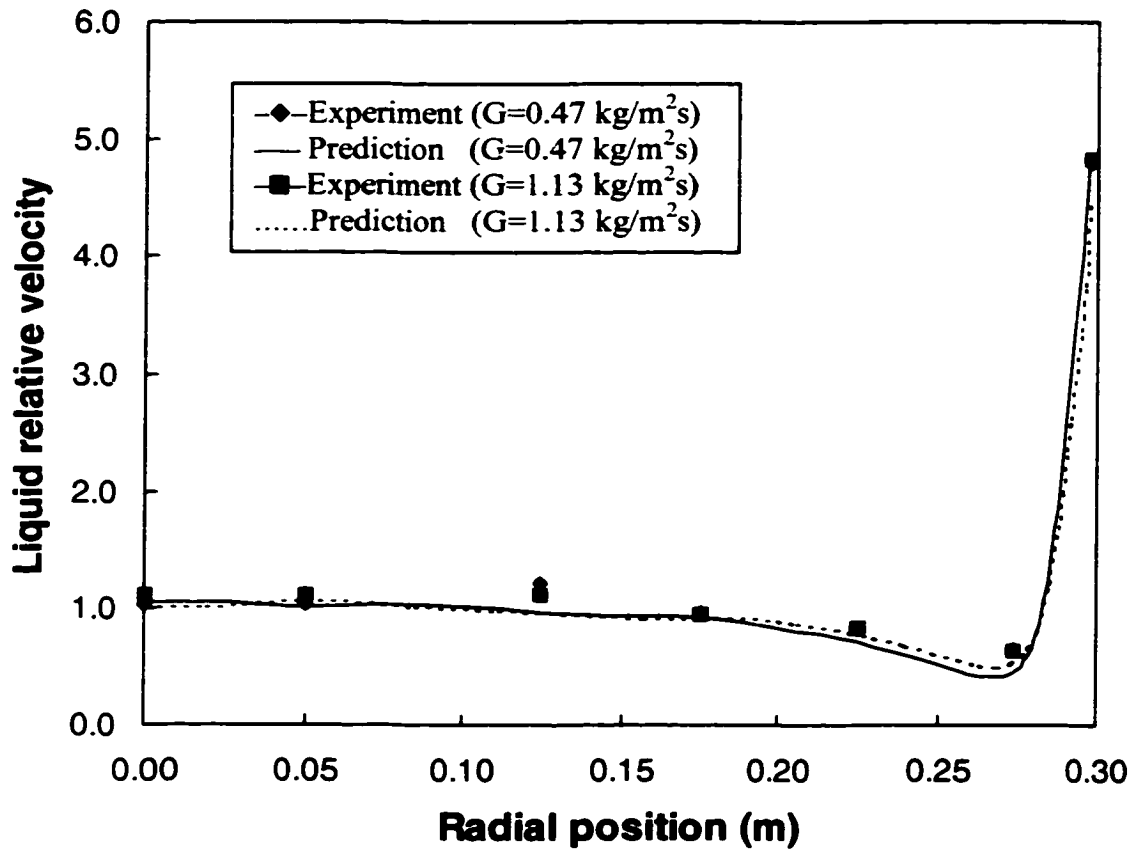
Figure 5.7. Comparison of liquid flow distribution at different gas flow rates for the uniform liquid inlet distribution, water/air system; H= 3.0 m; L=4.78 kg/m^{2}s.
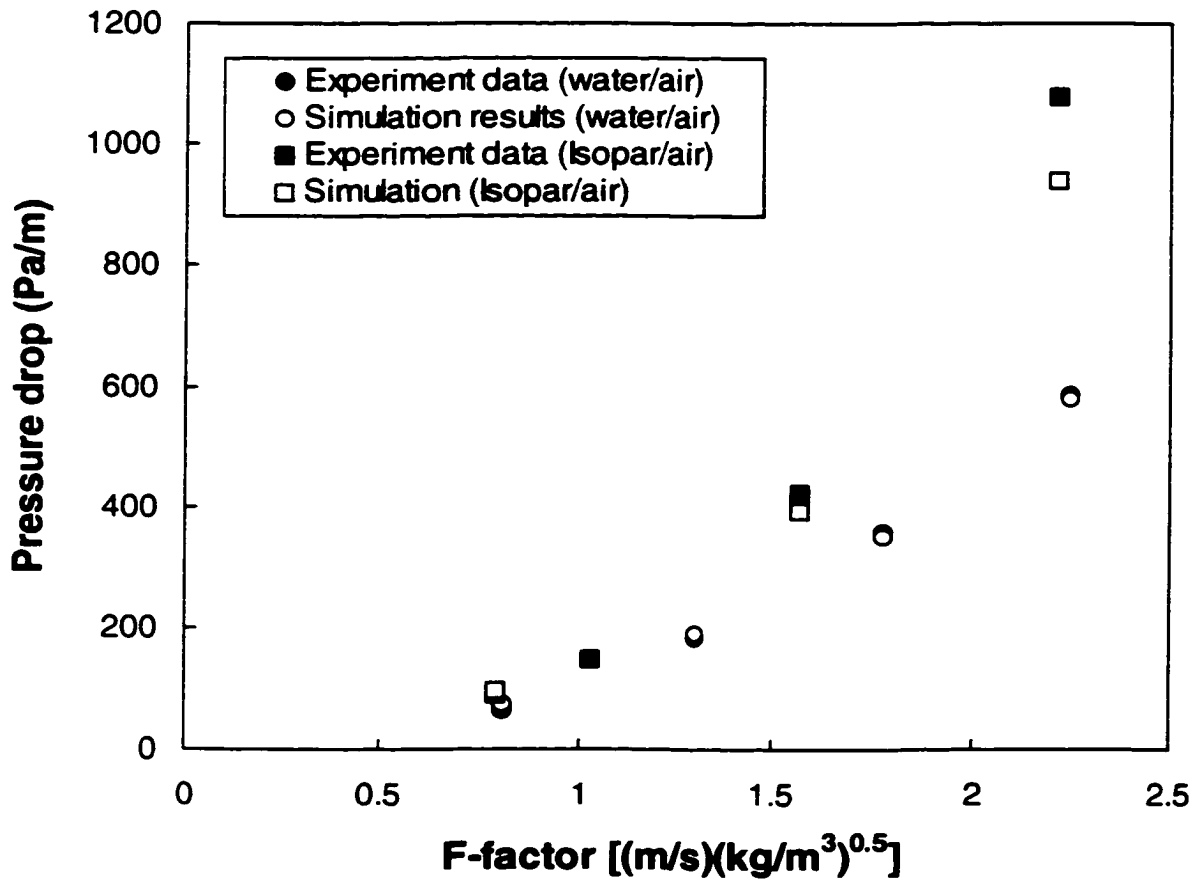
Figure 5.8. Comparison of predicted pressure drop with experiment, System: water/air (L=1.69 kg/m²s) and Isopar/air (L=4.78 kg/m²s); Liquid inlet distribution: uniform; H=3.0 m.

147
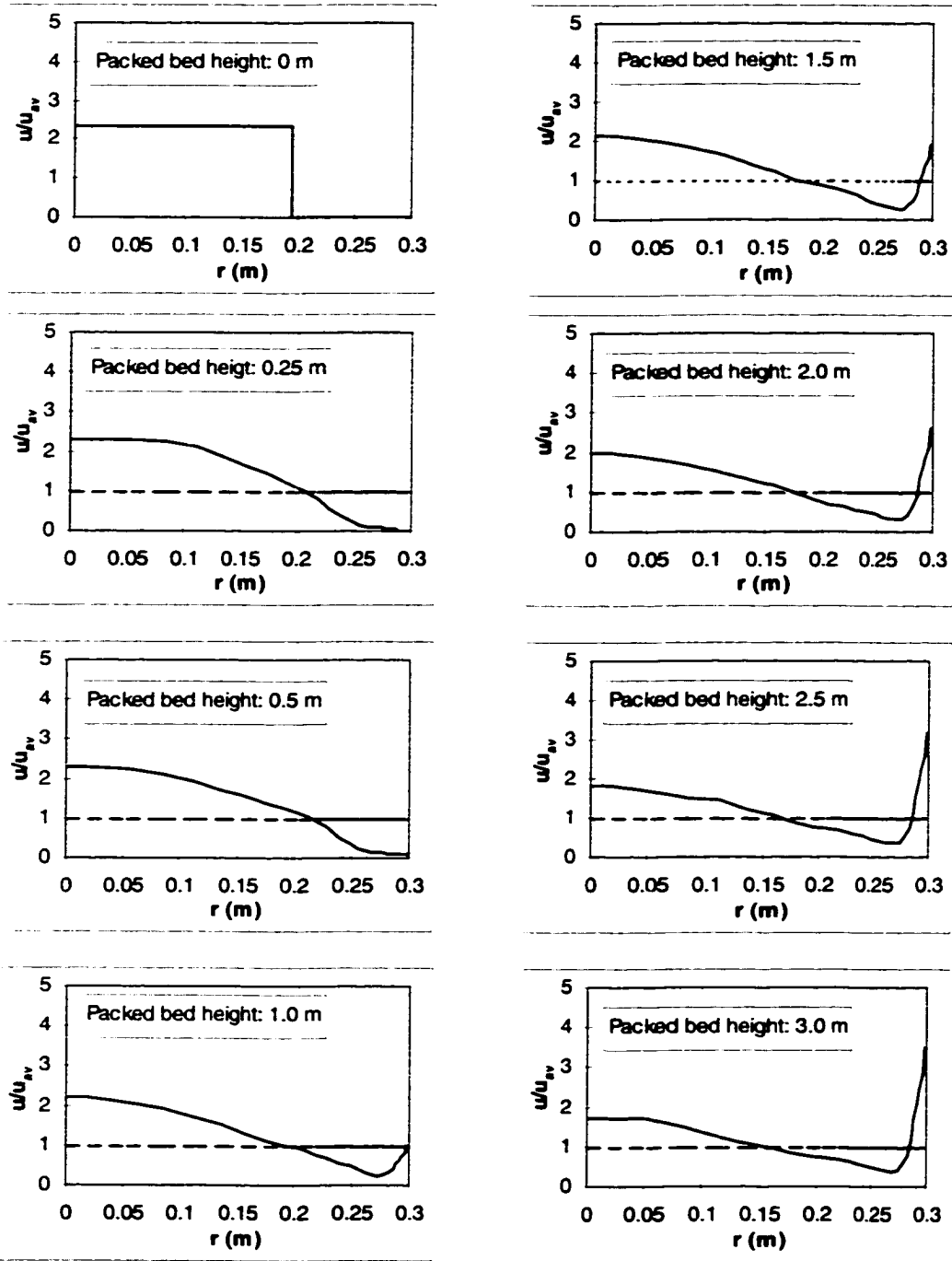
Figure 5.9. Development of predicted liquid flow patterns with the 43% liquid inlet distribution; water/air system; L=4.78 kg/m²s; G=0.75 kg/m²s.

148
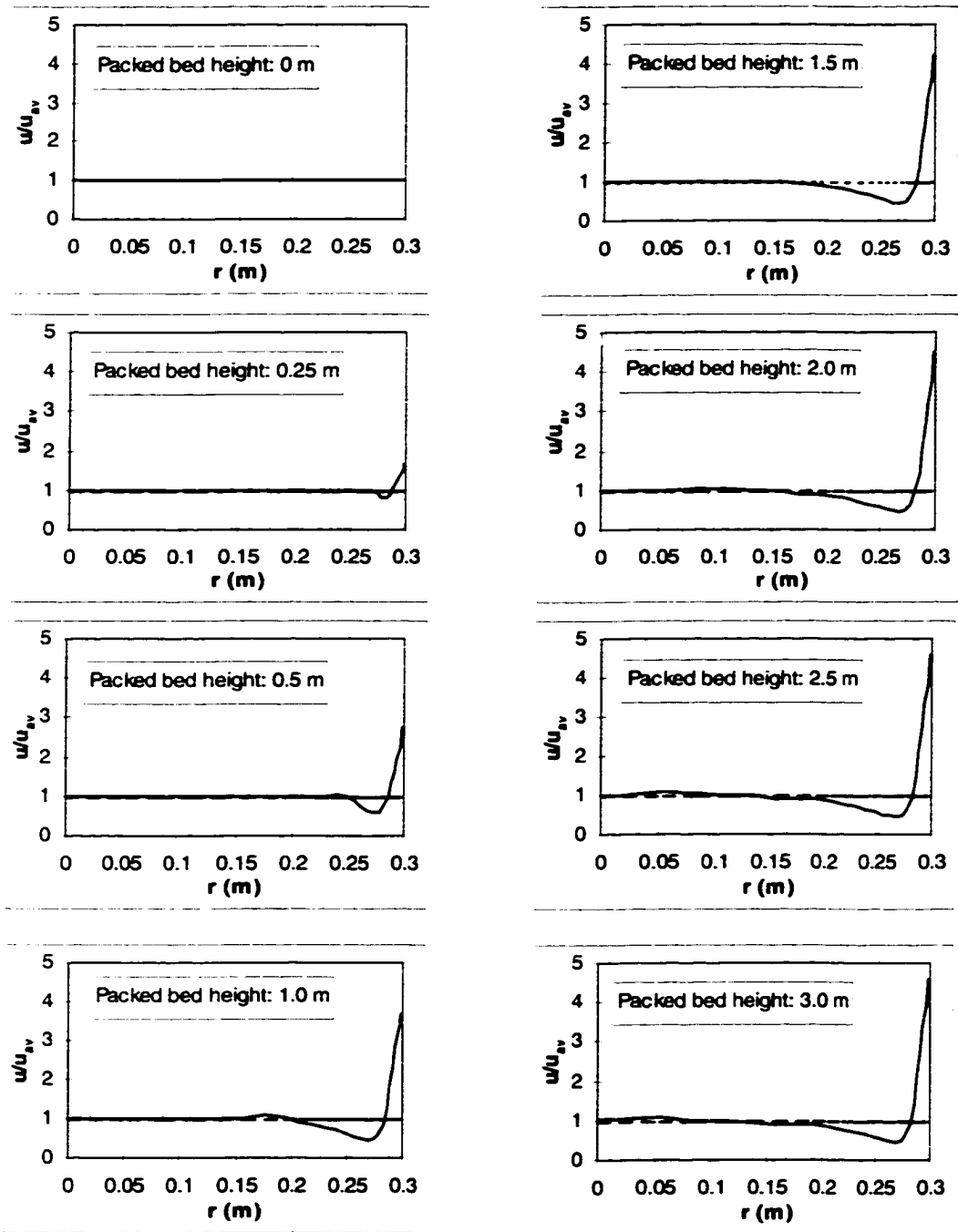
Figure 5.10. Development of predicted liquid flow patterns with the uniform liquid inlet distribution; water/air system; L=4.78 kg/m^{2}s; G=0.75 kg/m^{2}s.
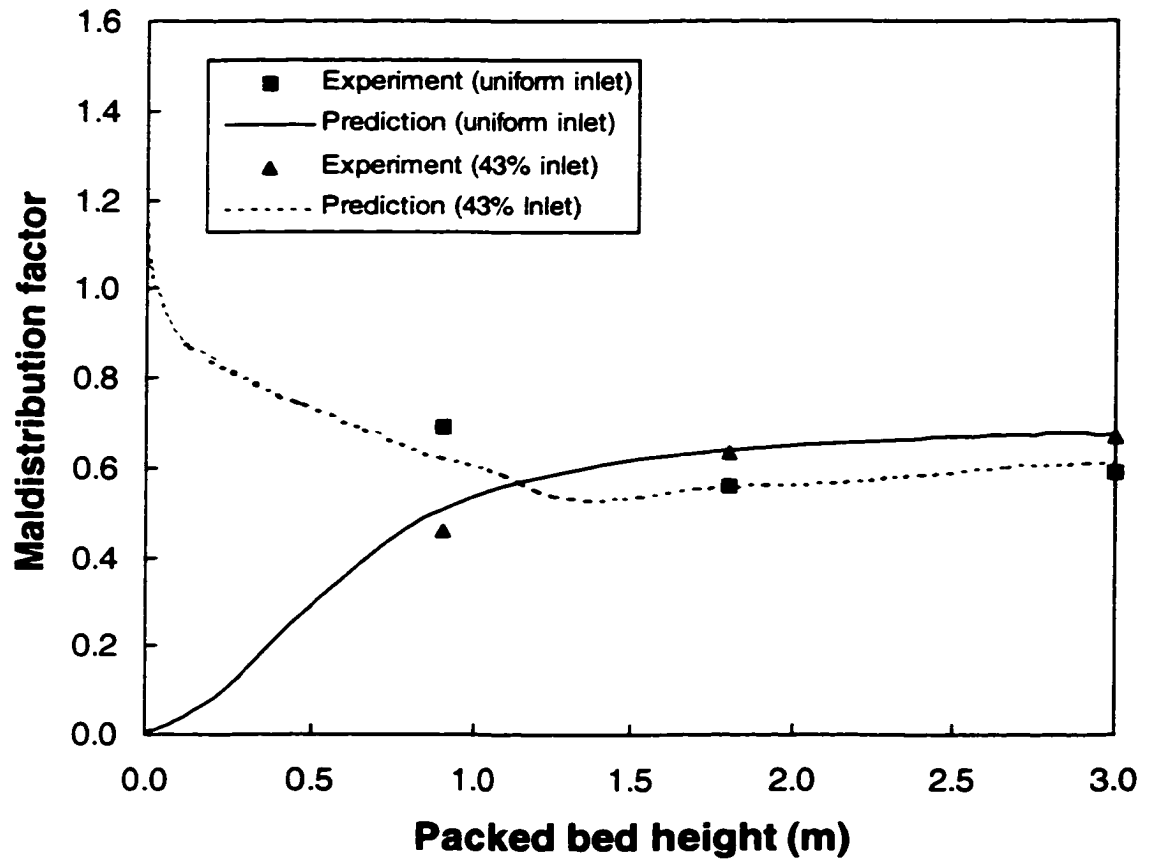
Figure 5.11. Comparison of liquid maldistribution factors with different liquid inlet distributions, water/air system; L=4.78 kg/m²s; G=0.75 kg/m²s.
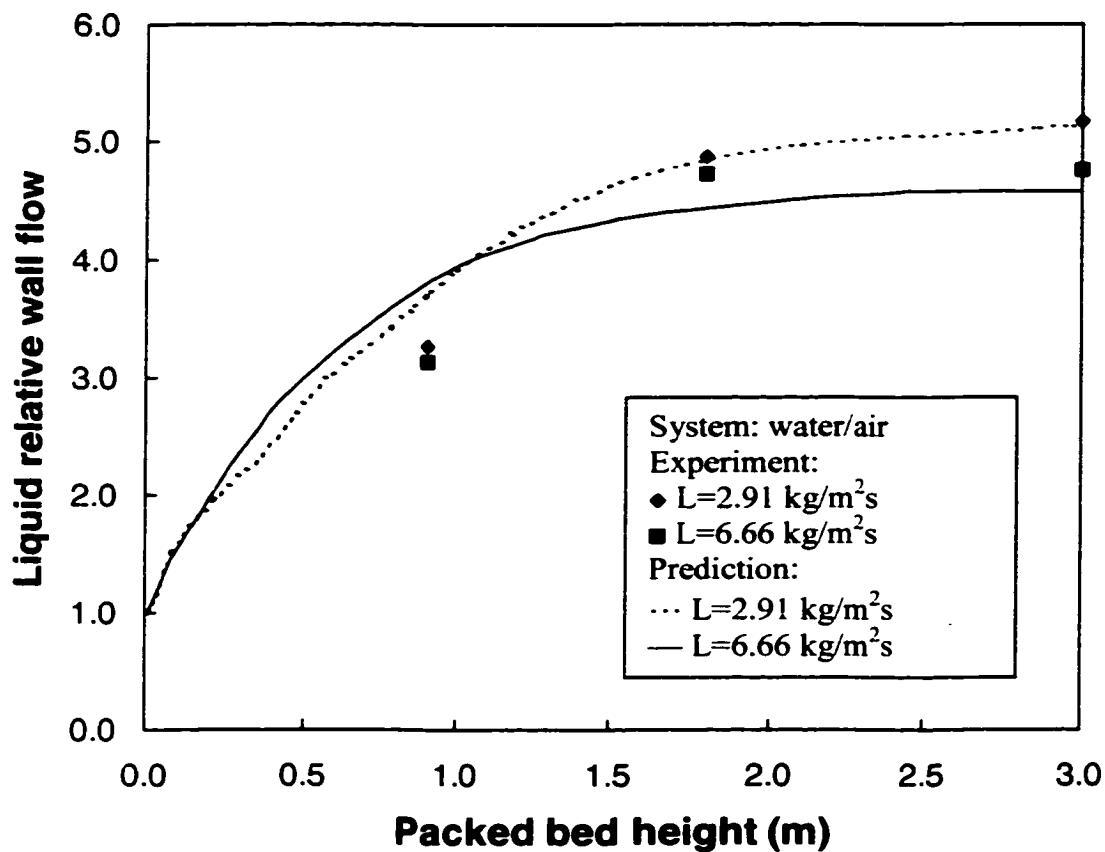
Figure 5.12. Development of liquid wall flow along the packed bed height at the gas flow rate of 0.75 kg/m²s for the uniform liquid inlet distribution.

151
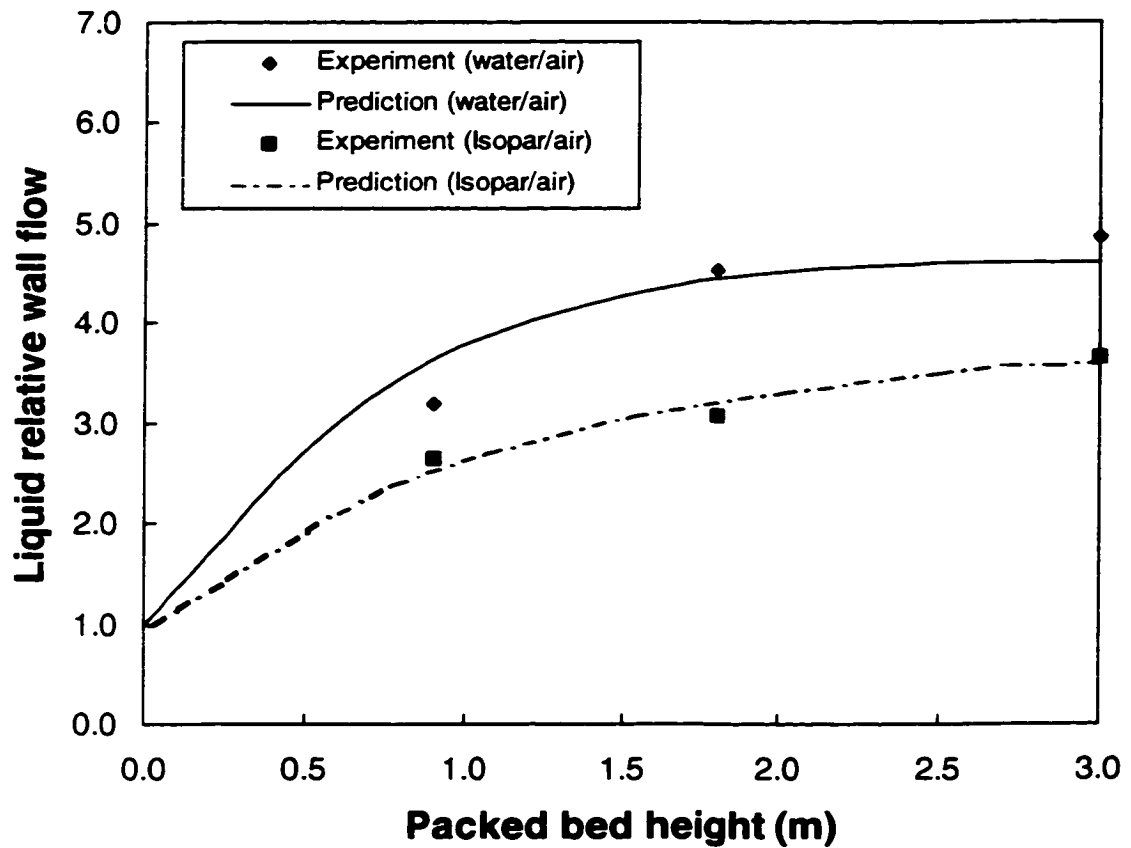
Figure 5.13. Development of liquid wall flow along the packed bed height for water/air and Isopar/air systems with a uniform liquid inlet distribution, $L=4.78$ kg/m^{2}s; $G=0.75$ kg/m^{2}s
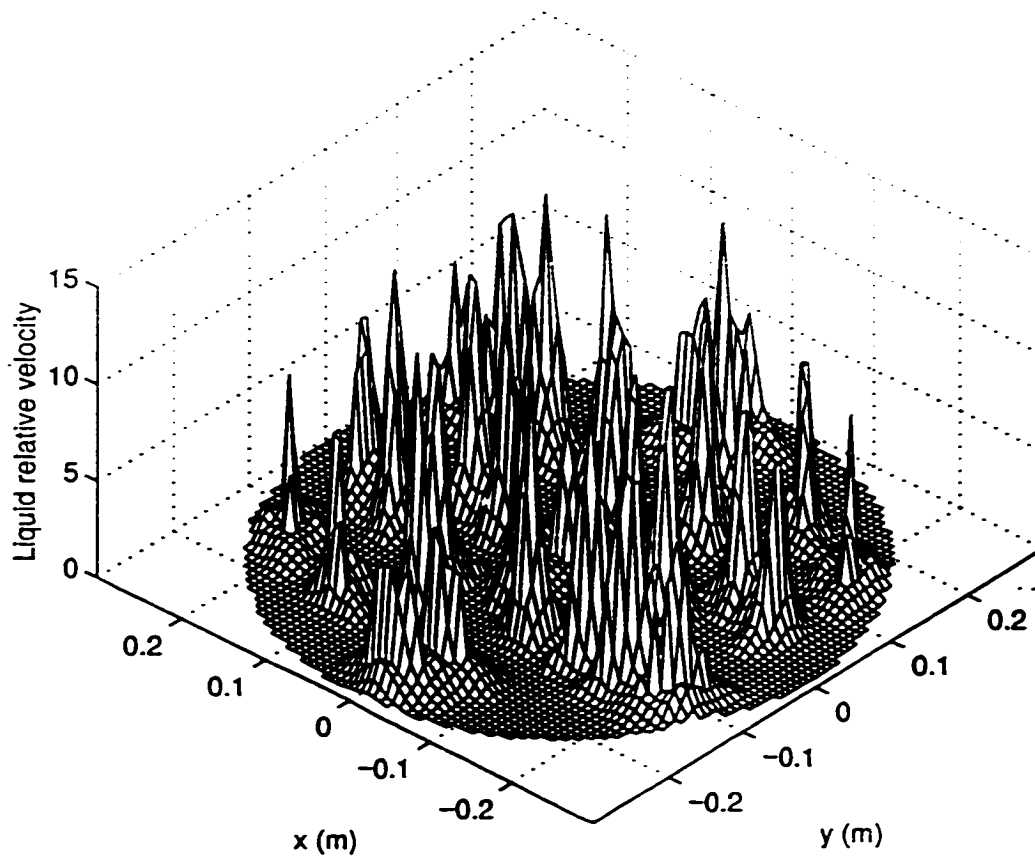
Figure 5.14. Liquid velocity profile generated from 3D simulation at the packed bed height of 0.0125 m, water/air system; L=4.78 kg/m^{2}s; G=0.75 kg/m^{2}s.
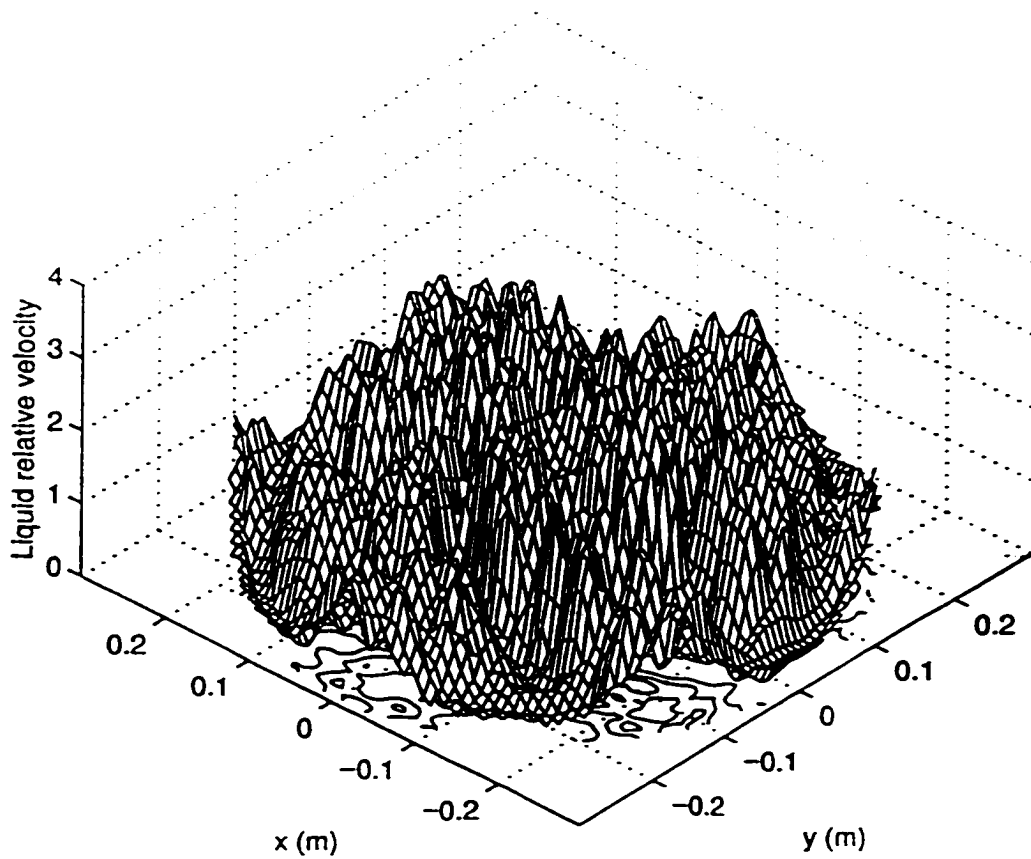
Figure 5.15. Liquid velocity profile generated from 3D simulation at the packed bed height of 0.0875 m, water/air system; L=4.78 kg/m^{2}s; G=0.75 kg/m^{2}s.

154
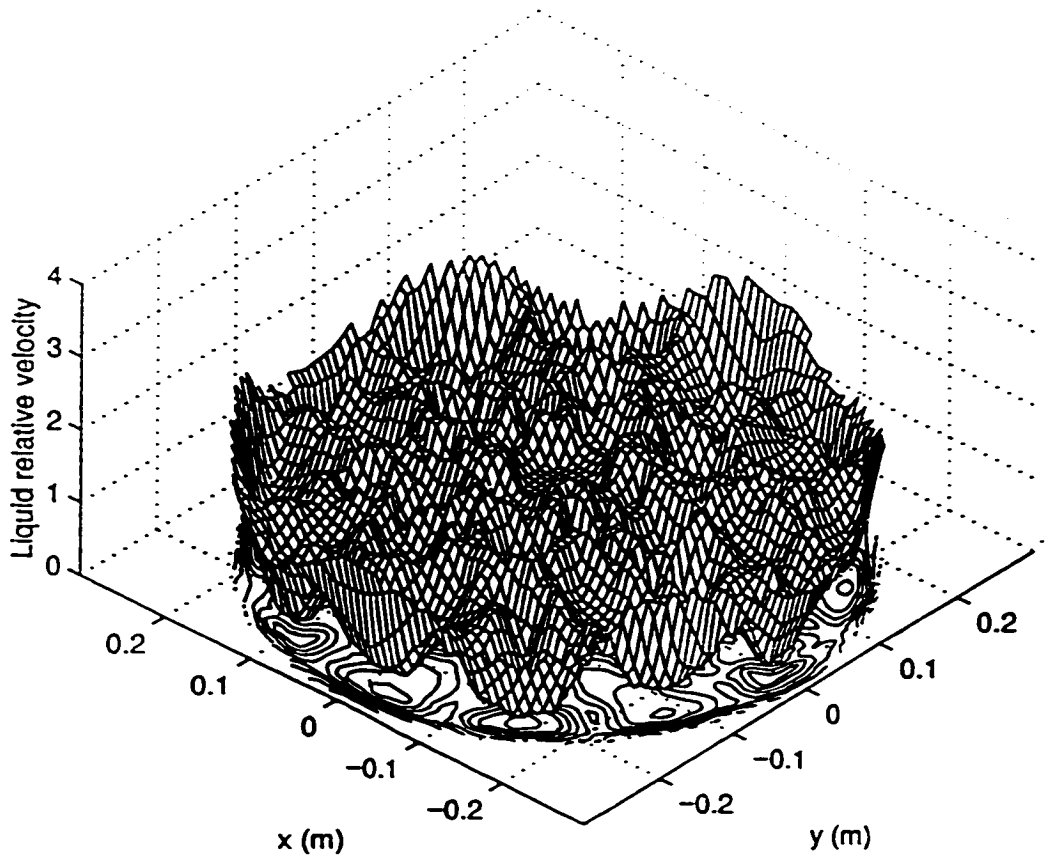
Figure 5.16. Liquid velocity profile generated from 3D simulation at the packed bed height of 0.2375 m, water/air system; L=4.78 kg/m^{2}s; G=0.75 kg/m^{2}s.
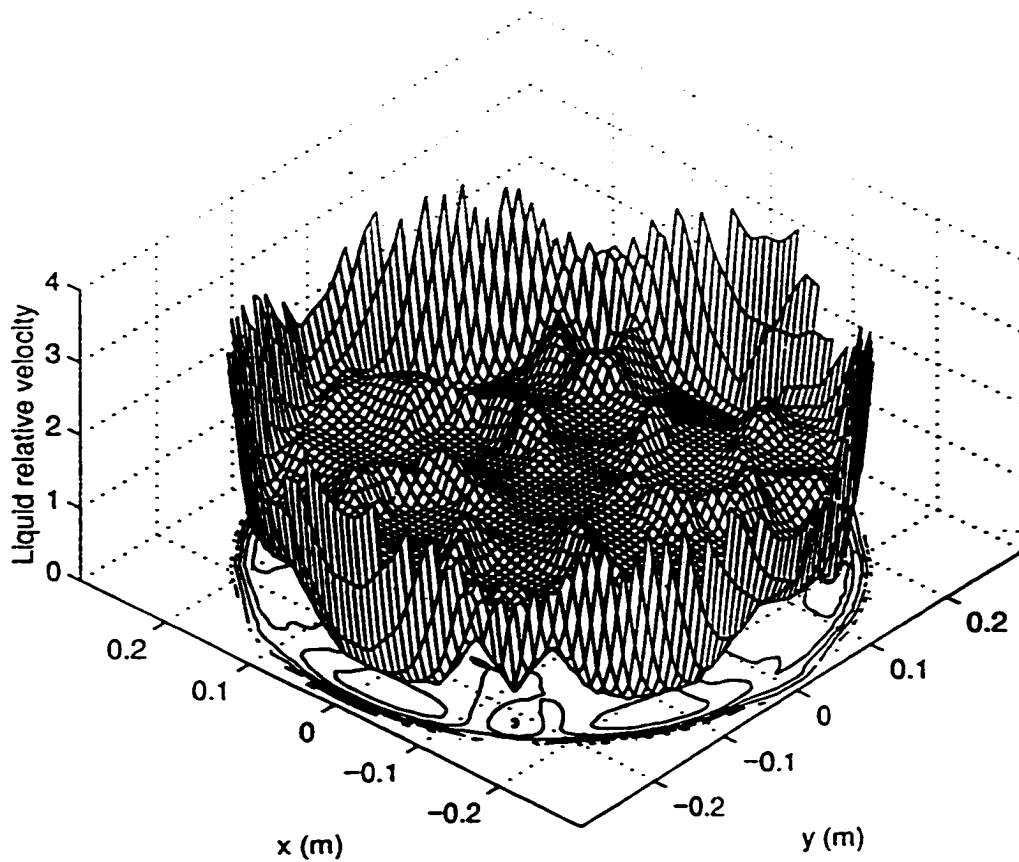
Figure 5.17 Liquid velocity profile generated from 3D simulation at the packed bed height of 0.4375 m, water/air system; L=4.78 kg/m^{2}s; G=0.75 kg/m^{2}s.
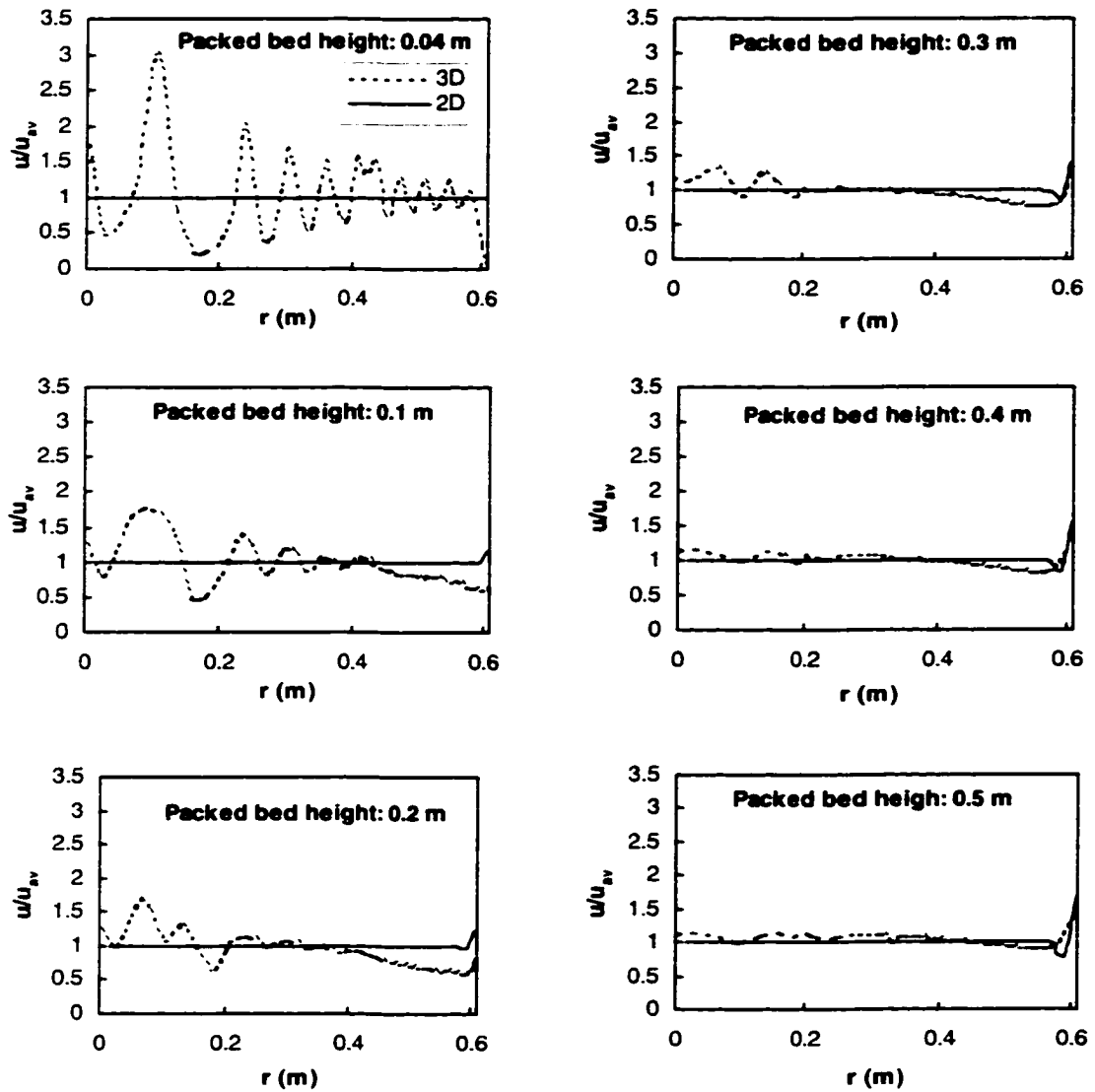
Figure 5.18. Comparison of liquid velocity profiles from two-dimensional and three-dimensional simulations, C_6/C_7 system; F-factor: 1.18 $(m/s)(kg/m^3)^{0.5}$; Operating pressure: 165.5 kPa; 25.4 mm Pall rings.

Chapter 6

CFD MODELING OF THE MASS TRANSFER PROCESSES

6.1 Introduction

Design, scale-up and performance analysis procedures for packed columns have been traditionally based on macroscopic mass balances, assuming homogeneous conditions along the radial direction. Such simple models lead to design procedures based on the unidirectional variation of concentration in the axial direction and hence to the concepts of HTU (Height of a Transfer Unit) and NTU (Number of Transfer Units). It is important to realize that these concepts rely on observations made at the macroscopic (or equipment) scale, i.e. only inlet and outlet flow rates and concentrations are measured (Wankat, 1988).

The standard design equation may be written as (Wankat, 1988; Kister, 1992)

$$Z = HTU \times NTU \tag{6-1}$$

$$HTU = \frac{G}{K_G a_e p M_A} \tag{6-2}$$

$$NTU = \int_{y_0}^{y_L} \frac{dy}{y^* - y} \tag{6-3}$$

Using macroscopic data and assuming the transfer processes (both flow conditions and interfacial mass transfer) to be uniform throughout the packed bed, the performance of the column can be analyzed. The overall mass transfer coefficient $K_G a_e$ is assumed to be uniform not only over a given cross sectional area, but also with height of the column.

158

The influence of the flow conditions on mass transfer is captured only indirectly through $K_G a_e$. If the flow distributions can not scale up properly with increasing equipment size, then a corresponding error in $K_G a_e$ will occur. For example, parameters such as wettability of the packing material and the interfacial system properties (such as surface tension) do not change with the equipment scale, however, other variables such as gas and liquid flow distributions in the packing, do change with the scale of the equipment.

Successful design and scale-up of packed columns require a model that captures the basic transport phenomena on the correct length scale. Concepts based on Height of a Transfer Unit (HTU) and Number of Transfer Units (NTU) obtained from the inlet and outlet conditions alone are not adequate for scale-up purposes as both HTU and NTU depend on the flow conditions and interface transfer taking place at the scale of the packing but not at the scale of the equipment. The existing design procedures for large diameter packed columns are uncertain due to lack of the understanding of liquid flow distribution in such columns (Olujic and de Graauw, 1989; Kister, 1992). Height Equivalent to a Theoretical Plate (HETP), characterizing the mass transfer efficiency of a packed column, varies very strongly and erratically with the changes in type and size of packing, liquid and gas flow conditions and fluid physical properties. The complex mechanisms that influence HETP have not been modeled in a rigorous way in the first generation models that assume conditions within a column to be homogeneous in the radial direction and neglect dispersion in all directions (Kister, 1992).

Chapter 4 has presented the flow distribution models and in Chapter 5 these models have been verified by comparison with experimental data. The next phase of the

159

packed column modeling is to incorporate flow hydrodynamic models into mass transfer models to simulate and analyze the mass transfer process. Having ability to capture radial and axial variations in flow and mass transfer conditions, the models will predict the overall separation efficiency based on the detailed local flow and mass transfer conditions. As outlined in Chapter 4 for the hydrodynamics simulations, the volume averaged mass transfer equations also require closure models to describe (a) the inter-phase mass transfer and (b) the mass dispersion coefficients. The simulation results using this set of closure models will be compared with the published FRI (Fractionation Research, Inc.) data, which were obtained from a commercial size 1.22 m diameter column (Shariat and Kunesh, 1995[*]). Since the experiments were conducted with a liquid distributor of relatively high drip point density (about 104 points/m^2), it can be assumed that the inlet distribution is uniform, thus permitting axisymmetric (or two-dimensional) simulations.

In this chapter, the necessary models to simulate the mass transfer process are presented. The reasons for choosing the FRI data to evaluate the simulation are: (1) they have reported all the necessary information required for the simulation purposes such as the column height, the column diameter, the packing size, inlet/outlet flow rates and concentrations; (2) they have reported not only the overall separation efficiency data, but also the concentration profiles along the packed bed height; and (3) they have reported data on different packing sizes over a wide range of operating conditions.

---

[*] Additional data were obtained through private communication with the authors.

6.2 Mathematical Models

6.2.1 Transport Equations for Mass Fraction

Transport equations for mass fractions $Y_{i\alpha}$ in the general form can be written as

$$\frac{\partial}{\partial t}(\gamma_\alpha \rho_\alpha Y_{i\alpha}) + \nabla \cdot [\gamma_\alpha (\rho_\alpha U_\alpha Y_{i\alpha} - \Gamma_\alpha \nabla Y_{i\alpha})] = \sum_{\beta=1,\beta \neq \alpha}^{N} \dot{m}_{\alpha\beta}^i \qquad \begin{array}{l} \alpha = 1,\cdots\cdots,N \\ \\ i = 1,\cdots\cdots,N_C \end{array} \qquad (6\text{-}4)$$

where γ is the volume fraction of a certain phase, Y is the mass fraction of the ith component in a particular phase, U is the interstitial velocity, ρ is the density, N is the number of phases, N_C is the number of components in each phase, Γ is the effective mass dispersion coefficient, and $\dot{m}_{\alpha\beta}^i$ is the mass of the ith component transferred from phase β to phase α per unit time per unit volume. For a fixed phase α, Equation (6-4) includes N_C equations, but only $N_C - 1$ equations are independent, since mass fraction Y must sum to one.

$$\sum_{i=1}^{N} Y_i = 1 \qquad (6\text{-}5)$$

Equations (6-4) are the general form of the transport equation for the mass fractions assuming species i is present in all phases. If a particular species is not present in a given phase, the mass fraction of that particular species is set to zero.

In solving Equations (6-4) for the concentration field, the variables such as interstitial velocities and volume fractions must be known. These variables can be determined in the same way as those outlined in Chapter 4.

6.2.2 The Closure Models

Before the set of partial differential equations describing the concentration fields for both the vapor and liquid phases can be solved, the following closure models are required.

6.2.2.1 Inter-Phase Mass Transfer

For binary distillation, both the liquid and vapor phases contain two components, say, A and B, with A being the more volatile component (see Figure 6.1). If phase equilibrium has not been reached, then mass transfer between liquid and gas phases will occur. According to the two-film theory, the mass transfer rate of component A can be calculated by one of the following two equations

$$\dot{m}_{LG}^{A} = k_{L} a_{e} M_{A} \left(x_{A} - x_{A}' \right) \tag{6-6}$$

$$\dot{m}_{LG}^{A} = k_{G} a_{e} M_{A} \left(y_{A}' - y_{A} \right) \tag{6-7}$$

where k_{L} and k_{G} are the individual mass transfer coefficients for the liquid and vapor phases, respectively, a_{e} is the effective interfacial area, M_{A} is the molecular weight of the more volatile component A, x_{A} and y_{A} are the mole fractions of component A in the liquid and vapor phases, respectively, and x_{A}' and y_{A}' are the interfacial mole fractions of component A in the liquid and vapor phase, respectively. The two-film theory assumes that there is no mass transfer resistance at the interface and this means that x_{A}' and y_{A}' must be in equilibrium which may be described by

$$y_{A}' = \frac{\alpha x_{A}'}{1 + (\alpha - 1) x_{A}'} \tag{6-8}$$

162

where α is the relative volatility.

Since $x_A + x_B = 1$ and $y_A + y_B = 1$ for binary systems, the phase equilibrium relation for component B can be readily obtained

$$y_B' = \frac{\frac{1}{\alpha}x_B'}{1 + \left(\frac{1}{\alpha} - 1\right)x_B'} \tag{6-9}$$

where y_B' and x_B' are the interfacial mole fractions of component B in the vapor and liquid phases, respectively.

Combining Equations (6-6), (6-7) and (6-8) results in (Appendix B)

$$\frac{\alpha - 1}{k_L k_G (a_e M_A)^2}(\dot{m}_{LG}^A)^2 + \left[\frac{(\alpha - 1)y_A - \alpha}{k_L a_e M_A} - \frac{(\alpha - 1)x_A + 1}{k_G a_e M_A}\right]\dot{m}_{LG}^A + \{\alpha x_A - [(\alpha - 1)x_A + 1]y_A\} = 0 \tag{6-10}$$

Equation (6-10) indicates that the local mass transfer rate $\dot{m}_{LG}^A$ is related to the local concentrations x_A and y_A, individual mass transfer coefficients k_L and k_G, and the interfacial mass transfer area a_e.

There are several correlations available in the literature that can be used to predict the mass transfer coefficients for random packings (Wagner et al. 1997; Kister, 1992). From preliminary studies, it was found that Onda's formulas provided the most reasonable results in terms of separation efficiency compared with the experimental data from FRI (Appendix C), therefore, Onda's formulas (1968a, b) were used in the simulation.

The k_L and k_G are calculated as (Onda et al., 1968 a,b)

163

$$k_L = 0.0051 \left(\frac{\mu_L g}{\rho_L} \right)^{\frac{1}{3}} \left(\frac{L}{a_w \mu_L} \right)^{\frac{2}{3}} \left(\frac{\mu_L}{\rho_L D_L} \right)^{-\frac{1}{2}} \left(a_p d_p \right)^{\frac{2}{5}} \qquad (6\text{-}11)$$

$$k_G = k_p \left(a_p D_G \right) \left(\frac{G}{a_p \mu_G} \right)^{\frac{7}{10}} \left(\frac{\mu_G}{\rho_G D_G} \right)^{\frac{1}{3}} \left(a_p d_p \right)^{-2.0} \qquad (6\text{-}12)$$

where k_p is the model parameter. According to Onda et al. (1968a,b), the value of the parameter k_p depends on the size of packing. For the ring size greater than 15 mm, k_p=5.23, otherwise, k_p=2.0.

The wetted surface area a_w was calculated by (Onda et al., 1968 a,b)

$$\frac{a_w}{a_p} = 1 - exp \left[-1.45 \left(\frac{\sigma_c}{\sigma} \right)^{\frac{3}{4}} \left(\frac{L}{a_p \mu_L} \right)^{\frac{1}{10}} \left(\frac{L^2 a_p}{\rho_L^2 g} \right)^{-\frac{1}{20}} \left(\frac{L^2}{\rho_L \sigma a_p} \right)^{\frac{1}{5}} \right] \qquad (6\text{-}13)$$

where σ_c is the critical surface tension of the packing material. For steel σ_c=75.0 dynes/cm (Kister, 1992).

The effective vapor-liquid interfacial mass transfer area was assumed to be equal to the wetted area in Onda's correlations (Onda et al., 1968 a,b)

$$a_e = a_w \qquad (6\text{-}14)$$

In Equations (6-4) the transport variables for mass are mass fractions. However mole fractions are normally used in mass transfer models. Mole fractions are related to mass fractions by

$$x_A = \frac{X_{AL}/M_A}{X_{AL}/M_A + X_{BL}/M_B} \qquad (6\text{-}15)$$

$$y_A = \frac{Y_{AG}/M_A}{Y_{AG}/M_A + Y_{BG}/M_B} \qquad (6\text{-}16)$$

164

where x and y represent mole fractions, and X and Y stand for the mass fractions.

6.2.2.2 Dispersion Coefficient

Mass dispersion tends to reduce the mass transfer driving force, thus having an adverse effect on the separation efficiency. Its effect can be taken into account through proper specification of the mass dispersion coefficients in the mass transfer equations. For the ring type of packing, the mass dispersion in the liquid phase and vapor phase can be modeled as (Wang et al., 1985; Zuiderweg and Nutter, 1992)

$$Pe_L = 5.337 \times 10^{-4} \, Re_L^{0.472} \, Re_G^{0.293} \left(\frac{d_e}{D_c} \right)^{-0.867} \tag{6-17}$$

$$Pe_G = \frac{u_G}{22 u_L + u_G} \tag{6-18}$$

where d_e is the equivalent diameter of the packed column and defined as

$$d_e = \frac{4 \varepsilon_p}{a_p} \tag{6-19}$$

and Re_L and Re_G are defined in terms of d_e

$$Re_L = \frac{d_e L}{\mu_L} \tag{6-20}$$

$$Re_G = \frac{d_e G}{\mu_G} \tag{6-21}$$

The dispersion coefficients for liquid phase and vapor phase can then be calculated as

$$\Gamma_L = \frac{\rho_L u_L d_e}{Pe_L} \tag{6-22}$$

165

$$\Gamma_G = \frac{\rho_G u_G d_p}{Pe_G}$$

(6-23)

6.2.3 Determination of Mass Transfer Efficiency

There are two conventional models used for mass transfer rate analysis in randomly packed columns. The HETP model, which treats a packed column as a series of theoretical stages, is based on the equilibrium-stage concept. Although the HETP concept is widely used for packed distillation column design, it lacks the fundamental mechanism involved in the mass transfer occurring in a packed column. The HTU model, on the other hand, is more physically sound because it is based on the mass transfer rate between the liquid and vapor phases.

In the HTU model, the packing height can be calculated as $Z = HTU \times NTU$. From the simulation, detailed information about the flow distribution and mass concentration distribution within the packed column is available, therefore the local Height of a Transfer Unit (HTU) and Number of Transfer Units (NTU) can be calculated as follows

$$N_{OGl} = \int_{y_{u}}^{y_{u,u}} \frac{dy}{y_A^* - y_A}$$

(6-24)

and

$$H_{OGl} = \frac{\Delta Z}{N_{OGl}}$$

(6-25)

where H_{OG} and N_{OG} are the height of an overall vapor phase transfer unit and the number of overall vapor phase transfer units, respectively. Similarly other local quantities such as

166

local individual film transfer units H_{Gl} and N_{Gl} can be defined. The relationship between the local overall height of a transfer unit and the local individual film transfer unit is given by

$$H_{OGl} = H_{GL} + m_l \frac{G_l}{L_l} H_{Ll} \qquad (6\text{-}26)$$

The local HETP at a point can be determined from the local H_{OG}

$$HETP_l = H_{OGl} \frac{ln\left(m_l \frac{G_l}{L_l}\right)}{m_l \frac{G_l}{L_l} - 1} \qquad (6\text{-}27)$$

In the above discussion, m_l is the local slope of the equilibrium line, defined as

$$m_l = \frac{\alpha}{\left[1 + (\alpha - 1)x_A\right]^2} \qquad (6\text{-}28)$$

6.3 Overview of CFD Based Models

In order to predict the mass transfer efficiency of a packed column, the detailed velocity distribution and concentration distribution are required. These distributions can be determined by CFD based models (the concentration distribution can be determined by Equations (6-4) and the results will be shown in the later sections). Figure 6.2 shows the block flow diagram of CFD based models developed for the simulation of hydrodynamics and mass transfer in packed columns. The inputs to the models are the details of the geometry of the process equipment and the system's physical properties such as density, viscosity, diffusivity and surface tension. The outputs from the models are detailed information on the velocity, volume fraction, pressure and concentration profiles at every

167

point within the geometry. Therefore, the CFD based models can be used to generate all the necessary information for the design and performance analysis of packed distillation columns.

6.4 Boundary Conditions

The boundary conditions for the velocity components and volume fractions were specified as those discussed in Chapter 4. The specifications of the mass fraction boundary conditions are as follows

(1) At the top of the column, the appropriate values for the component concentrations must be specified for both liquid and vapor phases;

(2) At the column wall, non-penetration of mass was specified for both liquid and vapor phases;

(3) At the bottom of the column, the Neumann boundary condition was specified for the mass fraction of the liquid phase. The Dirichlet boundary condition was specified for the mass fraction of vapor phase. This means that a specific value must be assigned to the mass fraction of the vapor phase;

(4) At the column axis, axisymmetry was specified for the mass fraction of both liquid and vapor phases.

6.5 Simulation Results and Discussion

The model was evaluated against the FRI data (Shariat and Kunesh, 1995). FRI conducted the distillation tests using the cyclohexane/n-heptane (C_6/C_7) system at total reflux and at two different operating pressures (33.3 and 165.5 kPa). The physical

168

properties of the system at these conditions are listed in Table 6.1. The test column, which was of a commercial size, had a diameter of 1.22 m and a height of 3.66 m. The packing used was 15.9 mm, 25.4 mm, and 50.8 mm metal Pall rings. Their characteristics can be found in Table 6.2. In the experiments, samples were withdrawn every 610 mm from the bed and the separation efficiency (HETP) was determined from the composition profiles using the Fenske equation (Shariat and Kunesh, 1995). The detailed description of the experimental set-up and operating procedures of the FRI unit can be found in the papers by Silvey and Keller (1966) and Shariat and Kunesh (1995). The simulations were carried out with all three sizes of Pall rings (15.9 mm, 25.4 mm, and 50.8 mm) over a wide range of operating conditions. The model has also been tested under operating pressures of 33.3 kPa and 165.5 kPa. For the two-dimensional simulation, the computational domain was divided into 120(axial)×50(radial) control volumes.

HETP is one of the most often used measures to characterize the separation efficiency of a packed column. The success of any hydrodynamics and mass transfer model relies on its ability to predict HETP accurately. Figure 6.3 shows the comparisons between the measured HETPs with the average HETPs determined from the simulation at an operating pressure of 165.5 kPa and a packed height of 3.66 m for the 15.9 mm, 25.4 mm, and 50.8 mm Pall rings, respectively. In developing their correlation for k_G, Onda et al. (1968, a, b) employed the experimental data for the packings with sizes greater than 25.4 mm and less than 15 mm. There was no data for the packings with sizes in the range of 15 mm to 25.4 mm. Since 15.9 mm is closer to 15 mm than to 25.4 mm, it is reasonable to use 2.0 for the value of k_p instead of 5.23. Thus, the k_p value in Equation (6-

12) was taken as 5.23 for the 25.4 mm and 50.8 mm Pall rings, and 2.0 for the 15.9 mm Pall rings.

In Figure 6.3, HETP data are plotted as a function of the F-factor. From this figure, it can be clearly seen that the simulation can predict the separation efficiency quite well over the range of operating conditions for all three sizes of Pall rings (average relative error (ARE) between prediction results and experimental data: for 15.9 mm Pall rings, ARE=6.07%; for 25.4 mm Pall rings, ARE=10.57%; for 50.8 mm Pall rings, ARE=4.99%). It can be seen that the simulation can track the HETP variation with the loading, which is one of the most important concerns in mass transfer modeling.

The more detailed comparison between the experimental data and simulation results is shown in Figures 6.4, 6.5 and 6.6. The composition on the y-axis is plotted as $\ln\left(\dfrac{x}{1-x}\right)$ to show the composition ratio variation with the packed bed height. In these figures, each composition x is an average value based on the detailed flow distribution over the column cross section at a fixed axial position. Again Figures 6.4, 6.5 and 6.6 show the good agreement between simulation and experimental results. While HETP is a single scalar measure at an operating condition, the composition profiles show important internal variations in the column. It is encouraging that both quantities agree well with the FRI data.

Depending on the separation requirements and system characteristics, packed distillation columns may operate under pressure or vacuum conditions. In order to determine the effect of operating pressure on the separation process, FRI ran the column at two different pressures: 165.5 kPa and 33.5 kPa. In both cases, the column packed

170

height was kept the same at 3.66 m. Figure 6.7 shows a comparison between the predicted HETP and measured HETP at operating pressure of 33.3 kPa for the 25.4 mm Pall rings. The agreement between simulation and experimental results is again reasonably good (ARE=7.86%). Comparing the results presented in Figures 6.3 and 6.7, one can see that with the increase of pressure, the separation efficiency improves for the C_6/C_7 system (HETP reduces). This favorable effect at high pressures for the C_6/C_7 system has also been reported in the literature (Zuiderweg and Nutter, 1992; Gualito et al., 1997) and can be explained by the improvement of the mass transfer parameters with increasing pressure. Table 6.1 shows that the liquid surface tension decreases with the increase of the operating pressure. A lower surface tension means better wetting of the packing, thus producing more mass transfer area and therefore higher separation efficiency. Furthermore, both the increase in liquid diffusion coefficient and decrease in liquid viscosity tend to increase the mass transfer coefficient of liquid phase and lead to higher separation efficiency.

Figure 6.8 shows a comparison between the predicted HETPs from two-dimensional simulations and one-dimensional models. In the one-dimensional model, the uniform radial distributions are assumed for both liquid and vapor phases. It can be seen that the predicted HETPs from one-dimensional models are lower than the measured HETPs for all the F-factors studied. Therefore, the flow maldistribution must be considered in order to obtain a better prediction of mass transfer efficiency.

171

6.6 Conclusions

The volume averaged momentum and mass transfer equations have been solved to obtain the detailed velocity and concentration distribution in a randomly packed distillation column. The effect of bed structure (void fraction variation) on the flow distribution has been included in the model. Also, the model has taken into account the dispersion effect in both the liquid and vapor phases. It has been shown through comparison with the experimental data over a wide range of operating conditions that the model can predict the mass transfer efficiency quite well.

The simulation was also used to predict the effect of packing size and operating pressure on separation efficiency. The increase of HETP with the packing size has been correctly captured by the simulation. For the cyclohexane/n-heptane system, the experimentally observed positive effect of the operating pressure on separation efficiency has also been confirmed in this study.

In general the simulation results for HETP and concentration profiles agree well with the experimental data. This is regarded as an encouraging sign that CFD models can play a useful role in studying separation processes.

6.7 Nomenclature

A   Component A

a_e Effective Interfacial Area Per Unit Volume, m^{-1}

a_p Total Surface Area of Packings Per Unit Volume, m^{-1}

a_w Wetted Surface Area Per Unit Volume, m^{-1}

B   Component B

D   Diffusivity, $m\ s^{-2}$

D_c Diameter of the Packed Column, m

d_e Equivalent Diameter of the Packed Column, m

d_p Size of Packing, m

F_{pd} Packing factor, m^{-1}

G   Flow Rate of Gas Per Unit Cross Sectional Area, $kg\ m^{-2}\ s^{-1}$

g   Gravitational Constant, $m\ s^{-2}$

HETP   Height Equivalent to a Theoretical Plate, m

H_{OG} Height of an Overall Vapor Phase Transfer Unit, m

H_G Height of a Vapor Phase Transfer Unit, m

HTU   Height of an Overall Vapor Phase Transfer Unit, m

K_G Overall Vapor Phase Mass Transfer Coefficient, $kmol\ s^{-1}\ m^{-2}\ Pa^{-1}$

k_G Vapor Phase Mass Transfer Coefficient, $kmol\ s^{-1}\ m^{-2}$

k_L Liquid Phase Mass Transfer Coefficient, $kmol\ s^{-1}\ m^{-2}$

k_p Parameter in Onda's Formula

L   Flow Rate of Liquid Per Unit Cross Sectional Area, $kg\ m^{-2}\ s^{-1}$

M   Molecular Weight, $kg\ kmol^{-1}$

m   Slope of Equilibrium Line

$\dot{m}$ Mass Transfer Rate, $kg\ s^{-1}\ m^{-3}$

173

N	Number of Phases
N_c	Number of Components in Each Phase
N_G	Number of a Vapor Phase Transfer Units
N_{OG}	Number of Overall Vapor Phase Transfer Units
NTU	Number of Overall Vapor Phase Transfer Units
p	Pressure, Pa
Pe	Peclet Number
Re	Reynolds Number
r	Radial Coordinate, m
t	Time, s
U	Interstitial Velocity Vector, m s^{-1}
u	Superficial Velocity. m s^{-1}
X	Mass Fraction of a Component in Liquid Phase
x	Mole Fraction of a Component in Liquid Phase
x^I	Interfacial Mole Fraction of a Component in Liquid Phase
Y	Mass Fraction of a Component in Vapor Phase
y	Mole Fraction of a Component in Vapor Phase
y^I	Interfacial Mole Fraction of a Component in Gas Phase
$y^\bullet$	Equilibrium Mole Fraction of a Component in Gas Phase
Z	Packed Bed Height, m
z	Axial Coordinate, m

Greek Symbols

α	Relative Volatility, Phase Index
β	Phase Index
ε_p	Void Fraction

174

Γ Effective Dispersion Coefficient, kg m^{-1} s^{-1}

γ Volume Fraction

σ Surface Tension, N m^{-1}

σ_c Critical Surface Tension of Packing Materials, N m^{-1}

μ Viscosity, kg m^{-1} s^{-1}

ρ Density, kg m^{-3}

θ Angular Coordinate

Subscripts

0   inlet

A   Component A

av   Average

B   Component B

G   Gas Phase

L   Liquid Phase

l   Local

z   Outlet

Superscripts

A   Component A

i   ith Component in a Phase

175

6.8 References

AEA Technology plc, (1997) *CFX-4.2: Solver*. Oxfordshire OX11 ORA, United Kingdom.

Gualito, J. J., Cerino, F. J., Cardenas, J. C. and Rocha, J. A., (1997) Design Method for Distillation Columns Filled with Metallic, Ceramic, or Plastic Structured Packings. *Ind. Eng. Chem. Res.* **36**, 1747-1757.

Kister, H. Z., (1992) *Distillation Design*, McGraw-Hill, New York.

Klemas, L. and Bonilla, J. A., (1995) Accurately Assess Packed-Column Efficiency. *Chem. Eng. Prog.* **July**. 27-44.

Kunesh, J. G., Lahm, L. and Yanagi, T., (1987) Commercial Scale Experiments That Provide Insight on Packed Tower Distributors. *Ind. Eng. Chem. Res.* **26**, 1845-1850.

Olujic, Z. and de Graauw J., (1989) Appearance of Maldistribution in Distillation Columns Equipped with High Performance Packings. *Chem. Biochem. Eng.* **Q3 (4)**, 181-196.

Onda, K., Takeuchi, H. and Okumoto. Y., (1968a) Mass Transfer Coefficients between Gas and Liquid Phases in Packed Columns. *J. Chem. Eng. Jpn.* **1**, 56-62.

Onda, K., Sada, E. and Takeuchi, H., (1968b) Gas Absorption with Chemical Reaction in Packed Columns. *J. Chem. Eng. Jpn.* **1**, 62-66.

Perry, D., Nutter, D. E. and Hale, A., (1990) Liquid Distribution for a Optimum Packing Performance. *Chem. Eng. prog.* **January**, 30-35.

Shariat, A. and Kunesh, J. G., (1995) Packing Efficiency Testing on a Commercial Scale with Good (and Not So Good) Reflux Distribution. *Ind. Eng. Chem. Res.* **34**,1273-1279.

Silvey, F. C. and Keller, G. J., (1966) Testing on a Commercial Scale. *Chem. Eng. Prog.* **62**, 68-74.

Wagner, I., Stichlmair, J. and Fair, J. R., (1997) Mass Transfer in Beds of Modern, High-Efficiency Random Packings. *Ind.Eng.Chem.Res.* **36**, 227-237.

Wang, S. T., Chen, S. Z., Xu, P. and Jia, S. Y., (1985) Longitudinal Mixing of the Liquid Phase with New-Type of Packing in a Packed Column. *Tianjin Daxue XueBao.* **2**, 57-68.

Wankat, P. C. (1988) Equilibrium Staged Separations. Prentice-Hall Inc., Englewood Cliffs, New Jersey.

Zuiderweg, F. J. and Nutter, D. E., (1992) Evidence of Vapor Backmixing in Packed Columns in the Case of High Pressure Distillation. *I. Chem. E. Symp. Ser. 128.* A481-488.

Table 6.1 Physical Properties of System Studied

C_6/C_7 System	P=165.5 kPa	P=33.3 kPa
Liquid density (kg/m^3)	636.7	713.4
Vapor density (kg/m^3)	4.907	1.162
Liquid viscosity (Pas)	0.23E-3	0.44E-3
Vapor viscosity (Pas)	8.5E-6	7.2E-6
Liquid diffusivity (m^2/s)	6.2E-9	2.7E-9
Vapor diffusivity (m^2/s)	2.1E-6	7.6E-6
Surface tension (N/m)	12E-3	20E-3
Relative volativity	1.6	1.9

178

Table 6.2 Characteristics of Metal Pall rings

Packing type	Nominal size (mm)	Specific area (1/m)	Void fraction	Packing factor (1/m)
	15.9	341	0.933	262
Metal Pall ring	25.4	207	0.940	174
	50.8	102	0.951	79

179

L, x_{A0}, x_{B0}

Liquid in | Gas out

Gas in | Liquid out

G, y_{A0}, y_{B0}
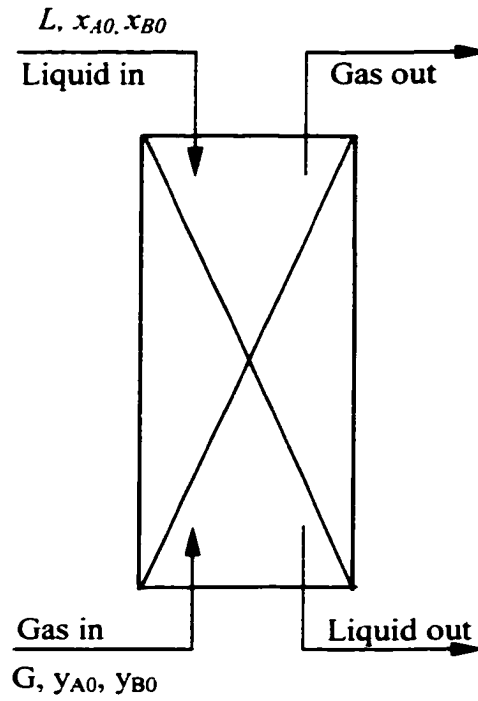
Figure 6.1. Sketch of a computational domain for a packed distillation column

180
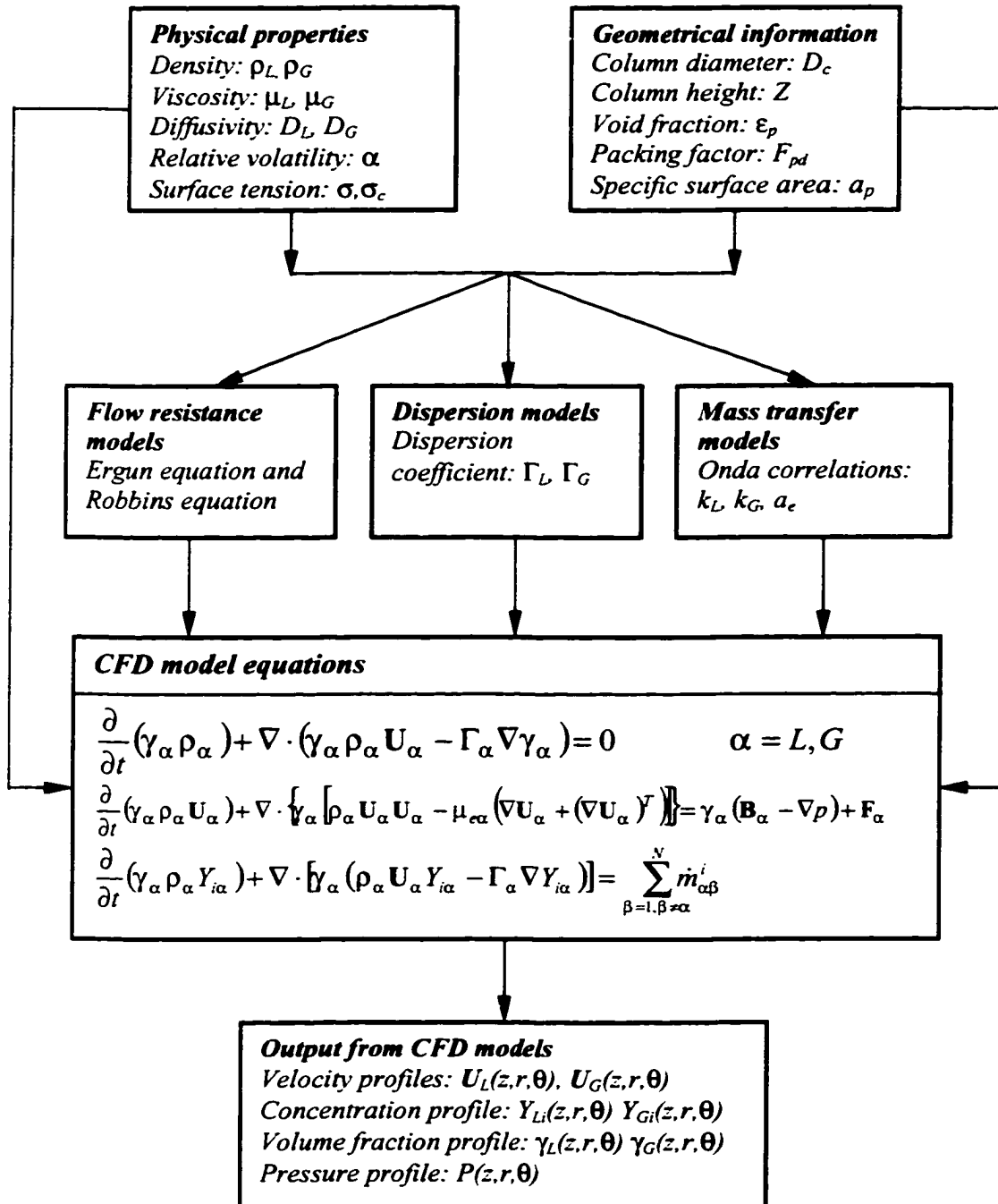
Figure 6.2. Overview of CFD based models for the simulation of the separation processes in packed columns
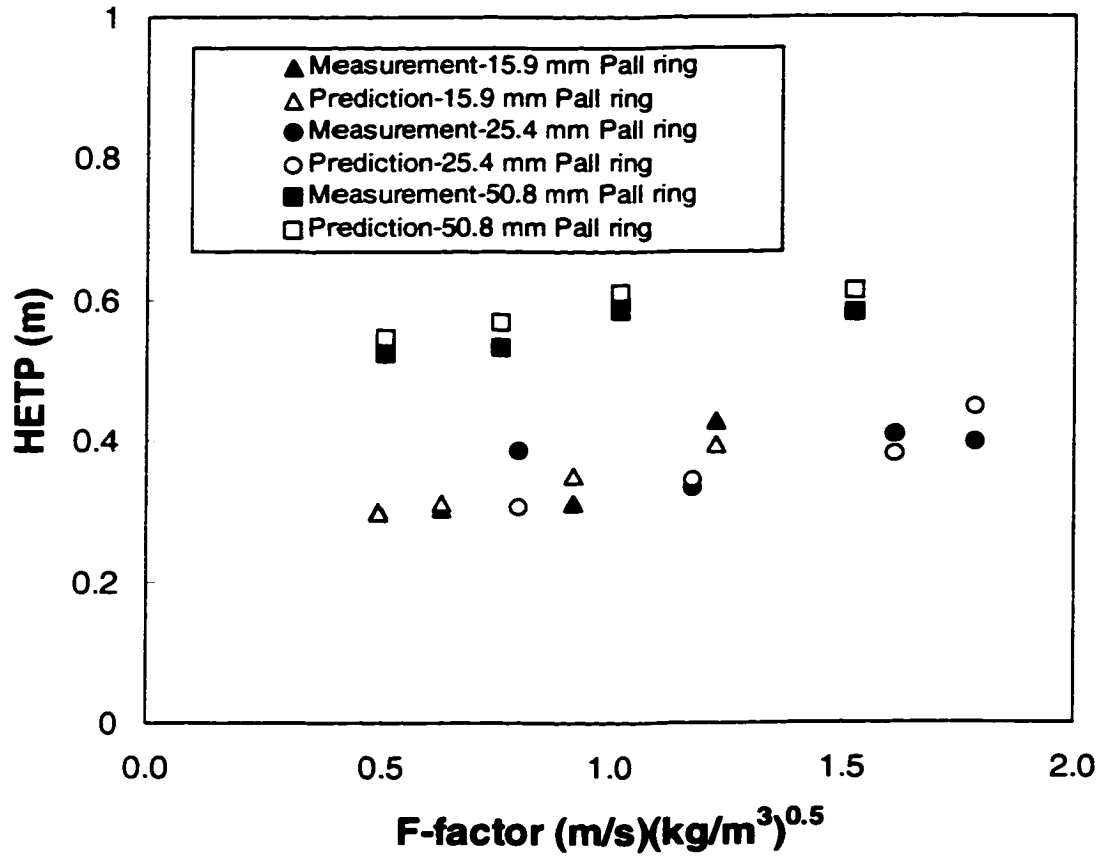
Figure 6.3. Comparison of predicted and measured HETP at an operating pressure of 165.5 kPa.
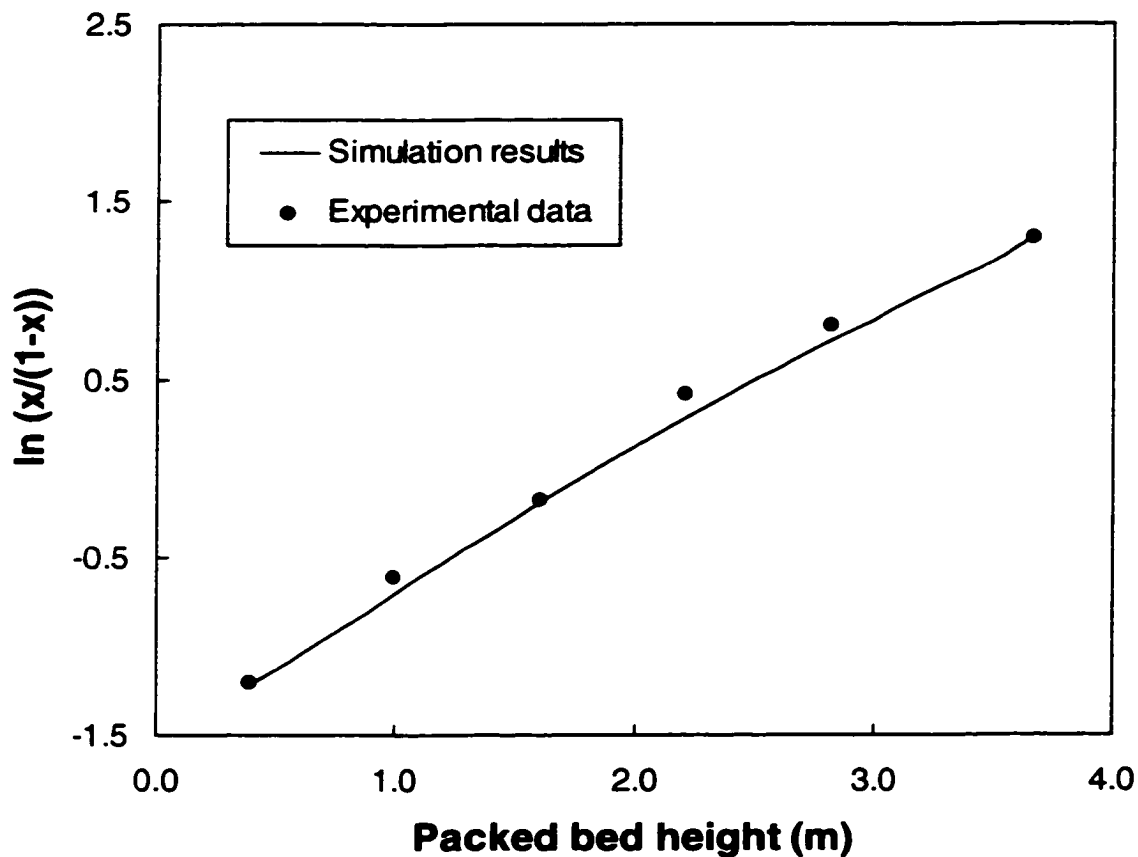
Figure 6.4. Comparison of predicted and measured composition profile of C_6 along the bed height at an operating pressure of 165.5 kPa, F-factor=0.76 $(m/s)(kg/m^3)^{0.5}$, 50.8 mm Pall rings.
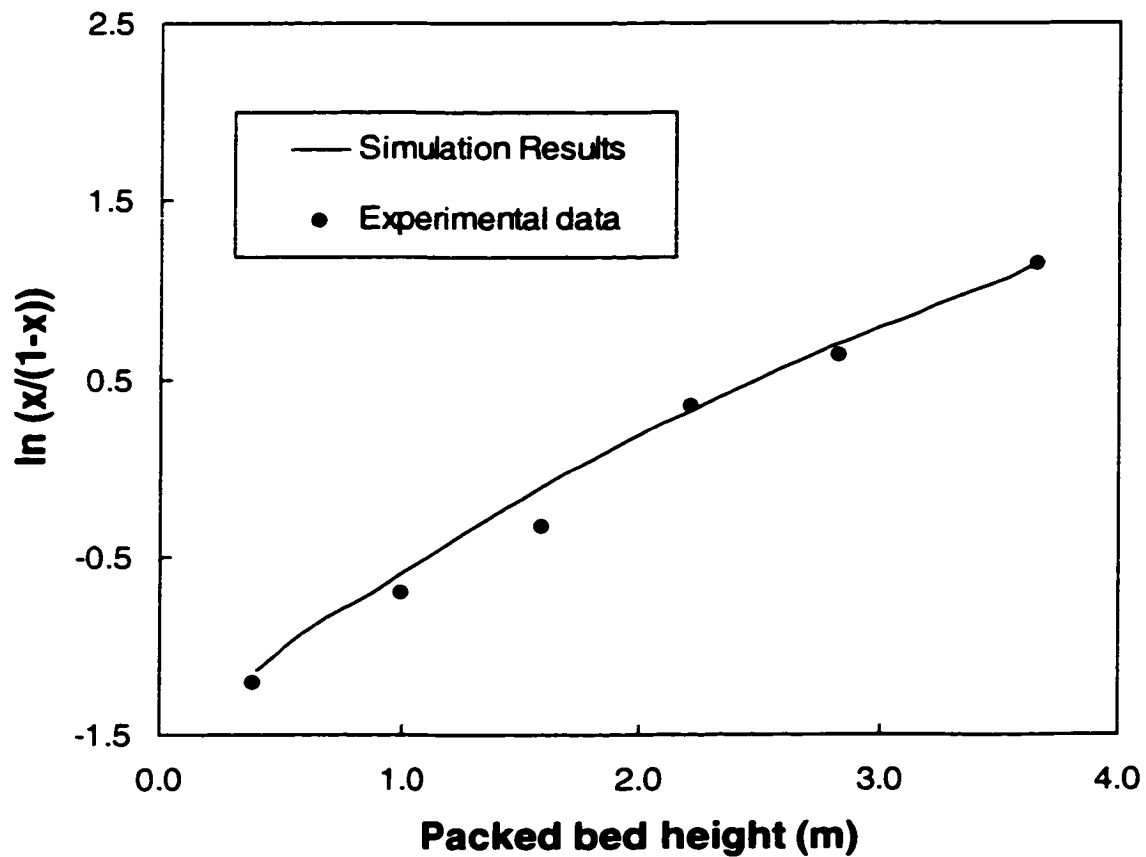
Figure 6.5. Comparison of predicted and measured composition profile of C_6 along the bed height at an operating pressure of 165.5 kPa, F-factor=1.02 $(m/s)(kg/m^3)^{0.5}$, 50.8 mm Pall rings.
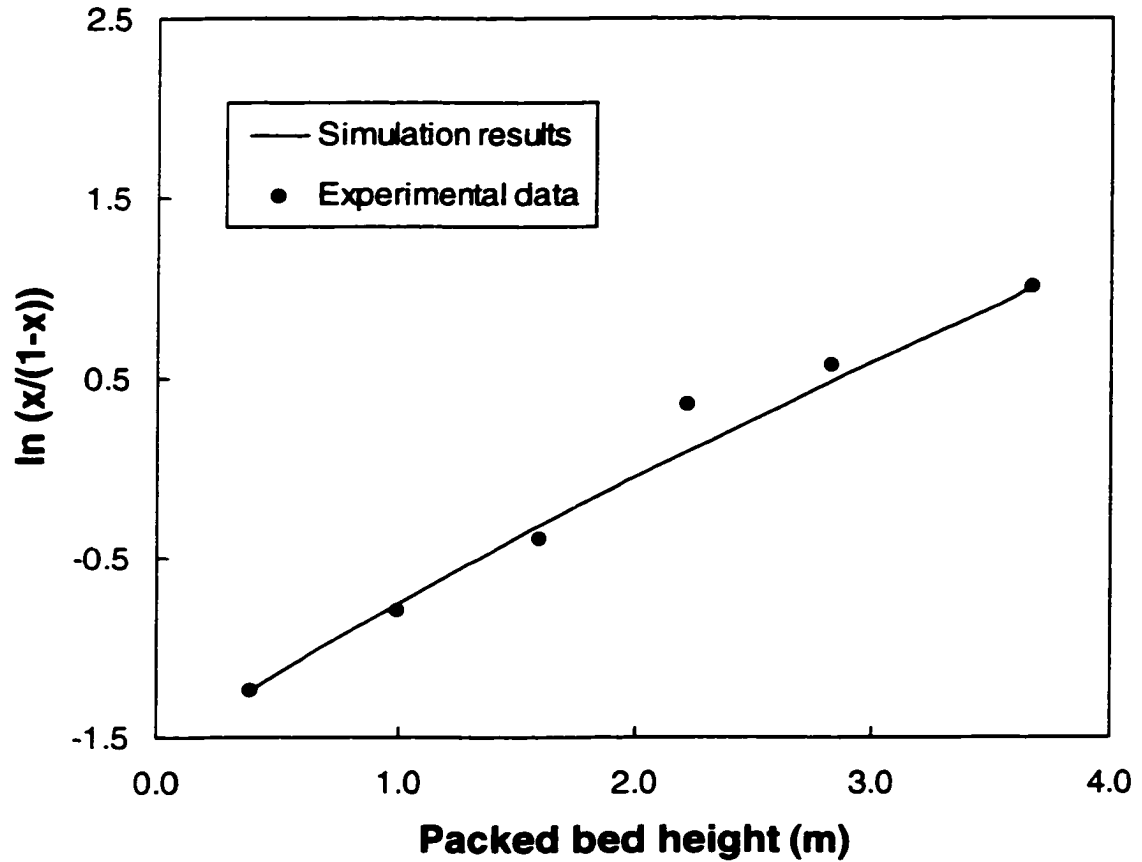
Figure 6.6. Comparison of predicted and measured composition profile of C_6 along the bed height at an operating pressure of 165.5 kPa, F-factor=1.52 $(m/s)(kg/m^3)^{0.5}$, 50.8 mm Pall rings.
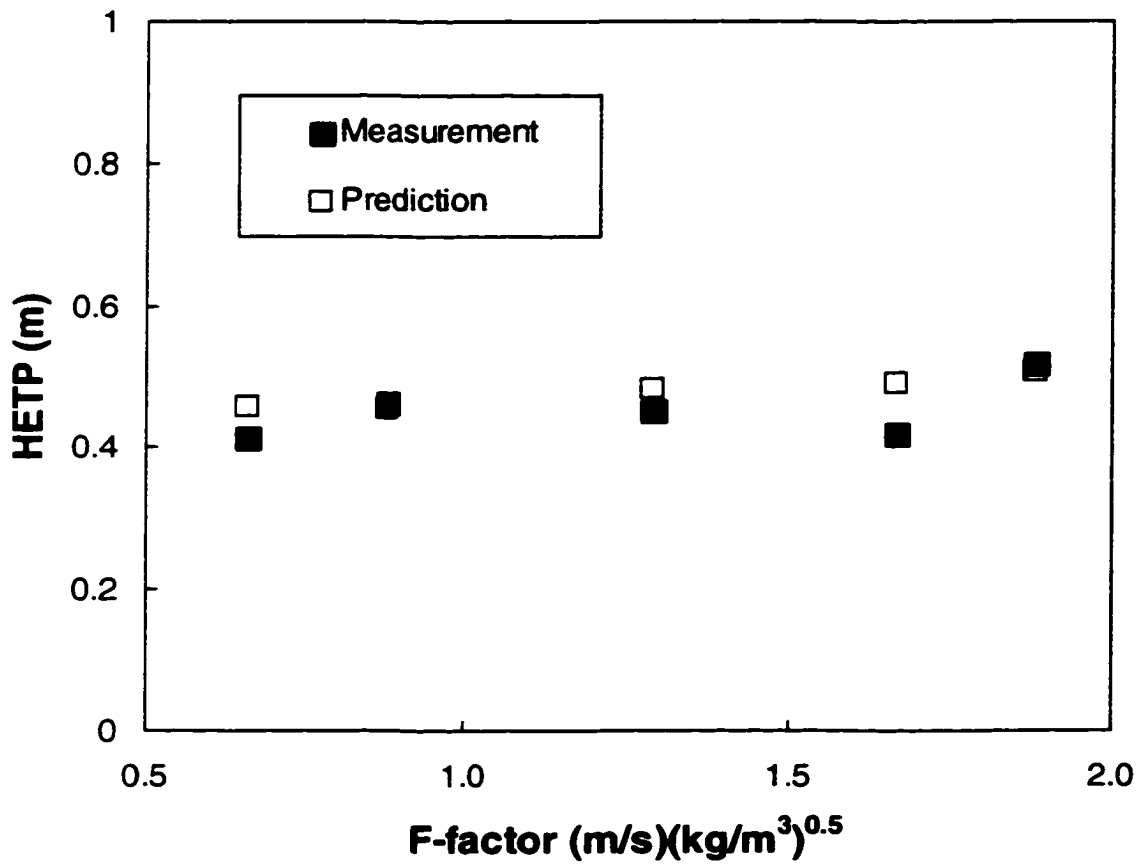
Figure 6.7. Comparison of predicted and measured HETP at the operating pressure of 33.3 kPa, 25.4 mm Pall rings.
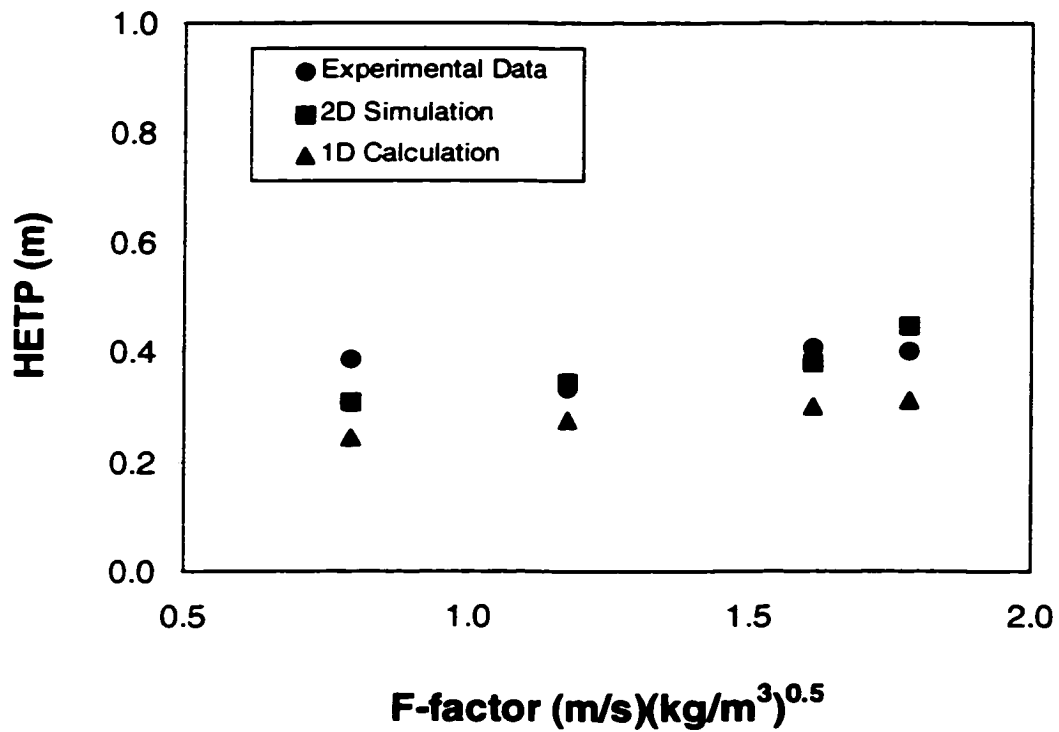
Figure 6.8. Comparison of predicted HETPs from two-dimensional simulations and one-dimensional models at the operating pressure of 165.5 kPa, 25.4 mm Pall rings.

Chapter 7

CONCLUSIONS AND RECOMMENDATIONS

Experimental data for liquid flow distribution in a randomly packed column show that the liquid velocity profile is not uniform. The main causes of the liquid maldistribution are non-uniform liquid inlet distribution and the formation of the liquid wall flow. The formation of the liquid wall flow is one of the most important characteristics associated with randomly packed columns. If the liquid is uniformly introduced into the column, the liquid wall flow will build up immediately. If the liquid is introduced into the central region of the column, the liquid will accumulate on the column wall but a portion of the packed bed height is required. The exact bed height required depends on the liquid distributor design, packing size, and operating conditions.

The design of the liquid distributor is very important to insure satisfactory performance of a packed column. If the liquid is not uniformly distributed over the top layer of the packing, a portion of packed bed height will remain unwetted and the result is that a portion of bed height provides little or no mass transfer.

Gas flow rate has a significant effect on the liquid distribution particularly at higher gas loadings. In the bulk region of the packed bed, the liquid distribution tends to become flatter with the increase of gas flow rate, however, in the wall region, the liquid wall flow shows a significantly increase.

With a increase in the liquid flow rate, the liquid relative wall flow is reduced at low gas loadings. The packed bed height required for the liquid to reach its fully developed state is also reduced.

The effect of liquid viscosity on liquid distribution depends on the gas flow rate. At a low gas flow rate, increased liquid viscosity tends to retard liquid spreading towards the column wall. However, viscous liquids also have a low loading point, thus experiencing more strong effect of gas flow at a higher gas loading.

Liquid surface tension shows little or no effect on the liquid distribution in large diameter packed columns.

The use of CFD based models for flow hydrodynamics and mass transfer in randomly packed columns have been shown. The spatial variation of void fraction was included to account for the effect of the bed structure. The models have the ability to capture the radial and axial variations in flow and mass transfer conditions, thus are a first significant step forward from one-dimensional models which assume conditions (flow distribution and concentration distribution) within a column to be uniform in the radial direction and neglect dispersion in all directions.

The good agreement between the simulation results and experimental data for liquid flow distribution, pressure drop, concentration profiles, and separation efficiency (HETP) indicates that the developed models can be used reliably to predict the hydrodynamic and mass transfer characteristics of gas and liquid two-phase flow in randomly packed columns.

189

The main advantage of the developed models is that they remain valid on any length scale, from laboratory to industrial size. Therefore they can be used as the basic tools for the rigorous design and scale-up of the packed columns.

Future work should be focused on additional laboratory experiments and improvement of the closure models used in this study.

Good model predictions have been shown for liquid flow distributions, pressure drops, axial concentration profiles and HETPs. However, the CFD models can also generate results for radial concentration distributions. Experimental data is lacking in literature. The radial concentration distribution could possibly be measured by a tracer technique.

The developed models are based on a set of closure models from the published correlations. As new experimental data becomes available, new correlations should be developed, included and validated as part of the possible improvements to the CFD models developed and tested in this study.

Appendix A

METHOD OF UNCERTAINTY ANALYSIS

Any experimental measurement involves some kind of errors, or uncertainties. If x_1, x_2, x_3, ..., and x_n are directly measured quantities, the dependence of a calculated result R on these quantities can be written as

$$R = f(x_1, x_2, x_3, \cdots, x_n)$$ (A-1)

The uncertainty in R due to the uncertainties in the measured variables can be determined as (Holman and Gajda, 1978)

$$e_R = \left[\left(\frac{\partial f}{\partial x_1} e_{x_1} \right)^2 + \left(\frac{\partial f}{\partial x_2} e_{x_2} \right)^2 + \left(\frac{\partial f}{\partial x_3} e_{x_3} \right)^2 + \cdots + \left(\frac{\partial f}{\partial x_n} e_{x_n} \right)^2 \right]^{1/2}$$ (A-2)

where e_R is the uncertainty in the calculated result R, and e_{x_1}, e_{x_2}, e_{x_3}, and e_{x_n} are the uncertainties in the directly measured quantities.

Based on Equation (A-2), the uncertainty in the experimental measurement of this study was calculated and added in the plots shown in Chapter 3.

Reference

Holman, J. P. and Gajda, W. J., (1978), *Experimental Methods for Engineers*, McGraw-Hill, New York.

191

Appendix B

Derivation of Equation (6-10)

The mass transfer rate of component A (more volatile component) from liquid phase to vapor phase can be calculated based on two-film theory

$$\dot{m}_{LG}^{A} = k_{L}a_{e}M_{A}\left(x_{A} - x_{A}'\right) \tag{B-1}$$

$$\dot{m}_{LG}^{A} = k_{G}a_{e}M_{A}\left(y_{A}' - y_{A}\right) \tag{B-2}$$

The interface compositions x_{A}' and y_{A}' are in equilibrium and can be described by

$$y_{A}' = \frac{\alpha x_{A}'}{1 + (\alpha - 1)x_{A}'} \tag{B-3}$$

From equation (B-1), x_{A}' can be determined as

$$x_{A}' = x_{A} - \frac{\dot{m}_{LG}^{A}}{k_{L}a_{e}M_{A}} \tag{B-4}$$

Substituting Equation (B-4) into Equation (B-3), results in

$$y_{A}' = \frac{\alpha\left(x_{A} - \dfrac{\dot{m}_{LG}^{A}}{k_{L}a_{e}M_{A}}\right)}{1 + (\alpha - 1)\left(x_{A} - \dfrac{\dot{m}_{LG}^{A}}{k_{L}a_{e}M_{A}}\right)} \tag{B-5}$$

Combining Equations (B-2) and (B-5) leads to

$$\frac{\alpha - 1}{k_{L}k_{G}\left(a_{e}M_{A}\right)^{2}}\left(\dot{m}_{LG}^{A}\right)^{2} + \left[\frac{(\alpha - 1)y_{A} - \alpha}{k_{L}a_{e}M_{A}} - \frac{(\alpha - 1)x_{A} + 1}{k_{G}a_{e}M_{A}}\right]\dot{m}_{LG}^{A} + \left\{\alpha x_{A} - \left[(\alpha - 1)x_{A} + 1\right]y_{A}\right\} = 0 \tag{B-6}$$

192

Appendix C

A Comparison of Predicted HETPs from Bravo and Fair's Correlations and Onda's Correlations

Figure C-1 shows a comparison of predicted HETPs based on Bravo and Fair's correlations and Onda's correlations for mass transfer coefficients and effective mass transfer area. It can be seen that the predicted HETP from Bravo and Fair's correlations is far off from the experimental data. Therefore, Onda's correlations were selected in this study.
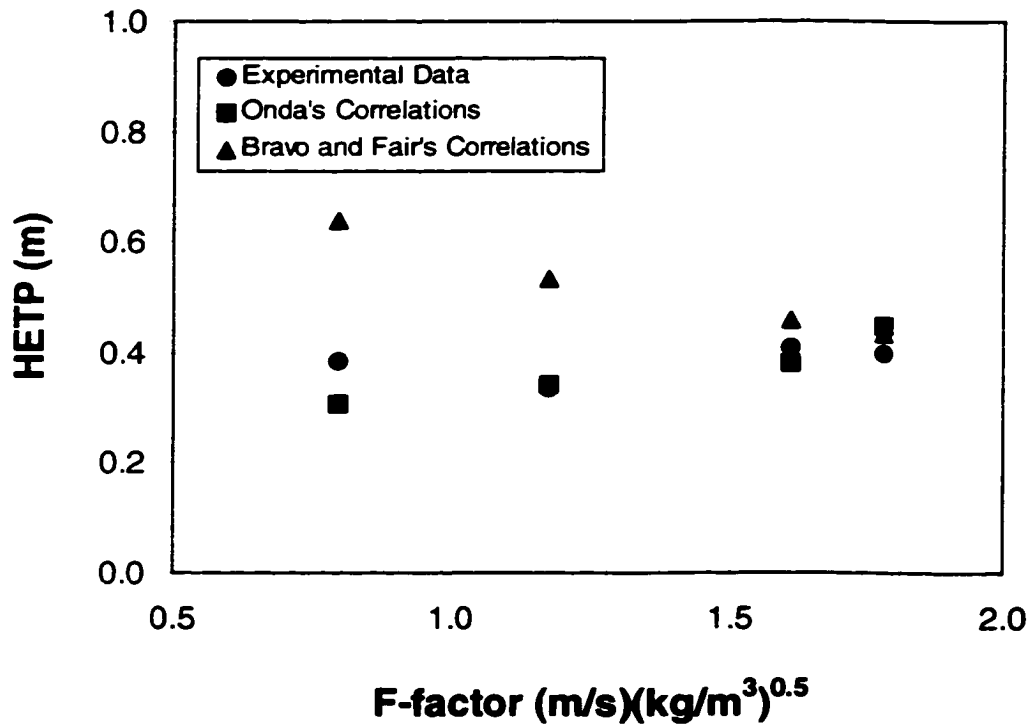
Figure C-1 A comparison of predicted HETPs from Bravo and Fair's correlations and Onda's correlations.

Appendix D: Experimental Data

Table D.1 Drip Point Flow Rate at Different Liquid Flow Rate (Water/Air)

Drip Point Number	L=0.81 kg/s		L=1.34 kg/s		L=2.39 kg/s	
	Drip Flow Rate (kg/s)	Average	Drip Flow Rate (kg/s)	Average	Drip Flow Rate (kg/s)	Average
1	0.0285	0.0280	0.0454	0.0441	0.0803	0.0795
2	0.0270	0.0280	0.0423	0.0441	0.0780	0.0795
3	0.0293	0.0280	0.0449	0.0441	0.0784	0.0795
4	0.0303	0.0280	0.0456	0.0441	0.0817	0.0795
5	0.0269	0.0280	0.0438	0.0441	0.0794	0.0795
6	0.0265	0.0280	0.0443	0.0441	0.0800	0.0795
7	0.0330	0.0280	0.0452	0.0441	0.0779	0.0795
8	0.0277	0.0280	0.0443	0.0441	0.0807	0.0795
9	0.0291	0.0280	0.0451	0.0441	0.0799	0.0795
10	0.0264	0.0280	0.0425	0.0441	0.0779	0.0795
11	0.0259	0.0280	0.0437	0.0441	0.0791	0.0795
12	0.0276	0.0280	0.0436	0.0441	0.0802	0.0795
13	0.0290	0.0280	0.0461	0.0441	0.0795	0.0795
14	0.0270	0.0280	0.0438	0.0441	0.0777	0.0795
15	0.0289	0.0280	0.0455	0.0441	0.0804	0.0795
16	0.0261	0.0280	0.0420	0.0441	0.0756	0.0795
17	0.0254	0.0280	0.0429	0.0441	0.0784	0.0795
18	0.0260	0.0280	0.0434	0.0441	0.0786	0.0795
19	0.0303	0.0280	0.0423	0.0441	0.0790	0.0795
20	0.0276	0.0280	0.0435	0.0441	0.0814	0.0795
21	0.0255	0.0280	0.0432	0.0441	0.0781	0.0795
22	0.0287	0.0280	0.0444	0.0441	0.0801	0.0795
23	0.0267	0.0280	0.0422	0.0441	0.0811	0.0795
24	0.0266	0.0280	0.0432	0.0441	0.0771	0.0795
25	0.0271	0.0280	0.0435	0.0441	0.0788	0.0795
26	0.0297	0.0280	0.0459	0.0441	0.0794	0.0795
27	0.0259	0.0280	0.0425	0.0441	0.0795	0.0795
28	0.0287	0.0280	0.0453	0.0441	0.0810	0.0795
29	0.0285	0.0280	0.0450	0.0441	0.0824	0.0795
30	0.0321	0.0280	0.0444	0.0441	0.0803	0.0795
31	0.0292	0.0280	0.0463	0.0441	0.0830	0.0795

Table D.2 Reproducibility Test for the Uniform Liquid Distributor
(Water/Air, H=0.9 m, L=4.78 kg/m^{2}s)

Radial Position	Liquid Relative Velocity	
mm	First Run	Second Run
0	1.152	1.170
50	1.152	1.170
125	1.189	1.170
175	1.047	1.070
225	0.842	0.831
272.4	0.698	0.716
296.6	3.183	2.979

195

Table D.3 Reproducibility Test for the Uniform Liquid Distributor
(Water/Air, H=0.9 m, L=4.78 kg/m²s, G=0.83 kg/m²s)

Radial Position	Liquid Relative Velocity	
mm	First Run	Second Run
0	1.234	1.103
50	1.234	1.103
125	1.189	1.140
175	1.222	1.207
225	0.860	0.878
272.4	0.515	0.575
296.6	3.189	3.310

196

Table D.4 Reproducibility Test for the Uniform Liquid Distributor
(Water/Air, H=0.9 m, L=4.78 kg/m²s, G=1.57 kg/m²s)

Radial Position	Liquid Relative Velocity	
mm	First Run	Second Run
0	1.167	1.118
50	1.167	1.118
125	1.144	1.127
175	1.173	1.167
225	0.884	0.904
272.4	0.542	0.552
296.6	3.552	3.460

197

Table D.5 Reproducibility Test for the Center Inlet Liquid Distributor
(Water/Air, H=0.9 m, L=4.78 kg/m²s, G=0.52 kg/m²s)

Radial Position	Liquid Relative Velocity	
mm	First Run	Second Run
0	2.343	2.152
50	2.343	2.152
125	1.839	1.862
175	1.183	1.269
225	0.588	0.602
272.4	0.264	0.264
296.6	0.869	0.840

Table D.6 Effect of Redumping on Liquid Distribution
(Water/Air, H=0.9 m, L=4.78 kg/m^{2}s)

Radial Position mm	Liquid Relative Velocity				
	Dump1	Dump2	Dump3	Dump4	Mean
0	1.134	1.082	1.305	1.306	1.207
50	1.134	1.082	1.305	1.306	1.207
125	1.307	1.243	1.095	1.080	1.181
175	1.238	1.229	1.180	1.193	1.210
225	0.832	0.863	0.931	0.920	0.887
272.4	0.519	0.538	0.513	0.525	0.524
296.6	3.113	3.265	3.090	3.077	3.136

Table D.7 Pressure Drop for Water/Air System
(Water/Air, H=0.9 m, L=4.78 kg/m^{2}s)

Gas Flow Rate kg/m^{2}s	Pressure Drop kPa/m
0.735	0.070
1.092	0.149
1.512	0.291
1.953	0.499
2.132	0.624
2.300	0.745
2.426	0.894
2.541	1.010
2.793	1.260
2.951	1.470
3.129	1.760
3.276	2.130
3.350	3.210

Table D.8 Pressure Drop for Isopar/Air System
(Water/Air, H=0.9 m, L=4.78 kg/m^{2}s)

Gas Flow Rate kg/m^{2}s	Pressure Drop kPa/m
0.870	0.090
1.130	0.147
1.720	0.420
2.420	1.079
2.530	1.373
2.630	1.848

Table D.9 Liquid Relative Velocity at the Different Packed Bed Heights for the Uniform and Center Inlet Liquid Distributors
(Water/Air, L=4.78 kg/m²s)

Radial Position (mm)	Uniform Liquid Distributor			Center Inlet Liquid Distributor		
	0.9 m	1.8 m	3.0 m	0.9 m	1.8 m	3.0 m
0	1.134	1.132	1.113	2.241	1.959	1.725
50	1.134	1.132	1.113	2.241	1.959	1.725
125	1.307	1.210	1.141	1.921	1.567	1.526
175	1.238	0.984	0.969	1.270	1.159	1.009
225	0.832	0.835	0.766	0.569	0.642	0.701
272.4	0.519	0.594	0.675	0.224	0.368	0.442
296.6	3.113	4.493	4.831	0.860	2.288	3.172

Table D.10 Liquid Relative Wall Flow for the Uniform Liquid Distributor (Water/Air)

Packed Bed Height m	G=0.0 kg/m²s		G=0.75 kg/m²s		G=1.57 kg/m²s	
	L=2.91 kg/m²s	L=6.66 kg/m²s	L=2.91 Kg/m²s	L=6.66 kg/m²s	L=2.91 kg/m²s	L=6.66 kg/m²s
0.9	3.272	2.864	3.259	3.139	3.329	3.461
1.8	4.614	4.595	4.873	4.730	5.059	4.907
3.0	5.220	4.610	5.171	4.752	5.307	5.174

203

Table D.11 Liquid Relative Wall Flow for the Center Inlet Liquid Distributor (Water/Air)

Packed Bed Height m	G=0.0 kg/m²s		G=0.75 kg/m²s		G=1.57 kg/m²s	
	L=2.91 kg/m²s	L=6.66 kg/m²s	L=2.91 Kg/m²s	L=6.66 kg/m²s	L=2.91 kg/m²s	L=6.66 kg/m²s
0.9	0.935	1.042	1.008	1.172	1.283	1.298
1.8	2.194	2.030	2.208	2.247	2.381	2.547
3.0	3.346	3.023	3.560	3.476	3.971	3.873
3.5	3.748	3.090	3.757	3.570	4.230	4.059

204

Table D.12 Liquid Relative Velocity for the Uniform Liquid Distributor
(Water/Air, H=0.9 m, L=2.91 kg/m^{2}s)

Radial Position mm	G=0.0 kg/m^{2}s	G=1.96 kg/m^{2}s	G=2.80 kg/m^{2}s
0	1.133	1.240	1.139
50	1.133	1.240	1.139
125	1.197	1.112	1.066
175	1.113	1.209	1.091
225	0.816	0.882	0.981
272.4	0.506	0.520	0.374
296.6	3.272	3.377	5.356

205

Table D.13 Liquid Relative Wall Flow for the Uniform Liquid Distributor
(Water/Air, L=4.78 kg/m^{2}s)

Packed Bed Height 0.9 m	G kg/m^{2}s	0	0.75	1.57	2.56	3.00
	u_w/u_{av}	3.113	3.181	3.460	4.788	6.113
1.8 m	G kg/m^{2}s	0	0.75		1.57	2.32
	u_w/u_{av}	4.493	4.537		4.906	5.275
3.0 m	G kg/m^{2}s	0	0.75	1.57	2.21	2.78
	u_w/u_{av}	4.831	4.870	5.073	5.342	6.123

Table D.14 Liquid Relative Velocity for the Uniform Liquid Distributor
(Water/Air, H=3.0 m)

Radial Position mm	L=2.91 kg/m^2s	L=4.78 kg/m^2s	L=6.66 kg/m^2s
0	1.116	1.113	1.174
50	1.116	1.113	1.174
125	1.161	1.141	1.127
175	0.958	0.969	1.002
225	0.780	0.766	0.768
272.4	0.613	0.675	0.659
296.6	5.220	4.831	4.610

Table D.15 Liquid Relative Velocity for the Uniform Liquid Distributor
(Water/Air, H=0.9 m, G=1.57 kg/m^{2}s)

Radial Position mm	L=2.91 kg/m^{2}s	L=4.78 kg/m^{2}s	L=6.66 kg/m^{2}s
0	1.243	1.167	1.119
50	1.243	1.167	1.119
125	1.164	1.144	1.138
175	1.190	1.173	1.135
225	0.864	0.884	0.901
272.4	0.530	0.542	0.570
296.6	3.330	3.552	3.461

208

Table D.16 Liquid Relative Velocity for the Uniform Liquid Distributor
(H=0.9 m, L=6.66 kg/m²s)

Radial Position mm	Water	Detergent Solution
0	1.129	1.113
50	1.129	1.113
125	1.254	1.098
175	1.258	1.155
225	0.838	1.029
272.4	0.556	0.542
296.6	2.864	2.864

Table D.17 Liquid Relative Velocity for the Uniform Liquid Distributor
(H=1.8 m, L=6.66 kg/m^{2}s, G=1.57 kg/m^{2}s)

Radial Position mm	Water/Air	Detergent Solution/Air
0	1.226	1.112
50	1.226	1.112
125	1.134	0.942
175	0.905	0.816
225	0.836	0.895
272.4	0.605	0.770
296.6	4.907	4.841

210

Table D.18 Liquid Relative Velocity for the Uniform Liquid Distributor
(H=3.0 m, L=6.66 kg/m^{2}s, G=3.00 kg/m^{2}s)

Radial Position mm	Water/Air	Detergent Solution/Air
0	0.970	0.864
50	0.970	0.864
125	1.019	0.824
175	0.829	0.832
225	0.979	0.882
272.4	0.627	0.704
296.6	6.315	5.965

Table D.19 Liquid Relative Velocity for the Uniform Liquid Distributor
$(H=0.9 \text{ m}, L=6.66 \text{ kg/m}^2\text{s})$

Gas Flow Rate kg/m²s	Water/Air	Detergent Solution/Air
0	2.864	2.864
0.75	3.139	2.962
1.57	3.461	3.643
2.45	4.521	4.326

212

Table D.20 Liquid Relative Velocity for the Uniform Liquid Distributor
(H=0.9 m, L=6.66 kg/m^{2}s)

Radial Position mm	Water	Isopar
0	1.129	1.301
50	1.129	1.301
125	1.254	1.251
175	1.258	1.187
225	0.838	0.867
272.4	0.556	0.615
296.6	2.864	1.998

Table D.21 Liquid Relative Velocity for the Uniform Liquid Distributor
(H=3.0 m, L=6.66 kg/m^{2}s,)

Radial Position mm	Water	Isopar
0	1.174	1.429
50	1.174	1.429
125	1.127	1.172
175	1.002	0.980
225	0.768	0.759
272.4	0.659	0.728
296.6	4.610	3.120

214

Table D.22 Liquid Relative Velocity for the Uniform Liquid Distributor
$$(H=0.9 \text{ m}, L=4.78 \text{ kg/m}^2\text{s}, G=0.75 \text{ kg/m}^2\text{s})$$

Radial Position mm	Water/Air	Isopar/Air
0	1.224	1.300
50	1.224	1.300
125	1.201	1.277
175	1.224	1.010
225	0.857	0.918
272.4	0.503	0.610
296.6	3.181	2.637

215

Table D.23 Liquid Relative Velocity for the Uniform Liquid Distributor
(H=3.0 m, L=4.78 kg/m^{2}s, G=0.75 kg/m^{2}s)

Radial Position mm	Water/Air	Isopar/Air
0	1.053	1.314
50	1.053	1.314
125	1.200	1.087
175	0.963	0.867
225	0.822	0.865
272.4	0.658	0.739
296.6	4.870	3.655

216

Table D.24 Liquid Relative Wall Flow for the Uniform Liquid Distributor
(H=0.9 m, L=2.91 kg/m²s)

	G kg/m²s	0	0.89	1.96	2.80
Water/Air	u_w/u_{av}	3.272	3.244	3.377	5.356
	G kg/m²s	0		0.92	1.82
Isopar/Air	u_w/u_{av}	1.829		2.171	3.913

217

Table D.25 Liquid Relative Velocity for the Uniform Liquid Distributor
(Water/Air, H=3.0 m, L=4.78 kg/m^{2}s)

Radial Position mm	G=0.47 kg/m^{2}s	G=1.13 kg/m^{2}s
0	1.032	1.120
50	1.032	1.120
125	1.210	1.119
175	0.970	0.942
225	0.821	0.825
272.4	0.648	0.628
296.6	4.810	4.830

218

Table D.26 HETP for Different Pall Rings (FRI Data)
(P=165.5 kPa)

Packing Size 15.9 mm	F-factor $(m/s)(kg/m^3)^{0.5}$	0.490	0.628	0.922	1.230
	HETP (m)	0.302	0.305	0.312	0.429
25.4 mm	F-factor $(m/s)(kg/m^3)^{0.5}$	0.795	1.180	1.610	1.780
	HETP (m)	0.386	0.335	0.409	0.399
50.8 mm	F-factor $(m/s)(kg/m^3)^{0.5}$	0.504	0.758	1.020	1.520
	HETP (m)	0.526	0.533	0.587	0.584

219

Table D.27 Concentration of C_6 at Different Packed Bed Height (FRI Data)
(P=165.5 kPa, 50.8 mm Pall Rings)

Packed Bed Height mm	Fs=0.760 $(m/s)(kg/m^3)^{0.5}$	Fs=1.020 $(m/s)(kg/m^3)^{0.5}$	Fs=1.520 $(m/s)(kg/m^3)^{0.5}$
3660	0.7857	0.7596	0.7328
2819	0.6914	0.6531	0.6385
2210	0.6035	0.5881	0.5881
1600	0.4576	0.4197	0.4018
991	0.3527	0.3306	0.3114
381	0.2314	0.2314	0.2246

220

Table D. 28 Pressure Drop for Different Pall Rings (FRI Data)
(p=165.5 kPa)

Packing Size	F-factor $(m/s)(kg/m^3)^{0.5}$	0.490	0.628	0.922	1.230
15.9 mm	Pressure Drop Pa/m	94.18	119.29	269.97	637.26
25.4 mm	F-factor $(m/s)(kg/m^3)^{0.5}$	0.584	0.795	1.180	1.610
	Pressure Drop Pa/m	66.22	122.62	250.96	671.96
50.8 mm	F-factor $(m/s)(kg/m^3)^{0.5}$	0.758	1.020	1.520	2.000
	Pressure Drop Pa/m	62.78	87.90	216.60	527.39

221

Table D. 29 HETP for the 25.4 mm Pall Rings (FRI Data)
(P=33.3 kPa)

F-factor $(m/s)(kg/m^3)^{0.5}$	HETP m
0.656	0.414
0.873	0.465
1.290	0.452
1.670	0.419
1.880	0.518

222